Navigating the immune system:

Improving CD8$^+$ T cell responses for vaccine design

Anouk Cecile Maria Platteel

COLOFON

ISBN: 978-90-393-6676-9

The research described in this thesis was performed within the framework of the European Union's Seventh Framework Programme ADITEC and supported through travel grants of the European Federation of Immunological Societies (EFIS) and Boehringer Ingelheim Fonds.

Research described in this thesis was performed at:
- the Department of Infectious Diseases and Immunology, Division of Immunology, Faculty of Veterinary Medicine, Utrecht University, Utrecht, The Netherlands.
- the Department of Immunology, Max Planck Institute for Infection Biology, Berlin, Germany.

Cover design: Suzanne Brouwer.
The boat embodies the immune system that is successfully navigated towards the desired $CD8^+$ T cell response for vaccination purposes, symbolized by the harbor of Den Helder.

Layout: Proefschrift-AIO
Printing: Proefschrift-AIO

Printing of this thesis was financially supported by KNCV Tuberculosis Foundation, the Infection & Immunity Center Utrecht and Coldskin.nl.

Navigating the immune system:

Improving CD8$^+$ T cell responses for vaccine design

Navigeren van het immuunsysteem:

Verbeteren van de CD8$^+$ T cel respons voor vaccinatie doeleinden

(met een samenvatting in het Nederlands)

Proefschrift

ter verkrijging van de graad van doctor aan de Universiteit Utrecht op gezag van de rector magnificus, prof. dr. G.J. van der Zwaan, ingevolge het besluit van het college voor promoties in het openbaar te verdedigen op donderdag 15 december 2016 des middags te 12.45 uur

door

Anouk Cecile Maria Platteel

geboren op 6 februari 1987
te Den Helder

Promotor: Prof. dr. W. van Eden
Copromotor: Dr. E.J.A.M. Sijts

Contents

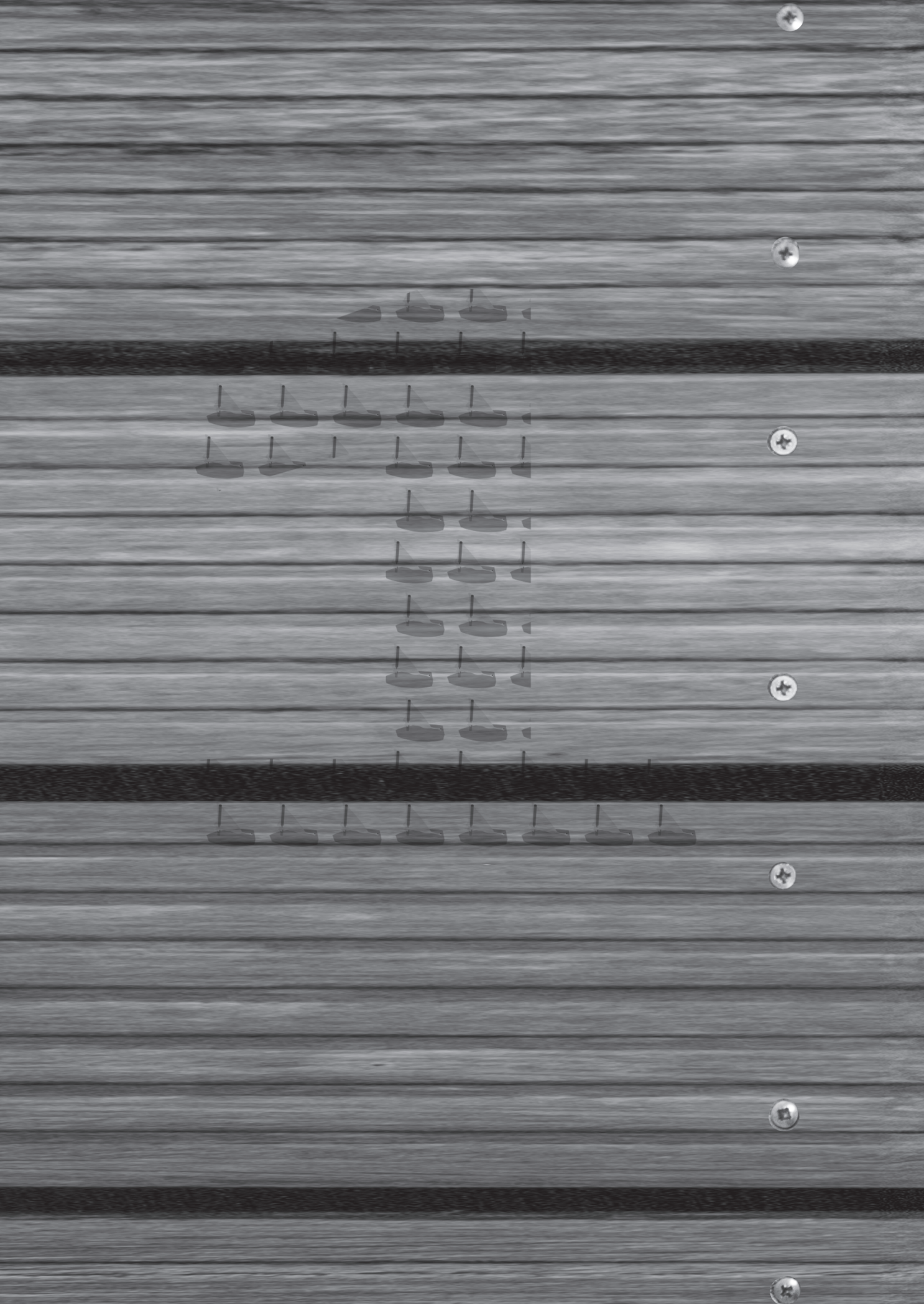

General introduction

Preface

The results of the research described in this thesis provide new insights in antigen processing, both in novel ways of $CD8^+$ T cell epitope generation as well as in strategies to modulate this process, in order to navigate the immune system towards a desired outcome in a vaccine setting. Currently, most vaccines rely on the protective effect of the humoral response. In case of intracellular- or rapidly mutating pathogens, humoral responses are less protective and instead the cellular response, mainly $CD8^+$ T cells, can convey protection. However, vaccine efficacy is hampered by insufficient knowledge of vaccine-antigen processing and subsequent activation of the cellular compartment [1]. Additionally, and most importantly, vaccine design in the future cannot be empirical; it needs to be rational, based on scientific knowledge of underlying mechanisms of immune responses targeted to vaccine-antigens. Therefore, the overall aim was to have a better understanding of antigen processing and subsequent initiation of a $CD8^+$ T cell response. In this introduction, the various components or influencing factors of antigen processing leading to a $CD8^+$ T cell response are first introduced. Thereafter, a short summary of the objectives of the different chapters is provided.

Antigen processing by the proteasome

Endogenous proteins, either self-derived or of microbial origin, are continuously degraded and replaced with newly synthesized proteins. A major role in the degradation of such proteins is played by the 26S proteasome, which is the central proteolytic enzyme complex of the ubiquitin–proteasome system (UPS). The UPS is present in every cell of an organism. In this system, a series of ubiquitin moieties is activated and transferred to protein substrates (Fig. 1). These poly-ubiquitylated proteins are thereby 'marked' for degradation and are channeled to the proteasome [2-4]. The 26S proteasome consists of two 19S regulatory caps and one 20S catalytic core. The 19S cap, also called PA700, is a proteasome activator and is responsible for substrate recognition and protein unfolding, thereby allowing entry to the channel of the barrel-shaped 20S core [5]. The 20S catalytic core is composed of two outer rings with seven α-subunits and two inner rings with seven β-subunits. Most mammalian tissues express constitutive proteasomes, which carry the proteolytic subunits β1, β2, and β5 in their core [2]. These β-subunits differ in their proteolytic activity; β5 preferably hydrolyses hydrophobic residues, β2 basic residues and β1 acidic residues. The activities are therefore referred to as chymotrypsin-like, trypsin-like, or caspase-like, respectively [6, 7]. Once the cell is in a pro-inflammatory milieu, these three constitutive subunits are replaced by alternative catalytically active subunits

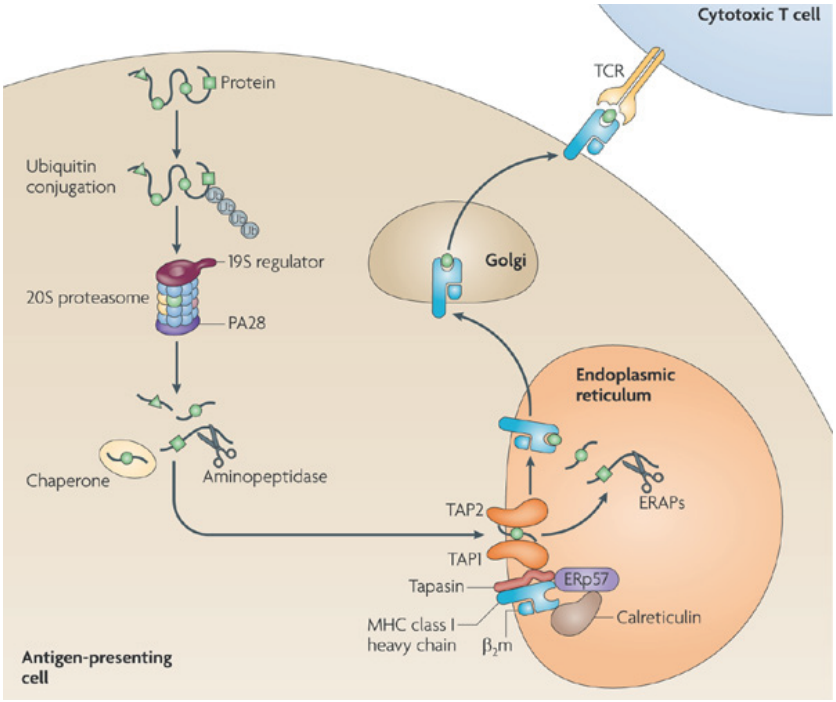

Figure 1. MHC class I antigen processing pathway. Adapted with permission from Groettrup et al., 2010 [4]. Endogenously present self- or microbial derived proteins are degraded in various steps into peptides that can be presented on the cell surface in the context of MHC class I to TCRs of $CD8^+$ T cells.

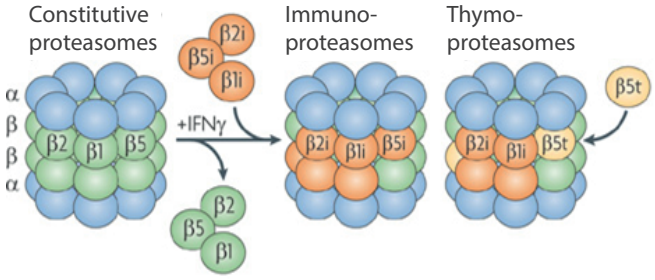

Figure 2. Constitutive, immuno- and thymic proteasomes. Adapted with permission from Klein et al., 2009 [86]. Constitutive proteasomes are present in every cell of an organism. If the cell resides in an inflammatory milieu, the immunosubunits are incorporated which has consequences for the peptides produced. In the thymus, thymoproteasomes are expressed, which have one of the immunosubunits replaced by β5t. Thymoproteasomes are important in positive and negative selection of T cells.

called β1i/LMP2, β2i/MECL1, and β5i/LMP7 to form immunoproteasomes [8] (Fig. 2). The incorporation of the immunosubunits is accompanied by expression of the alternative capping subunit PA28. PA28, also called 11S, attaches to the 20S core like the 19S complex, but has been shown to stimulate hydrolysis by the proteasome. There are even certain epitopes that are known to be dependent on PA28, suggesting a role of PA28 in antigen processing that is not fully understood yet [9, 10].

The changes in the catalytic subunit composition of β1, β2, and β5 in constitutive proteasomes or of the β1i, β2i and β5i subunits in immunoproteasomes were initially thought to result in qualitative differences of the peptide pool produced [11, 12]. Due to more sensitive detection methods, it has become clear that incorporation of the immunosubunits induce subtle modifications in the conformation in the active sites, which affect proteasome proteolytic dynamics, but with consequences for only the quantities of peptides produced [13-22]. The cause for this difference in peptide quantity was recently shown using an integrated experimental and modelling approach. It was proven that the transport of substrates into the proteasome is the rate-limiting step of hydrolysis. The transport efficiency varies between constitutive- and immuno-proteasomes, which results in differences in amounts of peptides produced [17]. Although the pool of peptides produced is only quantitatively different, there are qualitative differences in the immune responses specific for these peptides. This phenomenon has been intensively studied in mouse models lacking different combinations of the immunosubunits [23-25]. In infection, there is an almost 100% replacement of constitutive proteasomes for immunoproteasomes [26, 27]. In infected mice lacking immunoproteasomes, the need for this replacement is clear since the mice are not able to clear the pathogen [28] or they can even succumb to infection [29].

Proteasome-mediated cleavage and splicing

The generation of peptides by the proteasome can occur by simple peptide-bond cleavage as well as by proteasome-catalyzed peptide splicing (PCPS), which involves the linkage of fragments originally distant in the parental protein (Fig. 3) [30, 31]. Cleavage by the proteasome is the result of an attack on peptide bonds by the catalytic threonines of the β-subunits. This attack results in the formation of an acyl-enzyme intermediate. Rapid hydrolysis usually takes place, which gives rise to linear proteasome-generated products [32]. These products are stable and can leave the proteasome. However, when the acyl-enzyme intermediate is stabilized at the active site for an extended time span, the N-termini of released peptide fragments may outcompete hydrolysis and make a second attack on

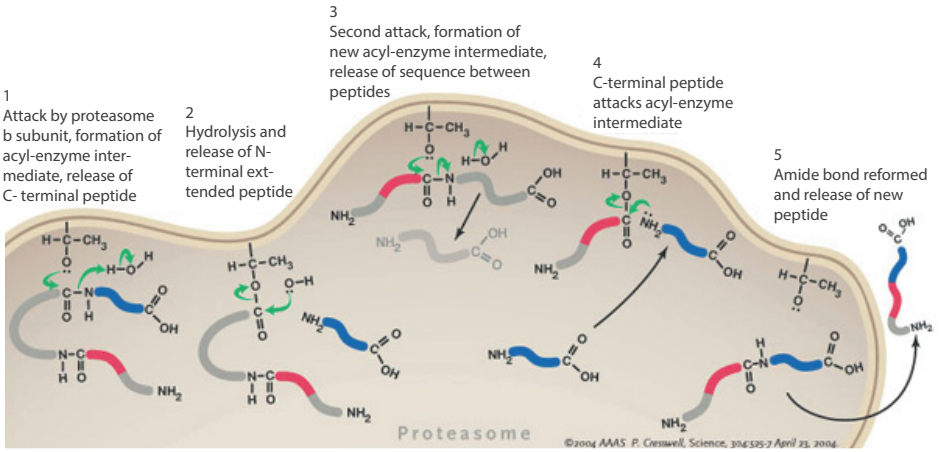

Figure 3. Proteasome catalyzed peptide splicing. Adapted with permission from Cresswell et al., 2004 [32]. Protein catalyzed peptide splicing (PCPS) involves linkage of two segments, originally distant in the parental protein, to be pasted together in several steps.

the ester bond of the acyl-enzyme intermediate, forming a new peptide bond and producing a proteasome-catalyzed spliced product [6]. The amount of specific spliced epitopes presented by human MHC class I molecules at the cell surface can be comparable to that of linear epitopes, as shown for $gp100^{mel}$ [33]. The proteasome-generated spliced epitopes that have been described until now are all derived of tumor-associated or other self-antigens [33-38].

In order to gain more knowledge on PCPS, accurate tools to predict spliced peptides are necessary. Some pioneering work has been done to set up 'splicing rules' [39] which are based on characteristics of the N- or C-terminal ligation partner. By combining such data with mathematical modelling, a reverse immunology approach can be set up for the prediction of potential spliced epitopes.

Transport to cell surface

Proteasomes usually generate the C-terminus of a peptide, while the N-terminus may need additional trimming. After generation by the proteasome, N-terminally elongated peptides enter the cytosol (Fig.1). Here, a substantial amount of proteasome-generated peptides is completely degraded by aminopeptidases [40, 41], but only N-terminal trimming can also take place. The peptides will be transported by TAP into the ER, where further N-terminal trimming can be carried out by aminopeptidase ERAP [42]. In the ER, peptides that contain a binding motive

will bind to the appropriate MHC class I molecule. To accomplish this, a chaperone protein called calreticulin maintains the MHC class I molecule in a partly unfolded state and tapasin links the MHC class I chains to TAP. The oxidoreductase ERp57 helps stabilizing the correctly sized peptide while it binds to this newly assembled MHC class I molecule. The binding induces a final folding and stabilization of the MHC class I-peptide complex, which then leaves the ER. Using Golgi vesicles, the complex is transported to the cell surface to be presented to the T cell receptor (TCR) of $CD8^+$ T cells.

T cell selection and repertoire

Since besides pathogen-derived peptides, also self-derived peptides are presented on MHC class I molecules, the $CD8^+$ T cells recognizing the self-peptides should be filtered out of the naive population to prevent auto-immunity. All progenitor T cells originate in the bone marrow but the major events in their development occur in the thymus. In the thymus, naive T cells are positively selected for their ability to recognize self-MHC, and then negatively selected to eliminate naive T cells bearing TCRs that recognize self-antigens. In this way, all T cells are able to recognize self MHC class I, but T cells recognizing self-derived peptides presented on MHC class I with high affinity are filtered out. The peptides used for positive- and negative selection are of major importance and are mainly generated by immunoproteasomes. It is therefore not surprising that immunoproteasomes have been associated with shaping the repertoire of $CD8^+$ T cells. Recently, a thymic proteasome subunit was identified, β5t [43-45], which was found to be expressed only in cortical thymical epithelial cells (cTEC), and to incorporate preferentially into proteasome precursor complexes containing β2i/MECL1, and β5i/LMP7 [46]. This incorporation selectively reduced the proteasomal chymotrypsin-like activity [46] and altered the cleavage site usage by the proteasome. The resulting altered pool of peptides available for MHC class I binding influences positive and negative selection [47] and thereby the naive T cell repertoire. This can have tremendous consequences, as illustrated in an influenza model, showing an enhanced susceptibility to infection in β5t deficient mice [48].

Dynamics of a T cell responses

Naive $CD8^+$ T cells can become activated if they recognize the right MHC class I-peptide complex and additional co-stimulatory molecules and cytokines are provided. All cells of an organism contain MHC class I, but only antigen presenting cells (APC), *i.e.* dendritic cells, B cells and macrophages, are able to give sufficient co-stimulation and activate naive $CD8^+$ T cells. After successful recognition, the $CD8^+$ T cell begins to divide, initiating the expansion phase,

during which the naive CD8+ T cell differentiates into a heterogeneous population of effector CD8+ T cells (T_{EFF}). When infected- or tumorigenic cells display the right MHC class I-peptide complex to these CD8+ T_{EFF} cells, they will be killed [49], which in infection will generally lead to the eradication of the pathogen. After successful clearance of the pathogen, the CD8+ T_{EFF} population starts to contract because not all cells are required for memory. In this contraction phase, the far majority of the activated CD8+ T_{EFF} cells go into apoptosis, leaving 5–10% to go on to differentiate into different types of memory T cells [50]. The memory T cell population can be divided into three subsets depending on their surface markers [51, 52]; effector memory (T_{EM}), central memory (T_{CM}) and tissue-resident memory (T_{RM}). The first two subsets can be distinguished by their localization, as T_{CM} home to secondary lymphoid organs and T_{EM} circulate through non-lymphoid tissues. T_{RM} have migratory properties and are found in peripheral tissues that require expression of specific homing receptors for T cell recruitment and retention, such as the skin. It is known that particularly memory CD8+ T cells are able to recognize epitopes presented on MHC class I molecules that share sequence similarity with the epitope that initiated their activation, a phenomenon called cross-reactivity [53]. The ability of a given TCR to recognize multiple epitopes has even be described as strictly necessary [53] because if every CD8+ T cell would solely recognize one epitope, the breadth of the CD8+ T cell response needed to eradicate the pathogen would not be achieved [54].

Immunodominance hierarchy

From the pool of pathogen-derived proteasome-generated peptides, the majority will not succeed in eliciting a CD8+ response with subsequent memory formation. Even if a sufficient amount of antigen is present, the peptide survives proteases, is transported by TAP, binds to a MHC class I molecule with sufficient strength and is compatible with enough naive CD8+ T cell precursors [55], the chances to be immunogenic are small [56]. Additionally, recognition of one peptide-MHC by the corresponding TCR, does not result in the same magnitude of the CD8+ T cell expansion as recognition of another peptide-MHC class I by its corresponding TCR. There appears to be a hierarchy of specific CD8+ T cells, whereby immunodominant peptides elicit the most vigourous CD8+ T cell expansion, and subdominant peptides induce less abundant CD8+ T cell expansion [56]. How the immunodominance hierarchy is accomplished is not fully understood yet, but as shown in viral infections, several factors play a role such as relative protein abundance; differential antigen processing; efficiency of peptide binding to MHC class I molecules; affinity of TCR to peptide-MHC class I complex and differences in CD8+ T cell precursor frequencies [55, 57-62].

CD8+ T cells in infection with intracellular (myco)bacteria

While studying CD8+ T cell responses, multiple tumor- or pathogen models can be chosen. For this thesis, pathogens *Listeria monocytogenes* and *Mycobacterium tuberculosis* were used.

Listeria monocytogenes is a gram-positive, facultative intracellular bacterium with a wide host range. It is a food-borne pathogen and therefore infections usually occur in the gastrointestinal tract, where *L. monocytogenes* attaches to intestinal epithelial cells through interaction of its surface protein Internalin A (InlA) with E-cadherin [63]. Bacteria enter the blood stream, after they have successfully crossed the epithelium, and infect cells in multiple other organs. *L. monocytogenes* specifically resides in hepatocytes [64, 65] but can also replicate in splenocytes [28]. Uptake by hepatocytes is elicited through the bacterial surface protein Internalin B (InlB), which binds to the hepatocyte growth factor receptor 66. Using this mechanism, the bacteria can not only be phagocytosed by professional phagocytes, but they can also induce their phagocytosis into cells that do not usually perform this process. After successful phagocytosis, the bacteria start to secrete virulence factors like listeriolysin O (LLO) and phospholipases (PlcA and PlcB), in order to disrupt the phagosomal membrane and subsequently escape the phagosome [67-69]. The metalloprotease Mpl is responsible for activation of PlcB and for the transport of this protein across the bacterial cell wall [70]. *L. monocytogenes* is able to infect neighboring cells without being in the extracellular compartment. This is facilitated by expression of actin-assembly-inducing-protein (ActA) which causes polymerization of cellular actin monomers of the cytoskeleton of the host, and subsequent propelling of the bacteria from one cell to the next [71]. For replication, the bacteria secrete cell wall hydrolyzing proteins, such as p60 [72]. Most known epitopes are derived of LLO and p60 [73]. In *L. monocytogenes* infection, CD8+ T cells are known to eradicate the bacteria and generate long-term protective immunity [74], which makes it an ideal pathogen to study CD8+ T cell responses.

Mycobacterium tuberculosis is the causative agent for Tuberculosis (TB). The bacterium has an unusual cell wall, rich in lipids, which makes it neither gram positive nor negative. *M. tuberculosis* is an air-borne pathogen, generally infecting the mammalian respiratory system. Within the lungs the bacteria primarily infect and persist in mononuclear phagocytes, although in the infected lung, bacilli interact with various cells in a multidisciplinary way [75]. Upon phagocytosis, the bacteria need to go to the interstitium of the lung to establish an infection. This

process is supported by deliverance of virulence factors like ESAT-6 into the host [76]. Once in the interstitium, the bacteria can be taken up by migrating cells like monocytes and dendritic cells, which are the prime events in triggering the adaptive immune response [77-79]. Immune responses to *M. tuberculosis* are complex since the infection manifests as a set of lesions, such as destruction of the alveolar and endothelial wall; perivascular and -bronchial infiltration; lipid and necrotic pneumonia; fibrosis; encapsulation; cavitation and granuloma formation, that coexist in the same lung. Mice are frequently used as a model to study *M. tuberculosis* infection. In this murine model, while innate immune responses are crucial as well [75], the cellular response, in particular the $CD4^+$ T_{CM} cells, can control infection in the lungs [80]. In humans, $CD4^+$ T cells play a critical role in orchestrating the host immunity, but $CD8^+$ T cells are required as well for an optimal and protective host response against the pathogen [81-83]. It is therefore that current vaccine design against *Mycobacterium tuberculosis* aims at inducing cellular responses. *Mycobacterium bovis* bacillus Calmette-Guérin (BCG) was introduced as a vaccine in 1924 [84] and is still the only approved vaccine against tuberculosis. It helped to reduce TB associated childhood mortality, however, the vaccine fails to prevent pulmonary TB and disease transmission. Additionally, it is associated with adverse events in HIV positive or otherwise immunocompromised people [85]. Research is conducted in order to develop vaccines that could replace or boost BCG, of which several are in clinical trials.

Scope of this thesis

The research described in this thesis explores how modulation of antigen processing affects $CD8^+$ T cell responses.

In the first chapters of the thesis we aim at proving the importance of the newly discovered antigen processing route PCPS in infection. In **Chapter 2** we report a newly developed multi-level *in silico* based prediction tool that we used to identify spliced epitopes targeted by $CD8^+$ T cells in infection. The $CD8^+$ T cells found, failed to recognize the non-spliced epitope parts in context of their natural flanking sequences. This proves that spliced epitope generation creates novel epitopes and expands the peptide pool produced in infection. We continue with proteasome-mediated splicing in **Chapter 3** in which we set out to illustrate the potential of the enhancement of the peptide pool by PCPS. We show an example of $CD8^+$ T cells that are primed by the linear epitope that can be cross-reactive to spliced epitopes that share sequence similarity. This cross-reactivity may reduce the chances of successful immune evasion by pathogens.

By discovering new immunological targets, possibilities for vaccine design are generated. The described method to identify spliced epitopes generated by PCPS could provide these new immunological targets. Next to this, vaccine efficacy can be increased by immunogenicity-enhancement of weakly immunogenic vaccine-derived epitopes. We aim at illustrating strategies to identify epitopes in model vaccine-antigens, and additionally increase their immunogenicity in **Chapter 4**. By using dermal DNA tattoo immunization with a model antigen of *Mycobacterium tuberculosis,* we provide a full strategy to modulate antigen processing and thereby enhance the $CD8^+$ T cell response. In the research described in **Chapter 5** the optimized antigen is tested as a potential booster vaccine for BCG using DNA tattoo immunization in combination with BCG in a heterologous prime-boost regimen. We aim at providing a full immunological profile in order to contribute to rational vaccine design against *Mycobacterium tuberculosis*. These studies were done at the Max Planck Institute of Infection Biology in Berlin.

The results reported in this thesis about several aspects of the MHC class I antigen processing pathway, important in successful navigation of $CD8^+$ T cells for vaccine design, are discussed in **Chapter 6**.

References

1. Rappuoli, R. Bridging the knowledge gaps in vaccine design. *Nat. Biotechnol.* **25,** 1361-1366 (2007).
2. Sijts, E. J. A. M. & Kloetzel, P. -. The role of the proteasome in the generation of MHC class I ligands and immune responses. *Cellular and Molecular Life Sciences* **68,** 1491-1502 (2011).
3. Kloetzel, P. -. Antigen processing by the proteasome. *Nat. Rev. Mol. Cell Biol.* **2,** 179-187 (2001).
4. Groettrup, M., Kirk, C. J. & Basler, M. Proteasomes in immune cells: More than peptide producers? *Nat. Rev. Immunol.* **10,** 73-78 (2010).
5. Ferrell, K., Wilkinson, C. R. M., Dubiel, W. & Gordon, C. Regulatory subunit interactions of the 26S proteasome, a complex problem. *Trends Biochem. Sci.* **25,** 83-88 (2000).
6. Mishto, M. *et al*. Driving forces of proteasome-catalyzed peptide splicing in yeast and humans. *Molecular and Cellular Proteomics* **11,** 1008-1023 (2012).
7. Mishto, M. *et al*. Modeling the in Vitro 20S Proteasome Activity: The Effect of PA28-aß and of the Sequence and Length of Polypeptides on the Degradation Kinetics. *J. Mol. Biol.* **377,** 1607-1617 (2008).
8. Aki, M. *et al*. Interferon-γ induces different subunit organizations and functional diversity of proteasomes. *J. Biochem.* **115,** 257-269 (1994).
9. Textoris-Taube, K. *et al*. The N-terminal flanking region of the TRP2360-368 melanoma antigen determines proteasome activator PA28 requirement for epitope liberation. *J. Biol. Chem.* **282,** 12749-12754 (2007).
10. Sun, Y. *et al*. Expression of the proteasome activator PA28 rescues the presentation of a cytotoxic T lymphocyte epitope on melanoma cells. *Cancer Res.* **62,** 2875-2882 (2002).
11. Toes, R. E. M. *et al*. Discrete cleavage motifs of constitutive and immunoproteasomes revealed by quantitative analysis of cleavage products. *J. Exp. Med.* **194,** 1-12 (2001).

12. Tenzer, S. *et al*. Quantitative Analysis of Prion-Protein Degradation by Constitutive and Immuno-20S Proteasomes Indicates Differences Correlated with Disease Susceptibility. *J. Immunol.* **172,** 1083-1091 (2004).
13. Dalet, A., Stroobant, V., Vigneron, N. & Van Den Eynde, B. J. Differences in the production of spliced antigenic peptides by the standard proteasome and the immunoproteasome. *Eur. J. Immunol.* **41,** 39-46 (2011).
14. Vigneron, N. & Van den Eynde, B. J. Proteasome subtypes and the processing of tumor antigens: Increasing antigenic diversity. *Curr. Opin. Immunol.* **24,** 84-91 (2012).
15. Sijts, A. J. A. M. *et al*. Efficient generation of a hepatitis B virus cytotoxic T lymphocyte epitope requires the structural features of immunoproteasomes. *J. Exp. Med.* **191,** 503-513 (2000).
16. Mishto, M. *et al*. Proteasome isoforms exhibit only quantitative differences in cleavage and epitope generation. *Eur. J. Immunol.* **44,** 3508-3521 (2014).
17. Liepe, J. *et al*. Quantitative time-resolved analysis reveals intricate, differential regulation of standard- and immuno-proteasomes. *eLife 2015;4:e07545* (2015).
18. Arciniega, M., Beck, P., Lange, O. F., Groll, M. & Huber, R. Differential global structural changes in the core particle of yeast and mouse proteasome induced by ligand binding. *Proc. Natl. Acad. Sci. U. S. A.* **111,** 9479-9484 (2014).
19. Ruschak, A. M. & Kay, L. E. Proteasome allostery as a population shift between interchanging conformers. *Proc. Natl. Acad. Sci. U. S. A.* **109** (2012).
20. Ossendorp, F. *et al*. A single residue exchange within a viral CTL epitope alters proteasome-mediated degradation resulting in lack of antigen presentation. *Immunity* **5,** 115-124 (1996).
21. Sijts, A. J. A. M. *et al*. MHC class I antigen processing of an adenovirus CTL epitope is linked to the levels of immunoproteasomes in infected cells. *Journal of Immunology* **164,** 4500-4506 (2000).
22. Van Hall, T. *et al*. Differential influence on cytotoxic T lymphocyte epitope presentation by controlled expression of either proteasome immunosubunits or PA28. *J. Exp. Med.* **192,** 483-494 (2000).
23. Deol, P., Zaiss, D. M. W., Monaco, J. J. & Sijts, A. J. A. M. Rates of processing determine the immunogenicity of immunoproteasome-generated epitopes. *Journal of Immunology* **178,** 7557-7562 (2007).
24. Chen, W., Norbury, C. C., Cho, Y., Yewdell, J. W. & Bennink, J. R. Immunoproteasomes shape immunodominance hierarchies of antiviral CD8+ T cells at the levels of T cell repertoire and presentation of viral antigens. *J. Exp. Med.* **193,** 1319-1326 (2001).
25. Kincaid, E. Z. *et al*. Mice completely lacking immunoproteasomes show major changes in antigen presentation. *Nat. Immunol.* **13,** 129-135 (2012).
26. Khan, S. *et al*. Immunoproteasomes largely replace constitutive proteasomes during an antiviral and antibacterial immune response in the liver. *J. Immunol.* **167,** 6859-6868 (2001).
27. Barton, L. F., Cruz, M., Rangwala, R., Deepe Jr., G. S. & Monaco, J. J. Regulation of immunoproteasome subunit expression in vivo following pathogenic fungal infection. *J. Immunol.* **169,** 3046-3052 (2002).
28. Strehl, B. *et al*. Immunoproteasomes are essential for clearance of Listeria monocytogenes in nonlymphoid tissues but not for induction of bacteria-specific CD8+ T cells. *Journal of Immunology* **177,** 6238-6244 (2006).
29. Tu, L. *et al*. Critical role for the immunoproteasome subunit LMP7 in the resistance of mice to Toxoplasma gondii infection. *Eur. J. Immunol.* **39,** 3385-3394 (2009).
30. Rammensee, H. -. Protein surgery. *Nature* **427,** 203-204 (2004).
31. Berkers, C. R., de Jong, A., Ovaa, H. & Rodenko, B. Transpeptidation and reverse proteolysis and their consequences for immunity. *International Journal of Biochemistry and Cell Biology* **41,** 66-71 (2009).

32. Cresswell, P. Cutting and Pasting Antigenic Peptides. *Science* **304,** 525-527 (2004).
33. Ebstein, F. *et al*. Proteasomes generate spliced epitopes by two different mechanisms and as efficiently as non-spliced epitopes. *Sci. Rep.* **6,** 24032 (2016).
34. Dalet, A. *et al*. An antigenic peptide produced by reverse splicing and double asparagine deamidation. *Proc. Natl. Acad. Sci. U. S. A.* **108,** E323-E331 (2011).
35. Hanada, K. -., Yewdell, J. W. & Yang, J. C. Immune recognition of a human renal cancer antigen through post-translational protein splicing. *Nature* **427,** 252-256 (2004).
36. Michaux, A. *et al*. A spliced antigenic peptide comprising a single spliced amino acid is produced in the proteasome by reverse splicing of a longer peptide fragment followed by trimming. *Journal of Immunology* **192,** 1962-1971 (2014).
37. Warren, E. H. *et al*. An antigen produced by splicing of noncontiguous peptides in the reverse order. *Science* **313,** 1444-1447 (2006).
38. Vigneron, N. *et al*. An Antigenic Peptide Produced by Peptide Splicing in the Proteasome. *Science* **304,** 587-590 (2004).
39. Berkers, C. R. *et al*. Definition of proteasomal peptide splicing rules for high-efficiency spliced peptide presentation by MHC class I molecules. *J. Immunol.* **195,** 4085-4095 (2015).
40. Reits, E. *et al*. A major role for TPPII in trimming proteasomal degradation products for MHC class I antigen presentation. *Immunity* **20,** 495-506 (2004).
41. Princiotta, M. F. *et al*. Cells adapted to the proteasome inhibitor 4-hydroxy-5-iodo-3-nitrophenylacetyl-Leu-Leu-leucinal-vinyl sulfone require enzymatically active proteasomes for continued survival. *Proc. Natl. Acad. Sci. U. S. A.* **98,** 513-518 (2001).
42. Heemels, M. -. & Ploegh, H. Generation, translocation, and presentation of MHC class I-restricted peptides. *Annu. Rev. Biochem.* **64,** 463-491 (1995).
43. Takada, K. *et al*. TCR affinity for thymoproteasome-dependent positively selecting peptides conditions antigen responsiveness in CD8$^+$ T cells. *Nat. Immunol.* **16,** 1069-1076 (2015).
44. Sasaki, K. *et al*. Thymoproteasomes produce unique peptide motifs for positive selection of CD8$^+$ T cells. *Nat. Commun.* **6** (2015).
45. Xing, Y., Jameson, S. C. & Hogquist, K. A. Thymoproteasome subunit-ß5T generates peptide-MHC complexes specialized for positive selection. *Proc. Natl. Acad. Sci. U. S. A.* **110,** 6979-6984 (2013).
46. Murata, S. *et al*. Regulation of CD8$^+$ T cell development by thymus-specific proteasomes. *Science* **316,** 1349-1353 (2007).
47. Kincaid, E. Z., Murata, S., Tanaka, K. & Rock, K. L. Specialized proteasome subunits have an essential role in the thymic selection of CD8(+) T cells. *Nat. Immunol.* **17,** 938-945 (2016).
48. Nitta, T. *et al*. Thymoproteasome Shapes Immunocompetent Repertoire of CD8$^+$ T Cells. *Immunity* **32,** 29-40 (2010).
49. Stinchcombe, J. C. & Griffiths, G. M. Secretory mechanisms in cell-mediated cytotoxicity. *Annu. Rev. Cell Dev. Biol.* **23,** 495-517 (2007).
50. Kaech, S. M. & Wherry, E. J. Heterogeneity and Cell-Fate Decisions in Effector and Memory CD8+ T Cell Differentiation during Viral Infection. *Immunity* **27,** 393-405 (2007).
51. Obar, J. J. & Lefrançois, L. Early events governing memory CD8$^+$ T-cell differentiation. *Int. Immunol.* **22,** 619-625 (2010).
52. Sarkar, S. *et al*. Functional and genomic profiling of effector CD8 T cell subsets with distinct memory fates. *J. Exp. Med.* **205,** 625-640 (2008).
53. Sewell, A. K. Why must T cells be cross-reactive? *Nature Reviews Immunology* **12,** 669-677 (2012).
54. Mason, D. A very high level of crossreactivity is an essential feature of the T- cell receptor. *Immunol. Today* **19,** 395-404 (1998).
55. Gilchuk, P. *et al*. Discovering naturally processed antigenic determinants that confer protective T cell immunity. *J. Clin. Invest.* **123,** 1976-1987 (2013).

56. Yewdell, J. W. Confronting Complexity: Real-World Immunodominance in Antiviral CD8+ T Cell Responses. *Immunity* **25,** 533-543 (2006).
57. Chen, W., Antón, L. C., Bennink, J. R. & Yewdell, J. W. Dissecting the multifactorial causes of immunodominance in class I- restricted T cell responses to viruses. *Immunity* **12,** 83-93 (2000).
58. Chen, W., Norbury, C. C., Cho, Y., Yewdell, J. W. & Bennink, J. R. Immunoproteasomes shape immunodominance hierarchies of antiviral CD8+ T cells at the levels of T cell repertoire and presentation of viral antigens. *J. Exp. Med.* **193,** 1319-1326 (2001).
59. Crowe, S. R. *et al*. Differential antigen presentation regulates the changing patterns of CD8+ T cell immunodominance in primary and secondary influenza virus infections. *J. Exp. Med.* **198,** 399-410 (2003).
60. Choi, E. Y. *et al*. Immunodominance of H60 is caused by an abnormally high precursor T cell pool directed against its unique minor histocompatibility antigen peptide. *Immunity* **17,** 593-603 (2002).
61. Zehn, D., Lee, S. Y. & Bevan, M. J. Complete but curtailed T-cell response to very low-affinity antigen. *Nature* **458,** 211-214 (2009).
62. La Gruta, N. L. *et al*. A virus-specific CD8+ T cell immunodominance hierarchy determined by antigen dose and precursor frequencies. *Proc. Natl. Acad. Sci. U. S. A.* **103,** 994-999 (2006).
63. Gaillard, J. -., Berche, P., Frehel, C., Gouln, E. & Cossart, P. Entry of L. monocytogenes into cells is mediated by internalin, a repeat protein reminiscent of surface antigens from gram-positive cocci. *Cell* **65,** 1127-1141 (1991).
64. Gregory, S. H., Sagnimeni, A. J. & Wing, E. J. Internalin B promotes the replication of Listeria monocytogenes in mouse hepatocytes. *Infect. Immun.* **65,** 5137-5141 (1997).
65. Conlan, J. W. & North, R. J. Neutrophil-mediated dissolution of infected host cells as a defense strategy against a facultative intracellular bacterium. *J. Exp. Med.* **174,** 741-744 (1991).
66. Ireton, K. Entry of the bacterial pathogen Listeria monocytogenes into mammalian cells. *Cell. Microbiol.* **9,** 1365-1375 (2007).
67. Bielecki, J., Youngman, P., Connelly, P. & Portnoy, D. A. Bacillus subtilis expressing a haemolysin gene from Listeria monocytogenes can grow in mammalian cells. *Nature* **345,** 175-176 (1990).
68. Portnoy, D. A., Chakraborty, T., Goebel, W. & Cossart, P. Molecular determinants of Listeria monocytogenes pathogenesis. *Infect. Immun.* **60,** 1263-1267 (1992).
69. Smith, G. A. *et al*. The two distinct phospholipases C of Listeria monocytogenes have overlapping roles in escape from a vacuole and cell-to-cell spread. *Infect. Immun.* **63,** 4231-4237 (1995).
70. Forster, B. M. *et al*. The metalloprotease of Listeria monocytogenes is regulated by pH. *J. Bacteriol.* **193,** 5090-5097 (2011).
71. Welch, M. D., DePace, A. H., Verma, S., Iwamatsu, A. & Mitchison, T. J. The human Arp2/3 complex is composed of evolutionarily conserved subunits and is localized to cellular regions of dynamic actin filament assembly. *J. Cell Biol.* **138,** 375-384 (1997).
72. Kohler, S., Leimeister-Wachter, M., Chakraborty, T., Lottspeich, F. & Goebel, W. The gene coding for protein p60 of Listeria monocytogenes and its use as a specific probe for Listeria monocytogenes. *Infect. Immun.* **58,** 1943-1950 (1990).
73. Geginat, G., Schenk, S., Skoberne, M., Goebel, W. & Hof, H. A novel approach of direct ex vivo epitope mapping identifies dominant and subdominant CD4 and CD8 T cell epitopes from Listeria monocytogenes. *Journal of Immunology* **166,** 1877-1884 (2001).
74. Mcgregor, D. D., Koster, F. T. & Mackaness, G. B. Biological sciences: The short lived small lymphocyte as a mediator of cellular immunity. *Nature* **228,** 855-856 (1970).
75. Dorhoi, A. & Kaufmann, S. H. E. Pathology and immune reactivity: understanding multidimensionality in pulmonary tuberculosis. *Semin. Immunopathol.* **38**(2):153-66 (2015).

76. Simeone, R., Bottai, D. & Brosch, R. ESX/type VII secretion systems and their role in host-pathogen interaction. *Curr. Opin. Microbiol.* **12,** 4-10 (2009).
77. Wolf, A. J. *et al*. Initiation of the adaptive immune response to Mycobacterium tuberculosis depends on antigen production in the local lymph node, not the lungs. *J. Exp. Med*. **205,** 105-115 (2008).
78. Urdahl, K. B., Shafiani, S. & Ernst, J. D. Initiation and regulation of T-cell responses in tuberculosis. *Mucosal Immunol.* **4,** 288-293 (2011).
79. Park, J. S., Tamayo, M. H., Gonzalez-Juarrero, M., Orme, I. M. & Ordway, D. J. Virulent clinical isolates of Mycobacterium tuberculosis grow rapidly and induce cellular necrosis but minimal apoptosis in murine macrophages. *J. Leukocyte Biol.* **79,** 80-86 (2006).
80. Bold, T. D., Banaei, N., Wolf, A. J. & Ernst, J. D. Suboptimal activation of antigen-specific cD4+ effector cells enables persistence of M. tuberculosis in vivo. *PLoS Pathog.* **7** (2011).
81. Woodworth, J. S. M. & Behar, S. M. Mycobacterium tuberculosis-specific $CD8^+$ T cells and their role in immunity. *Crit. Rev. Immunol.* **26,** 317-352 (2006).
82. Woodworth, J. S., Wu, Y. & Behar, S. M. Mycobacterium tuberculosis-specific $CD8^+$ T cells require perforin to kill target cells and provide protection in vivo. *J. Immunol.* **181,** 8595-8603 (2008).
83. Lewinsohn, D. M., Briden, A. L., Reed, S. G., Grabstein, K. H. & Alderson, M. R. Mycobacterium tuberculosis-reactive $CD8^+$ T lymphocytes: The relative contribution of classical versus nonclassical HLA restriction. *J. Immunol.* **165,** 925-930 (2000).
84. Calmette, A. Sur la vaccination préventive des enfants nouveau-néscontre la tuberculose par le BCG. Ann Inst Pasteur, **41**:201–232 (1927).
85. Hesseling, A. C. *et al*. Disseminated bacille Calmette-Guérin disease in HIV-infected South African infants. *Bull. WHO* **87,** 505-511 (2009).
86. Klein, L., Hinterberger, M., Wirnsberger, G. & Kyewski, B. Antigen presentation in the thymus for positive selection and central tolerance induction. *Nat. Rev. Immunol.* **9,** 833-844 (2009).

1

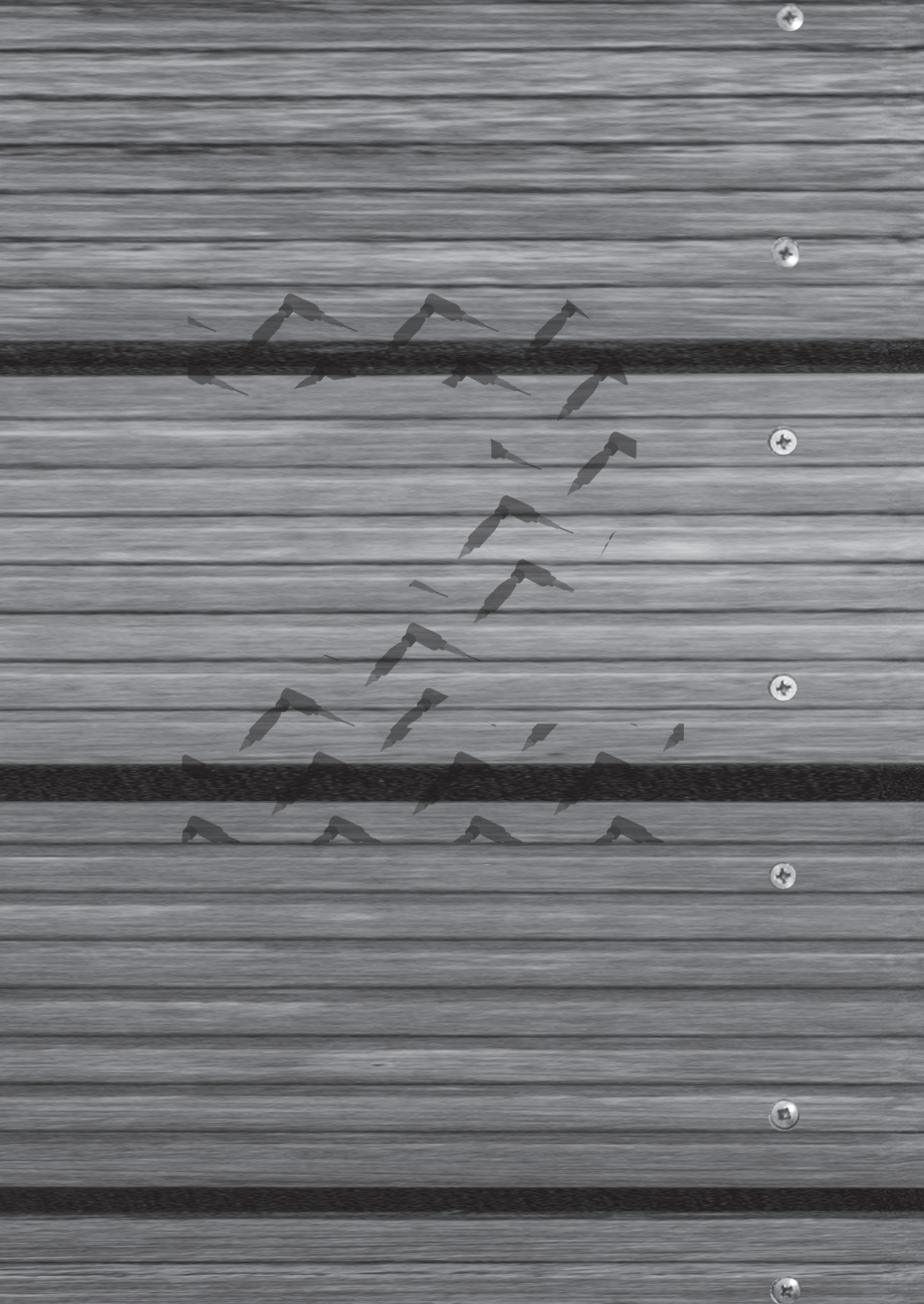

Multi-level strategy identifies spliced epitopes targeted by CD8$^+$ T cells in *Listeria monocytogenes* infection

Anouk C. M. Platteel[1,a], Juliane Liepe[2,a], Kathrin Textoris-Taube[3,4], Hanna H. Schalkwijk[1], Peter M. Kloetzel[3,4], Michele Mishto[3,4,b], and Alice J. A. M. Sijts[1,b]

[1] Division of Immunology, Faculty of Veterinary Medicine, Utrecht University, Utrecht, The Netherlands.
[2] Centre for Integrative Systems Biology and Bioinformatics, Department of Life Sciences, Imperial College London, SW7 2AZ, UK.
[3] Institut für Biochemie, Charité - Universitätsmedizin Berlin, 10117 Berlin, Germany.
[4] Berlin Institute of Health, Berlin, Germany.

[a] These authors contributed equally
[b] These authors contributed equally

In review

Abstract

Proteasome-catalyzed peptide splicing (PCPS) generates peptides that are presented by MHC I molecules but, as their identification is challenging, the immunological relevance of spliced peptides remains unclear. Here we developed a novel reverse immunology-based multi-level approach to identify proteasome-generated spliced epitopes. Applying this strategy to a murine *Listeria monocytogenes* infection model, we identified two novel spliced epitopes within the secreted bacterial phospholipase PlcB that were recognized by CD8+ T cells of *L. monocytogenes*-infected mice. While reacting to the spliced epitopes, these CD8+ T cells failed to recognize the non-spliced epitope parts in context of their natural flanking sequences. This is the first evidence that PCPS expands the CD8+ T cell response against pathogens by exposing yet undiscovered spliced epitopes on the cell surface. Moreover, the developed multi-level strategy opens new opportunities to systematically investigate proteins for spliced epitope candidates and, therewith, new possibilities for immunotherapies or vaccine design.

Introduction

CD8+ T cell responses play an important role in the clearance of intracellular pathogens and in protection to subsequent infections. CD8+ T cells react to epitopes presented by major histocompatibility complex class I (MHC I) molecules at the cell surface. Epitope generation usually starts by processing of pathogen-derived intracellular proteins by proteasomes. Peptides released by the proteasome are translocated by the transporter associated with antigen processing (TAP) into the ER, where they may undergo N-terminal trimming by ERAP [1-3] and are loaded onto MHC I molecules for presentation at the cell surface [4].

Given the central role of proteasomes in MHC I antigen processing, their catalytic activity plays a fundamental role in shaping of the pathogen-derived peptide repertoire towards which CD8+ T cells may react. The catalytic activity of proteasomes is displayed by three subunits, β1, β2 and β5, which are replaced by the induced catalytic subunits β1i/LMP2, β2i/MECL1 and β5i/LMP7 when cells are exposed to an inflammatory milieu [5]. The changes in the catalytic subunit composition induce subtle modifications in the conformation in the active sites, that affect proteasome proteolytic dynamics, with consequences for the quantities of peptides produced [6-10]. Proteasomes can simply hydrolyze the peptide-bonds of the antigen, thereby releasing canonical non-spliced peptides, or splice two distal fragments of the antigen, thereby generating peptides with a novel sequence [11]. The latter mechanism is called proteasome-catalyzed peptide splicing (PCPS) [12, 13].

Despite the well-established crucial role of proteasomes in MHC I antigen processing, the immunological relevance of PCPS is still a matter of debate, in part because only few proteasome-generated spliced epitopes, mainly derived from tumor-associated antigens [11, 14-18], have been described so far. Few recent studies however hint at a strong relevance of PCPS in the MHC I antigen presentation. It was reported that proteasome-generated spliced peptides represent one third of the self-antigenic peptides presented by MHC I molecules, as shown for different cell types, and one third of the MHC I-presented self-antigens are represented only by spliced peptides [19]. Such a significant increase in the variety of peptides potentially recognized by CD8+ T cells due to PCPS is also strengthened by their amount, which has been calculated in the order of one fourth of the MHC I-restricted self-peptides [19]. This is in agreement with the amount of tumor-associated spliced epitopes presented by human MHC I molecules at the cell

surface, that can be comparable to that of non-spliced epitopes as shown for the gp100^{mel} antigen [18].

The relevance of PCPS in the cell-mediated immune response during infections is still unknown. We recently described cross-reactivity of CD8+ T cells, primed during *L. monocytogenes* by the dominant listeriolysin O (LLO)-derived epitope $LLO_{296-304}$, towards the spliced epitope $LLO_{294/297-304}$ [20]. Nevertheless, so far, no clear evidence that PCPS triggers a specific CD8+ T cell response during infection has been found. The sparsity of knowledge on the role of PCPS in immune recognition mostly illustrates the main difficulty in the identification of immunologically relevant spliced epitopes, lying in adopting a reverse immunology approach, which would need a complex *in silico – in vitro* workflow. To propel further investigation into the role of PCPS in antigen processing, we here developed a novel multi-level spliced epitope identification strategy, which we tested in the murine *L. monocytogenes* infection model. *L. monocytogenes* is a gram positive bacterium that primarily infects phagocytes and then mobilizes the host cell cytoskeleton to spread to neighboring cells. To enter the cytosol of infected cells, the bacteria secrete LLO and the phospholipases PlcA/phosphatidylinositol-specific phospholipase C (PI-PLC) and PlcB/phosphatidylcholine-preferring phospholipase C (PC-PLC) [21-23]. Bacterial clearance during *L. monocytogenes* infection is mediated by CD8+ T cells specific for the secreted bacterial proteins. Therefore, to test and validate our novel spliced epitope identification approach, we decided to use the secreted PlcA and PlcB proteins as model antigens.

Material and methods

In silico generation of spliced peptide target list

Given the PlcA (AEO05212.1) or PlcB (AEO05216.1) sequences, we first computed all potential non-spliced and spliced peptides of length L=8 and L=9, resulting in N peptides, denoted as [n-p1]-[p2-c], where N can be obtained via equation 1 derived from [37].

$$N = \sum_{L=8}^{9} \sum_{n=1}^{S} \sum_{p1=n}^{n+L-2} \sum_{p2}^{S-L+p1-n+1} 1 \quad , \qquad \text{(equation 1)}$$

where S is the length of the parental antigen (PlcA and PlcB, respectively).This list was then reduced by excluding all spliced peptides generated through *trans* PCPS. This means that for a given spliced peptide denoted as [n-p1]-[p2-c] all peptides with p1 < p2 (for PCPS in same order as in parental antigen) or c > n

(for PCPS in reverse order compared to the parental antigen) are maintained in the reduced database). We next removed all peptides with intervening sequence length l larger than 40 amino acids, where l is defined as l = p2-p1-1 for splicing in normal order, and l = c-n-1 for splicing in reverse order. For all remaining 8 and 9mer spliced peptides we computed *in silico* the IC_{50} as a measure for binding strength to the murine H-2K^{b} or the human HLA-A*01:01, -A*02:01, -A*03:01, -B*07:02, -B*44:02, and –B*44:03 haplotypes using the offline version of the SMM algorithm [26]. We considered all spliced peptides with predicted IC_{50} < 100 nM and a further IC_{50} cut-off of 16 nM.

Peptide synthesis and 20S proteasome purification

The $PlcB_{159\text{-}171/185\text{-}196}$ (KFDTAFYKLGLAINFTAISYPPGYH) polypeptide substrate and all non-spliced and spliced peptides derive from PlcA (AEO05212.1) or PlcB (AEO05216.1) from *L. monocytogenes*. They were synthesized using Fmoc solid phase chemistry. 20S proteasomes were purified from 5 pooled spleens of C57BL/6 mice infected or uninfected by *L. monocytogenes* [20]. The purity of the proteasome preparation is shown in Fig. S7. The differences in proteasome subunit composition were disclosed elsewhere [20].

Identification and quantification of peptide products from *in vitro* digestions by proteasomes

The synthetic polypeptide $PlcB_{159\text{-}171/185\text{-}196}$ (20 µM) was digested by 2 µg 20S proteasomes in 100 µl TEAD buffer (Tris 20 mM, EDTA 1 mM, NaN_3 1 mM, DTT 1 mM, pH 7.2) over time at 37°C. The identification of the polypeptide digestion products was performed by liquid-chromatography mass spectrometry (LC-MS) analyses as following: 15µl digested samples were analysed directly by nanoscale LC-MS/MS using an Ultimate 3000 and LTQ Orbitrap XL mass spectrometer (Thermo Fisher Scientific). The system comprises a 5 mm × 300 µm, 100 Å trapping column (PepMap C18, 5 µm; Dionex) and a PicoChip analytical column (Reprosil-pur; 3 µm; New Objective). The mobile phase (A) was 0.1% (v/v) formic acid in water, and (B) was 80:20 (v/v) acetonitrile/water containing 0.1% (v/v) formic acid. The elution was carried out using a gradient 15-50% B in 35′ with a flow rate of 300 nl / min. Full MS spectra (*m/z* 300–2,000) were acquired in an Orbitrap instrument at a resolution of 60,000 (FWHM). At first, the most abundant precursor ion was selected for either data-dependent CID fragmentation with parent list (1^+, 2^+ charge state included). Fragment ions were detected in an Ion Trap instrument. Dynamic exclusion was enabled with a repeat count of 2- and 60-s exclusion duration. Additional, the theoretically calculated precursor ions of the expected spliced peptides were pre-elected for two Orbitrap CID- (*m/z* 350-2,000) and

HCD- (*m/z* 100-1500) fragmentation scans. The maximum ion accumulation time for MS scans was set to 200 ms and for MS/MS scans to 500 ms. Background ions at *m/z* 391.2843 and 445.1200 act as lock mass. Peptides were identified by PD1.4 software (Thermo Fisher Scientific) based on their merged tandem mass spectra (MS/MS) of CID and HCD. In addition for spliced peptides we compared the retention time and the merged MS/MS of CID and HCD with the fragmentation pattern of their synthetic counterparts. The database used for the LC-MS/MS analyses was generated by applying the SpliceMet's ProteaJ algorithm thereby allowing the identification of non-spliced and spliced peptides [37].

The polypeptide digestion kinetics were analysed with the ESI-ion trap instrument DECA XP MAX (ThermoFisher Scientific, USA) as previously described [37]. The quantification of peptides produced in the *in vitro* digestion kinetics was carried out by applying QME (Quantification with Minimal Effort) method to the LC-MS analyses [33]. QME estimates the absolute content of spliced and non-spliced peptide products based on their MS peak area measured in the digestion probe. The QME algorithm parameters were empirically computed in our previous study [33], and here applied.

Cell culture

RMA-S cells were cultured in IMDM (Invitrogen Life Technologies), supplemented with 10% FCS-HI (LONZA), 2 mM L-glutamine, 30 µM 2-mercaptoethanol, and penicillin/streptomycin.

MHC I - peptide stability assays

RMA-S off rate assays were performed as described [38]. In short, TAP-deficient RMA-S cells were incubated overnight in the presence or absence of 100 µM synthetic peptide, at 37 °C. Cells are harvested, washed 3 times with phosphate-buffered saline (PBS), and chased in the absence of peptide, at 37 °C for 8 hours, stained for H-2K^b class I expression with a conformation-sensitive, biotin-conjugated mouse Ab (AF6-88.5; BD Bioscience) and PE-conjugated SA (eBioscience) and analysed using FACS Canto II (BD Bioscience) and FlowJo software (Tree Star). The $t_{1/2}$ of the H-2K^b – peptide complex at the cell surface was computed as described elsewhere [39], based on the mean fluorescence levels of peptide-pulsed cells corrected for background levels from cells that were not incubated with peptide.

Mice and infection

L. monocytogenes strain 10403S was grown in brain-heart infusion medium (Sigma-Aldrich) and harvested while in log phase. Six to eight weeks old female C57BL/6 mice were purchased from Charles River. For infection, mice were inoculated intravenously in the tail vain with 2000 bacteria (0.1 LD50) in 200 µl PBS. All animal experiments were approved by the Animal Ethics Committee from Utrecht University (DEC 2014.II.11.081 and DEC 2014.II.01.003).

Intracellular IFNγ staining of $CD8^+$ T cells

Erythrocyte depleted single cell suspensions were made from the spleens and 0.5×10^6 of these splenocytes were incubated with or without 1 µg/ml synthetic peptide for 6 h in 1 ml RPMI 1640 medium supplemented with 10% FCS (Lonza), 2 mM L-glutamine, 30 µM 2-mercaptoethanol, and penicillin/streptomycin containing 50 µg/ml gentamycin (GIBCO) and 10 µM monensin (eBioscience), at 37 °C. Subsequently, cells were stained with an APC-conjugated anti-mouse CD8 antibody (53-6.7; eBioscience) in the presence of anti-mouse CD16/CD32 antibody (clone 2.4G2; made in house). Cells were fixed with 2% paraformaldehyde and then stained with PE-conjugated anti-mouse IFNγ antibody (XMG1.2; eBioscience) in the presence of 0.5% saponin and analysed on a FACS Canto II (BD Biosciences) using FlowJo software (Tree Star). Percentages of specific $IFN\gamma^+$ $CD8^+$ splenocytes were calculated by subtracting the background $IFN\gamma^+$ $CD8^+$ level of splenocytes incubated without peptide per individual mouse.

Statistical Analysis

Data were tested for normality distribution and homoscedasticity by Kolmogorov-Smirnov, Shapiro-Wilk and Levene tests and the following tests were applied accordingly. To identify significant differences between splenocytes stimulated with the synthetic peptides we applied an unpaired ANOVA test with Bonferroni Post Hoc correction for multiple comparisons and Welch's correction. To compare the frequency of $CD8^+$ T cells specific for the synthetic peptides in infected *vs* uninfected mice we applied an unpaired t-test with Welch's correction. For the correlations we applied a Spearman test. $P < 0.05$ was considered to be significant.

Results

Identification of *L. monocytogenes* derived spliced epitope candidates

$LLO_{296-304}$ and its spliced variant $LLO_{294/297-304}$ are the main, known, targets of $CD8^+$ T cells responding to *L. monocytogenes* infection in C57BL/6 mice [20, 24]. The PlcA and PlcB antigens used in this study to develop a reverse immunology-based spliced epitope prediction method lack known H-$2K^b$ presented epitopes. These proteins possess 317 residues and 292 residues, respectively. In commonly used reverse immunology approaches to identify non-spliced epitopes, the antigen sequence is first screened *in silico* for peptides predicted to bind to the MHC molecule of interest, and subsequently the predicted epitopes are investigated *in vivo*. This approach cannot be directly applied to identify spliced epitopes because all available tools/algorithms for MHC I - peptide binding predictions only test non-spliced sub-sequences of a given length for binding. To be able to identify the potential spliced epitopes, we first computed all possible 8mer and 9mer non-spliced and spliced peptides from the two antigens (Fig. 1). Here, the peptide length was restricted to reduce the number of potential epitopes since 8mer and 9mer peptides represent the large majority of the mouse MHC I ligandome. The resulting database contained in total $1.56*10^6$ sequences (Fig. 2A, B). We then reduced the number of sequences by introducing further restrictions, which were based on previous studies. In particular, among the peptide candidates we: (i) set a maximal distance of 40 residues between the two splice reactants – *i.e.* the intervening sequence and (ii) excluded spliced peptides that were generated by binding of splice-reactants derived from two distinct antigens or from two molecules of the same antigen (*i.e. trans* PCPS), as suggested by the study of Dalet and colleagues [25]. Thus, from this point onwards only *cis* spliced peptides, *i.e.* peptides generated from fragments of the same molecule, were included. This reduced database contained $4.67*10^5$ entries for potential 8-9mer spliced peptides and 1188 entries for the potential 8-9mer non-spliced peptides (Fig. 2A, B). Because we were interested in antigenic peptides efficiently presented in the H-$2K^b$ cleft we further reduced the database by selecting only those peptides that were predicted to bind H-$2K^b$ molecules with an IC_{50} < 100 nM using the algorithm SMM [26] (Fig. 1, Fig. 2C, Fig.2D). This selection step reduced the PlcA and PlcB candidate list to 989 spliced peptides and 5 non-spliced peptides. From these we selected the 22 peptides with the lowest predicted IC_{50}, *i.e.* lower than 16 nM, which were all spliced peptides (Table 1, Fig. S1, Fig. S2), for further testing in *ex vivo* $CD8^+$ T cell recognition assays (Fig. 1).

In summary, we applied several reduction steps *in silico* based on previously collected experimental evidence in order to obtain a candidate list of 22 predicted PlcA and PlcB spliced epitopes, starting from $1.56*10^6$ potential spliced peptides. This led to a progressive emergence of a peptide sequence pattern in the reduced databases, which included the known H-2K^b anchor sites [27] (Fig. 2E,F).

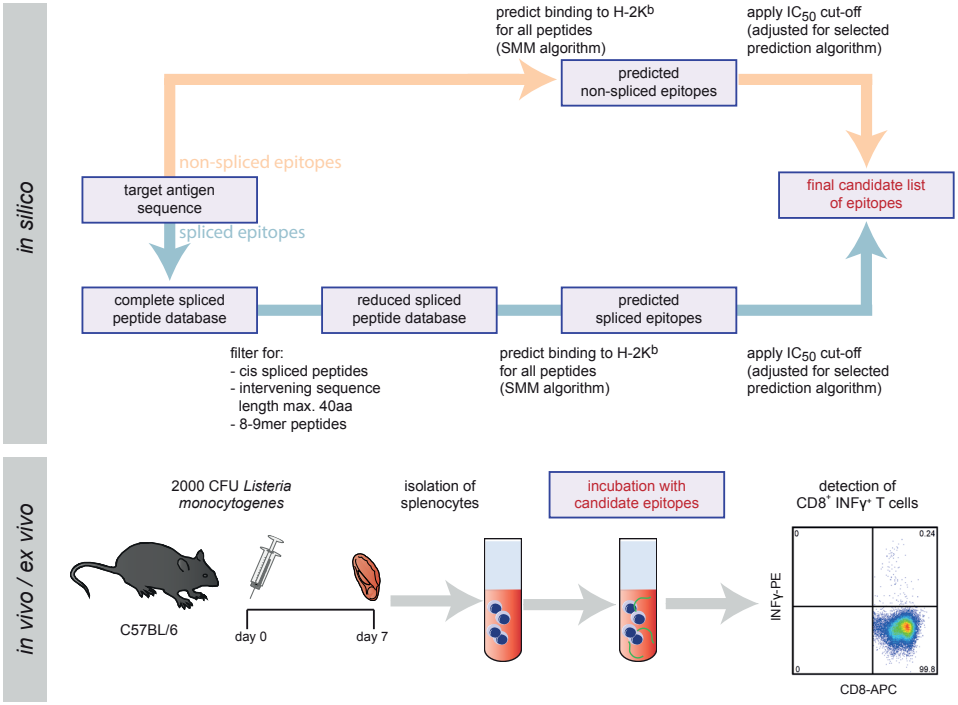

Figure 1. Reverse immunology approach to identify immunogenic spliced peptides *in vivo*. The systematic identification of immunogenic peptides requires a combined *in silico* – *in vitro* approach. Illustrated is the identification of non-spliced peptides (pink arrows) and identification of spliced peptides (blue arrows). For the latter, we first computed the complete list of theoretically possible spliced peptides from a given antigen and reduced this step-by-step to a number of spliced peptides predicted to bind to the H-2K^b molecule. The final candidate list of epitopes then was tested *ex vivo*. C57BL/6 mice were infected with *L. monocytogenes*. After 7 days the splenocytes were isolated and incubated with the spliced peptides from the final candidate list. Peptides that triggered IFNγ production in CD8$^+$ T cells *ex vivo* (*i.e.*, CD8$^+$ IFNγ$^+$ T cells) were targeted by the *L. monocytogenes*-induced CD8$^+$ T cell response *in vivo*.

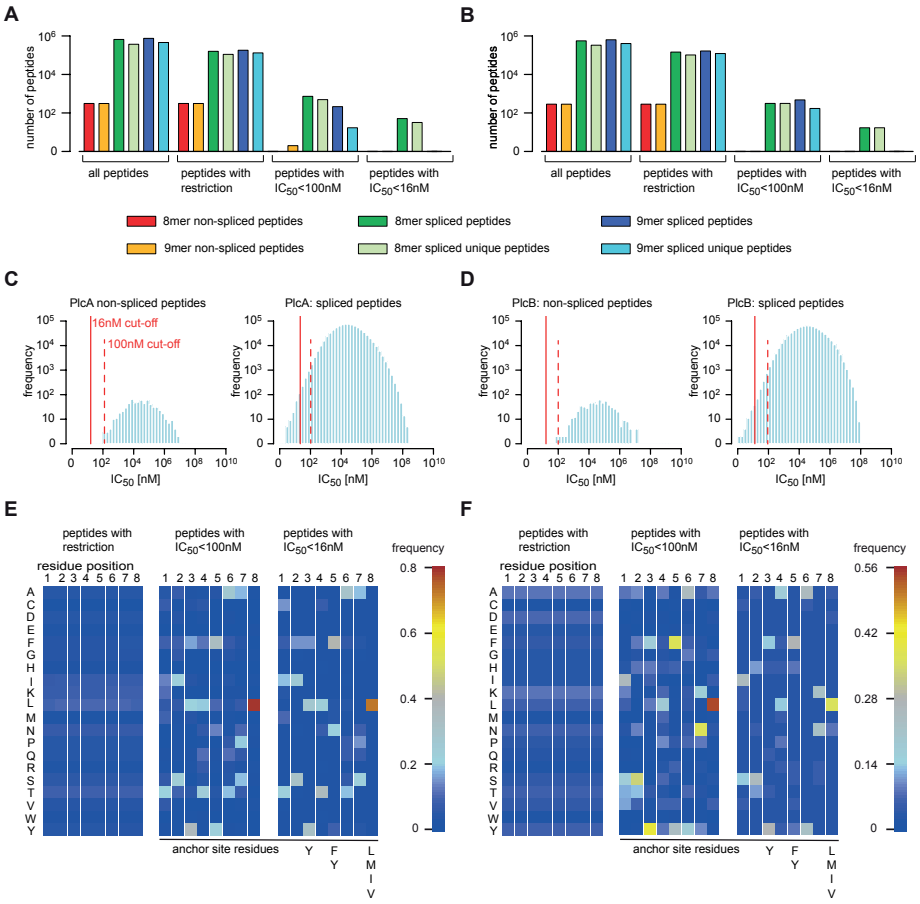

Figure 2. *In silico* identification of a spliced peptide candidate list. (A-B) All possible 8mer and 9mer non-spliced and spliced peptides were computed for (**A**) PlcA and (**B**) PlcB. Shown is the reduction of the number of potential peptides based on the spliced peptide characteristics. It is often possible to produce the same sequence through different PCPS events from the same antigen, resulting in duplicate sequences. We therefore report both, the total number of sequences and the number of unique sequences. (**C-D**) For all 8mer and 9mer non-spliced peptides and for all 8mer and 9mer *cis*-spliced peptides with a maximum intervening sequence length of 40 amino acids the IC_{50} of binding to the H-2K^b molecule was predicted, shown as histograms in (**C**) PlcA and (**D**) PlcB. The IC_{50} cut-offs are indicated as red lines. (**E-F**) The sequence profiles of 8mer spliced peptides after each reduction step are shown in (**E**) PlcA and (**F**) PlcB. The frequencies represent the marginal probability distributions for each amino acid residue in the 8mer spliced sequence. Below, the known anchor sites of the H-2K^b variants are denoted [27].

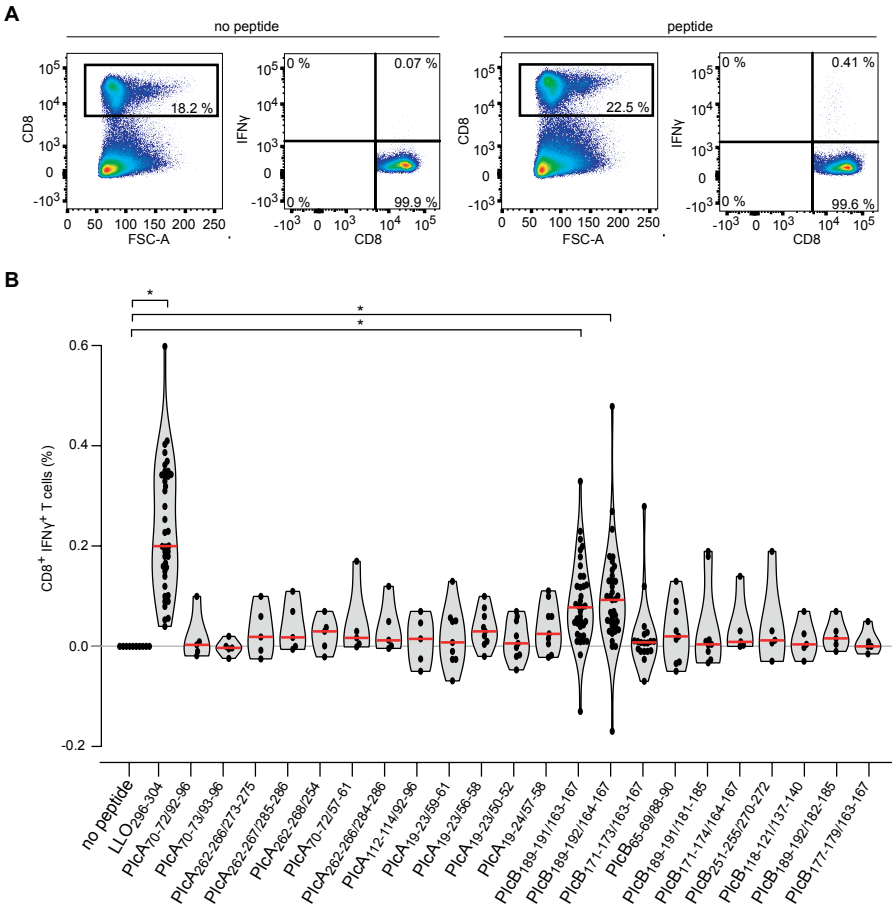

Figure 3. CD8⁺ T cells from infected mice specifically recognize PlcB spliced epitopes. (**A,B**) C57BL/6 mice were infected with *L. monocytogenes* and 7 days later the frequency of CD8⁺ T cells specific for synthetic peptides among the splenocytes of infected mice was measured *ex vivo* by intracellular staining of IFNα in CD8⁺ T cells. (**A**) Representative FACS plots of the staining in presence or absence of the target peptide $LLO_{296\text{-}304}$ is here depicted. (**B**) Frequency of IFNγ⁺ CD8⁺ T cells, upon *ex vivo* stimulation with the PlcA or PlcB spliced peptides and the non-spliced $LLO_{296\text{-}304}$ epitope, among splenocytes derived from infected mice (n = 5 - 43). Accumulated data of five independent experiments are shown, corrected for IFNγ background measured in control samples incubated without peptide. The violin plots indicate the density of the measurements on each side, with all single mice indicated as dots. Red lines indicate the median of the measurements. Significant differences between the splenocytes incubated with or without the peptides are marked as * (ANOVA with Bonferroni and Welch's corrections; $LLO_{296\text{-}304}$, $PlcB_{189\text{-}191/163\text{-}167}$ and $PlcB_{189\text{-}192/164\text{-}167}$, $p < 0.001$).

PlcB derived proteasome-generated spliced epitope specific CD8+ T cells are activated in *L. monocytogenes* infection

To test the immunogenicity of the selected antigenic spliced peptide candidates, C57BL/6 mice were infected *i.v.* with 2000 CFU *L. monocytogenes*. At the peak of the response [28], their splenocytes were isolated and the frequency of CD8+ T cells producing IFNγ upon recognition of the spliced peptides was measured *ex vivo* (Fig. 3A). A significant expansion of specific CD8+ T cells in infected mice was observed for two PlcB spliced epitopes - *i.e.* $PlcB_{189\text{-}191/163\text{-}167}$ and $PlcB_{189\text{-}192/164\text{-}167}$ - as well as for the known control epitope $LLO_{296\text{-}304}$ (Fig. 3B).

The CD8+ T cell response in *L. monocytogenes* infected mice specific for spliced epitopes could result from cross-reactivity of CD8+ T cells primed by non-spliced epitope variants, as we have recently demonstrated for the LLO antigen [20]. To address this possibility, we compared the frequency of CD8+ T cells in *L. monocytogenes* infected mouse spleen that were specific for the spliced epitopes $PlcB_{189\text{-}191/163\text{-}167}$ and $PlcB_{189\text{-}192/164\text{-}167}$, to the response elicited by the two non-spliced peptides $PlcB_{160\text{-}167}$ and $PlcB_{189\text{-}196}$, which shared part of the N- or C-terminus with the spliced epitopes. Only the spliced epitopes were specifically recognized by CD8+ T cells primed during the *L. monocytogenes* infection (Fig. 4A), thereby ruling out a possible cross-reaction of the CD8+ T cells towards non-spliced peptides derived from that antigen.

To confirm that the specific CD8+ T cell-mediated response towards the spliced epitopes in infected mice was the outcome of the infection, we compared the frequencies of spliced epitope-specific IFNγ+ CD8+ T cells amongst splenocytes of infected mice to those of uninfected mice. For both the spliced ($PlcB_{189\text{-}191/163\text{-}167}$ and $PlcB_{189\text{-}192/164\text{-}167}$) and non-spliced ($LLO_{296\text{-}304}$) epitopes we observed a significantly larger prevalence of IFNγ+ CD8+ T cells in samples from infected mice compared to those from uninfected mice (Fig. 4B). Additionally, when performing a blast search to check for non-spliced peptides with full sequence similarity with $PlcB_{189\text{-}191/163\text{-}167}$ or $PlcB_{189\text{-}192/164\text{-}167}$ in any proteome of prokaryotes or eukaryotes, no hits were found (data not shown). From these data we conclude that proteasome-generated spliced PlcB-derived epitopes participate in the priming of CD8+ T cell responses upon *L. monocytogenes* infection.

PlcB derived spliced epitopes are generated by the proteasome

All spliced epitopes described so far were produced by proteasomes and PCPS did not occur in absence of this enzyme [11, 14, 16, 18, 29]. However, as proof of principle to confirm that also the PlcB-derived spliced epitopes were generated

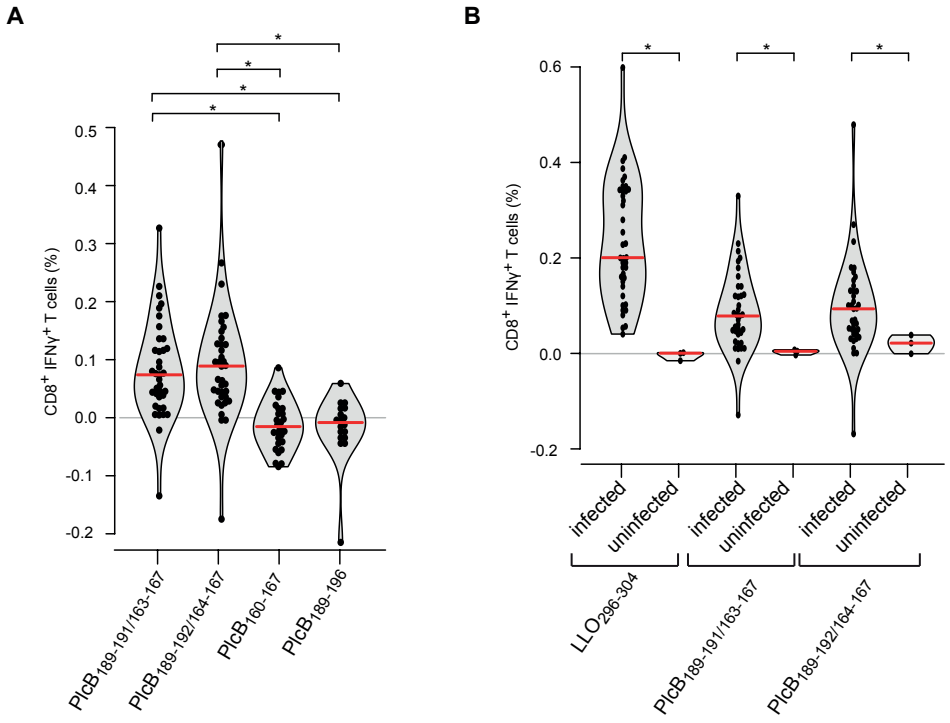

Figure 4. PlcB spliced epitope-specific CD8⁺ T cells are not cross-reactive to PlcB non-spliced peptides and are not activated in uninfected mice. (**A**) Frequency of IFNγ⁺ CD8⁺ T cells, upon *ex vivo* stimulation with the $PlcB_{189\text{-}191/163\text{-}167}$ and $PlcB_{189\text{-}192/164\text{-}167}$ spliced epitopes and the $PlcB_{160\text{-}167}$ and $PlcB_{189\text{-}196}$ non-spliced peptides, among splenocytes derived from *L. monocytogenes* infected mice (n = 18 - 37) is shown. Accumulated data of five independent experiments is shown per peptide corrected for IFNγ background level as measured in control samples that were incubated without peptide. The violin plots indicate the density of the measurements on each side, with all single mice indicated as dots. Red lines indicate the median of the measurements. Significant differences between the splenocytes incubated with spliced epitopes and non-spliced peptides are marked as * (ANOVA upon Bonferroni and Welch's corrections; $PlcB_{189\text{-}191/163\text{-}167}$ or $PlcB_{189\text{-}192/164\text{-}167}$ vs $PlcB_{160\text{-}167}$ or $PlcB_{189\text{-}196}$, $p < 0.001$). (**B**) Frequency of IFNγ⁺ CD8⁺ T cells, upon *ex vivo* stimulation with $LLO_{296\text{-}304}$, $PlcB_{189\text{-}191/163\text{-}167}$, and $PlcB_{189\text{-}192/164\text{-}167}$, among splenocytes derived from infected (n = 37 - 40) or uninfected (n = 3) mice. Accumulated data of five independent experiments is shown. Significant differences between infected and uninfected mice are marked as * (t-student with Welch's correction; $LLO_{296\text{-}304}$, and $PlcB_{189\text{-}191/163\text{-}167}$, $p < 0.001$; $PlcB_{189\text{-}192/164\text{-}167}$, $p = 0.001$).

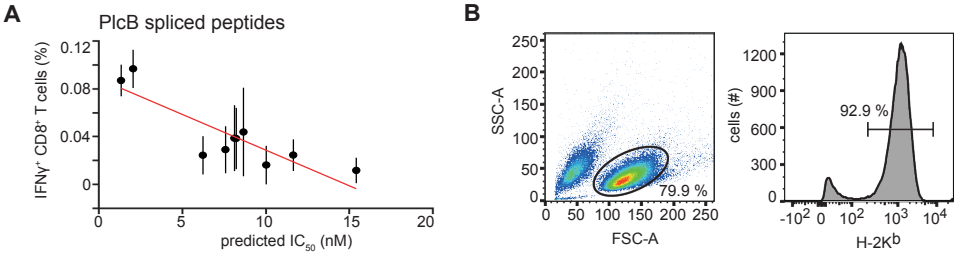
A
PlcB spliced peptides
IFNγ⁺ CD8⁺ T cells (%)
predicted IC50 (nM)
B
SSC-A
FSC-A
79.9 %
cells (#)
92.9 %
H-2Kb

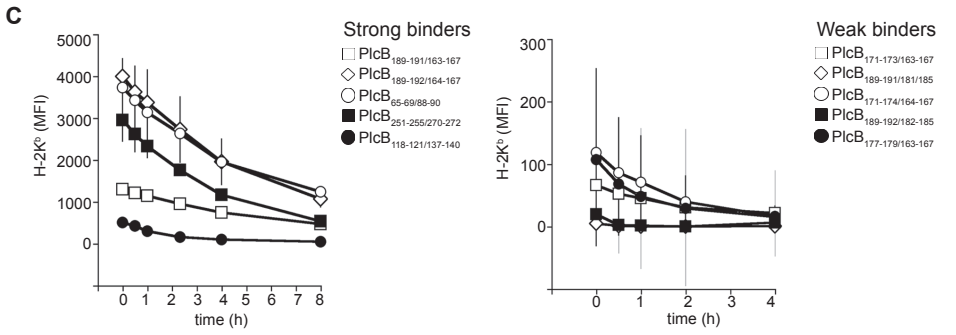
C
H-2Kb (MFI)
time (h)
Strong binders
PlcB189-191/163-167
PlcB189-192/164-167
PlcB65-69/88-90
PlcB251-255/270-272
PlcB118-121/137-140
Weak binders
PlcB171-173/163-167
PlcB189-191/181/185
PlcB171-174/164-167
PlcB189-192/182-185
PlcB177-179/163-167

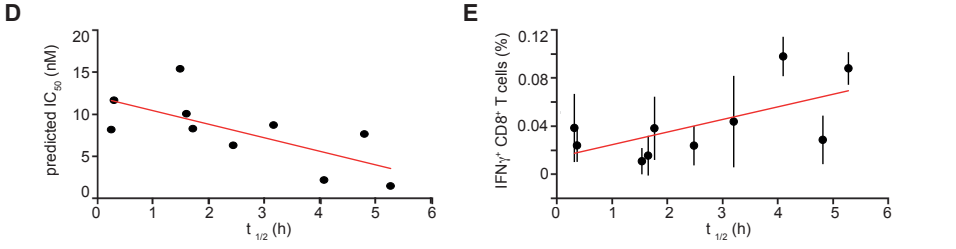
D
predicted IC50 (nM)
t 1/2 (h)
E
IFNγ⁺ CD8⁺ T cells (%)
t 1/2 (h)

Figure 5. Correlation between predicted IC_{50}, H-2K^b – peptide stability and frequency of specific CD8$^+$ T cells in infected mice. (A) Correlation between the predicted IC_{50} of PlcB spliced peptides and the frequency of IFNγ$^+$ CD8$^+$ T cells specific for the peptides among splenocytes derived from *L. monocytogenes* infected mice (for all PlcB peptides tested on 5 - 37 mice). There is a significant inverse correlation (Spearman correlation test $p < 0.001$, C value = -0.559). Values are the mean and bars the SEM of tested mice for each peptide (n = 5 - 37). IC_{50} of the peptides for the H-2K^b complex was predicted by the SMM algorithm [26]. (**B**) H-2K^b – peptide stability was measured with RMA-S cells incubated with synthetic peptides and chased in the absence of peptide. At different time points the remaining H-2K^b – peptide complexes were measured using FACS and measured in MFI (mean fluorescence index). (**C**) The stability of the H-2K^b complexes bound to each PlcB spliced peptide is shown. Peptides were divided in strong binders (with MFI > 500 at t = 0; left panel) or weak binders (with MFI < 200 at t = 0; right panel). Incubation without peptide resulted in a background MFI level of ~ 40. Values are the mean MFI ± SD of two independent experiments. (**D**) Correlation between the predicted IC_{50} of the PlcB spliced peptides (n = 10) and the H-2K^b – peptide half-life at the cells surface is shown. Values are the mean of two independent experiments. There is a significant inverse correlation (Spearman correlation test $p = 0.022$, C value = -0.709). (**E**) Correlation between the H-2K^b – peptide stability and the frequency of IFNγ$^+$ CD8$^+$ T cells responsive against the spliced peptides among splenocytes derived from infected mice (for all peptides tested on 5 - 37 mice). There is a significant correlation (Spearman correlation test $p < 0.001$, C value = 0.498). Values are the mean and bars the SEM of mice tested for each peptide (n = 5 - 37).

by the proteasome, we performed *in vitro* digestions of the synthetic substrate $PlcB_{159\text{-}171/185\text{-}196}$ with 20S proteasomes purified from spleens of *L. monocytogenes* infected or uninfected mice. The substrate sequences were derived from the original PlcB protein although part of the intervening sequence ($PlcB_{172\text{-}184}$) was removed to facilitate the *in vitro* reaction as previously demonstrated [25]. Mass spectrometry (MS) analysis of the digests demonstrated the proteasome-mediated generation of the spliced epitopes $PlcB_{189\text{-}191/163\text{-}167}$ and $PlcB_{189\text{-}192/164\text{-}167}$ (Fig. S3). By applying the quantitative method QME to samples collected at different time intervals of *in vitro* digestion of $PlcB_{159\text{-}171/185\text{-}196}$, we measured the generation kinetics of the spliced epitopes $PlcB_{189\text{-}191/163\text{-}167}$ and $PlcB_{189\text{-}192/164\text{-}167}$. No remarkable differences in generation kinetics of the two spliced epitopes were detected between reactions carried out by proteasomes purified from uninfected or infected mouse spleens. Similar results were obtained for the non-spliced peptides $PlcB_{160\text{-}167}$ and $PlcB_{189\text{-}196}$ (Fig. S4).

Table 1. Predicted spliced epitope candidates

Peptide[a]	Sequence	IC_{50} (nM)[b]	$T_{1/2}$ (h)[c]
$LLO_{296-304}$[d]	VAYGRQVYL	8	1.4 ± 0.2
$PlcA_{70-72/92-96}$	MSYLYQQL	2.5	
$PlcA_{70-73/93-96}$	MSYNYQQL	3.2	
$PlcA_{262-266/273-275}$	TSLTFAAL	3.5	
$PlcA_{262-267/285-286}$	TSLTFTNL	5.7	
$PlcA_{262-268/254}$	TSLTFTPL	6.7	
$PlcA_{70-72/57-61}$	MSYNLAAL	5.3	
$PlcA_{262-266/284-286}$	TSLTFLNL	7.3	
$PlcA_{112-114/92-96}$	KIYLYQQL	8.4	
$PlcA_{19-23/59-61}$	CFFTFAAL	3.8	
$PlcA_{19-23/56-58}$	CFFTFTNL	6.1	
$PlcA_{19-23/50-52}$	CFFTFSAL	8.7	
$PlcA_{19-24/57-58}$	CFFTFPNL	7.0	
$PlcB_{189-191/163-167}$	ISYAFYKL	1.1	5.25 ± 0.92
$PlcB_{189-192/164-167}$	ISYPFYKL	1.9	4.05 ± 1.07
$PlcB_{171-173/163-167}$	IHYAFYKL	6.1	2.39 ± 0.71
$PlcB_{65-69/88-90}$	VNTHYANL	7.5	4.78 ± 1.69
$PlcB_{189-191/181-185}$	ISYMHANN	8.0	0.17 ± 0.12
$PlcB_{171-174/164-167}$	IHYYFYKL	8.1	1.66 ± 0.63
$PlcB_{251-255/270-272}$	KSYLVARL	8.6	3.13 ± 0.56
$PlcB_{118-121/137-140}$	STFLFANA	9.9	1.54 ± 0.25
$PlcB_{189-192/182-185}$	ISYPHANN	11.6	0.22 ± 0.14
$PlcB_{177-179/163-167}$	ISQAFYKL	15.4	1.43 ± 0.73
$PlcB_{160-167}$[e]	FDTAFYKL	2949	[f]
$PlcB_{189-196}$[e]	ISYPPGYH	10840	[f]

[a] Spliced epitope candidates PlcA and PlcB antigens were predicted by applying the *in silico* computation method shown in Fig. 1.

[b] The predicted IC_{50} for binding to the H-2K^b MHC I molecule was calculated using SMM algorithm [26].

[c] The H-2K^b – peptide complex stability was empirically measured; mean half-life ($T_{½}$) and SD of two independent experiments are shown.

[d] The half-life of $LLO_{296-304}$ was in agreement with previous studies [20].

[e] The two non-spliced peptides listed here were used as negative controls, to exclude potential cross-reactivity of spliced epitope-specific CD8+ T cells.

[f] -, peptides failed to stabilize H-2K^b molecules.

Thus, we confirmed that the spliced epitopes $PlcB_{189\text{-}191/163\text{-}167}$ and $PlcB_{189\text{-}192/164\text{-}167}$ were generated by the proteasome, both early in infection when proteasome composition has not yet been changed as result of the inflammatory milieu (see results with proteasomes of uninfected mouse spleens) and in later stages of infection. The two non-spliced peptides that share sequence similarity with the spliced epitopes are also generated by the proteasome, which suggests that other factors, *e.g*. affinity for the H-2K^b molecule (see below), are responsible for the fact that they are not targeted by the *L. monocytogenes*-induced CD8$^+$ T cell response.

The measured H-2K^b-spliced peptide stability and the predicted binding affinity correlate with the relative frequency of specific CD8$^+$ T cells in infected mice

During the development of our *in silico* strategy for selecting the best peptide candidates for this study we assumed, based on earlier studies [30-32], a correlation between the predicted IC_{50} (*i.e*. H-2K^b binding affinity) and the recognition of peptides by specific CD8$^+$ T cells. Therefore we restricted the list of spliced peptides that might be recognized during *L. monocytogenes* infection by their predicted IC_{50}. The validity of this approach was evaluated on the results of the *ex vivo* stimulation of splenocytes derived from infected mice with the PlcB spliced peptides. In agreement with our assumption, we observed a significant inverse correlation between the predicted IC_{50} of the spliced peptides and the specific response (measured as frequency of IFNγ$^+$ CD8$^+$ T cells *ex vivo*) in infected mice (Fig. 5A, Table 1).

As proof of principle we experimentally measured another parameter depicting the affinity between MHC I and peptide, *i.e.* the stability of H-2K^b-peptide complexes at the cell surface of RMA-S cells (Fig. 5B). Five out of ten spliced epitope candidates tested, including $PlcB_{189\text{-}191/163\text{-}167}$ and $PlcB_{189\text{-}192/164\text{-}167}$, upregulated H-2K^b levels on RMA-S cells (Fig. 5C, left panel), indicating that these peptides bound to and stabilized RMA-S-expressed H-2K^b molecules. The other spliced epitope candidates tested (Fig 5C, right panel) as well as the non-spliced peptides $PlcB_{160\text{-}167}$ and $PlcB_{189\text{-}196}$ (data not shown), only weakly upregulated or failed to upregulate H-2K^b on RMA-S cells. This difference in peptide binding capacity was illustrated by the half-lives that we computed based on chase analyses of peptide-pulsed RMA-S cells (Table 1), which varied from 5,25 h for H-2K^b complexed with "strong" binders to 0,17 h for weak binders. Of note, the two identified spliced epitopes $PlcB_{189\text{-}191/163\text{-}167}$ and $PlcB_{189\text{-}192/164\text{-}167}$ were amongst the three highest affinity H-2K^b binders (Table 1), with computed half-lives

exceeding these of H-2K^b molecules complexed with the control epitope LLO$_{296-304}$. Comparing the data for all spliced peptides tested, we found a significant correlation between the predicted IC$_{50}$ and the measured half-lives of H-2K^b-peptide complexes at the cell surface (Fig. 5D). Accordingly, we also found a significant inverse correlation between the half-lives of H-2K^b-peptide complexes and the relative frequency of IFNγ$^+$ CD8$^+$ T cells amongst infected mouse' splenocytes for the spliced peptides derived from PlcB (Fig. 5E). Thus, selection of spliced epitope candidates based on predicted IC$_{50}$ is a valid approach to focus *ex vivo* analyses on the most promising epitope candidates.

Discussion

We here present a novel multi-level spliced epitope identification approach which will be instrumental in uncovering the role of PCPS in immune recognition, both of pathogen-derived and self-antigens. Application of this approach enabled us to gain more insight in the contribution of PCPS to MHC I antigen processing. Focusing on two *L. monocytogenes* proteins as model antigens, we show that PCPS generates novel spliced epitopes that participate in CD8$^+$ T cell priming following infection.

The method developed for this study to identify spliced epitope candidates uses an *in silico* guided-approach for the identification of spliced peptides, combined with experimental outcomes and the SMM prediction algorithm. As part of this approach, *in silico* predicted epitope candidates are selected based on their low predicted IC$_{50}$, which showed to be the right approach since we observed a correlation between predicted IC$_{50}$ (and H-2K^b – peptide complex stability) and the expansion of specific CD8$^+$ T cells during infection, in agreement with earlier published works [30-32].

The demonstration that proteasome-generated spliced epitopes trigger a specific CD8$^+$ T cell response during *L. monocytogenes* infection in mice could represent a mile stone in the investigation of T cell immunity against pathogens. The ability of PCPS to expand the epitope variety could be a key means of the immune system to tackle the high mutation frequency and therewith the escape mechanisms of some pathogens. The enormous number of potential combinations of spliced peptides derived from an antigen could also be a means for allowing the immune system to target antigens with few or none non-spliced antigenic peptides that could be effectively presented by the MHC I molecules of a person. Indeed, we have recently shown that one third of the self-antigens were represented only by spliced epitopes [19]. This might also

apply to PlcB because there are no potential non-spliced antigenic peptides with strong binding affinity for the H-2K^b complex.

Thus, the so far neglected possibilities for epitopes generated by PCPS may be a tremendous asset for vaccination approaches focusing on single pathogen-derived proteins. To illustrate this, we performed a preliminary *in silico* analysis to identify PlcA and PlcB epitope candidates for the most frequent human MHC I haplotypes (Fig. S5, S6). We calculated that the number of potential spliced peptides predicted to bind with high affinity to the most frequent HLA-A or –B variants largely exceeds that of the non-spliced peptides. Thus, no non-spliced epitope candidates with a predicted IC_{50} below 100 nM were found in PlcB or in PlcA in combination with HLA-A*01:01, -A*03:01, -B*44:02, or -B*44:03, while four and three non-spliced candidates were predicted for the PlcA antigen in combination with HLA-A*02:01 and -B*07:02, respectively. In contrast, there are hundreds of potential spliced epitopes for both antigens predicted to bind to each of the investigated MHC I haplotypes (Fig. S5, S6). Therefore, spliced peptides could be the answer to yet undiscovered immunological targets as well as a key means of the immune system to tackle pathogens.

To further facilitate studies into the contribution of PCPS to MHC I antigen processing, the here reported approach may be further optimized. Initial *in silico* selection of the spliced peptide targets could be streamlined by performing *in vitro* digestion assays with purified proteasomes. In our study the *in vitro* digestion of synthetic polypeptides confirmed to be a reliable method for the identification and characterization of immunogenic peptides in case of positive identification of the target peptides by MS/MS. However, as happened for other studies [18, 33-35], the assay can fail to identify samples that are produced and are immunogenic *in vivo*. Improvement of the MS devices would in the future allow for the reduction in the number of false negatives and would likely lead to the identification of a larger number of spliced peptides, thereby providing a more complete view of the PCPS occurrence both *in vitro* and *ex vivo*. Another way to optimize the initial *in silico* selection of the spliced peptide targets could be the development of an algorithm predicting the PCPS events, which would be an enormous asset, in particular in studies focusing on the contribution of proteasome-generated spliced peptides to the development of auto immune diseases. The first pioneering attempt in this direction done by Berkers et al. [36] was limited to a single peptide model and the HLA-A*02:01 haplotype. Other strategies should be identified and applied to expand the size and number of the datasets mandatory for the development of such a prediction algorithm.

Taken together, our newly developed multi-level strategy to systematically investigate proteins for spliced epitope candidates opens novel opportunities to unravel the so far poorly understood contribution of PCPS to immune recognition of both pathogens and self-antigens. Possibilities to predict spliced epitopes may further find its application in vaccination approaches or immunotherapies.

Acknowledgements

Support was by European Union's Seventh Framework Programme [FP7/2007-2013] - Grant No. 280873 ADITEC to A.S., Berlin Institute of Health (BIH, CRG1-TP1) and the Einstein Stiftung Berlin (A2013-174) to P.M.K. and NC3Rs through a David Sainsbury Fellowship to J.L. (NC/K001949/1). We thank P. Henklein, P.Kunert, B. Brecht-Jachan, and C. Keller (Charité Berlin) and Rebeca F. Cardoso (Utrecht University) for technical assistance.

Abbreviations

PCPS proteasome-catalyzed peptide splicing
PlcA phosphatidylinositol-specific phospholipase C (PI-PLC)
PlcB phosphatidylcholine-preferring phospholipase C (PC-PLC)

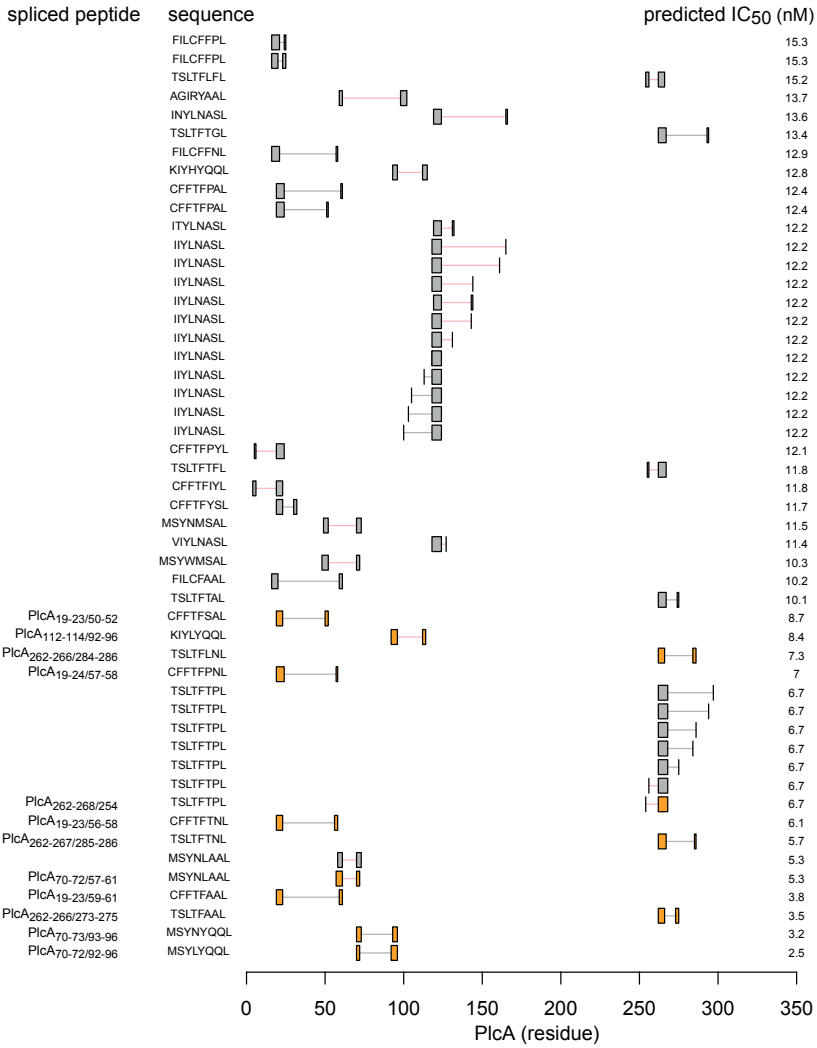

Supplementary figure 1. List and location of predicted spliced peptide candidates for the PlcA antigen. Shown are all spliced peptides derived from PlcA that passed the described reduction steps (Fig. 1) and that have a predicted IC_{50} of binding to H2-K^b molecule smaller than 16 nM. Rectangles depict the N- and C-terminal splice reactants. *Ex vivo* tested spliced peptides are marked with orange rectangles. Rectangles are located relative to the position in the parental antigen PlcA and are connected by a line; a grey line indicates PCPS in normal order (*i.e.* same order as the splice-reactants appear in the antigen), a pink line indicates PCPS in reverse order. The spliced peptides are ordered with increasing predicted IC_{50} (from bottom to top). The corresponding sequences are shown on the left; the corresponding predicted IC_{50} are shown on the right. Of note, all spliced sequences including duplicate sequences that are generated by PCPS of different splice-reactants are shown.

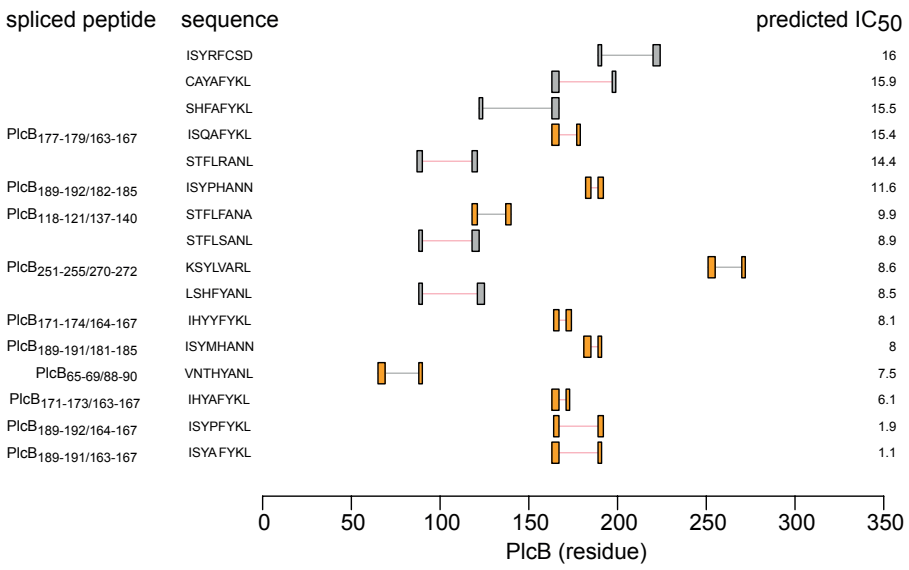

Supplementary figure 2. List and location of predicted spliced peptide candidates for the PlcB antigen. Shown are all spliced peptides derived from PlcB that passed the described reduction steps (Fig. 1) and that have a predicted IC_{50} of binding to H2-K^b molecules smaller than 16 nM. Rectangles depict the N- and C-terminal splice reactants. *Ex vivo* tested spliced peptides are marked with orange rectangles. Rectangles are located relative to the position in the parental antigen PlcB and are connected by a line; a grey line indicates PCPS in normal order (*i.e.* same order as the splice-reactants appear in the antigen), a pink line indicates PCPS in reverse order. The spliced peptides are ordered with increasing predicted IC_{50} (from bottom to top). The corresponding sequences are shown on the left; the corresponding predicted IC_{50} are shown on the right. Of note, all spliced sequences including duplicate sequences that are generated by PCPS of different splice-reactants are shown.

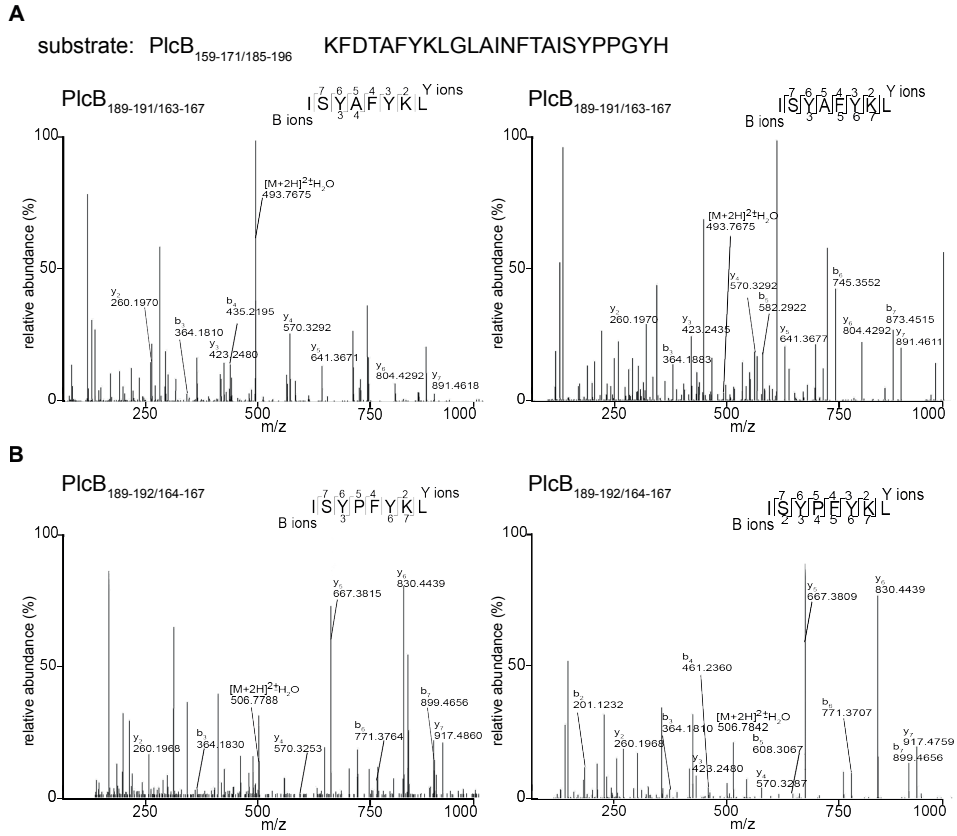

Supplementary figure 3. MS/MS of the PlcB spliced epitopes. (**A, B**) The MS/MS of the two spliced epitopes (**A**) $PlcB_{189\text{-}191/163\text{-}167}$ (*m/z* 502.7576, +2) and (**B**) $PlcB_{189\text{-}192/164\text{-}167}$ (*m/z* 515.7832, +2) are shown. In the left panel the MS/MS spectra of the peptides identified among the products of *in vitro* digestion of the synthetic substrates $PlcB_{159\text{-}171/185\text{-}196}$ by 20S proteasome purified from spleens of mice infected by *L. monocytogenes*. In the right panel the MS/MS spectra of the corresponding synthetic peptides. Detected doubly charged $[M+2H]^{2+}$-H_2O are enclosed in parenthesis. Single charged B-, Y-ions (related sequence is demonstrated in brackets) and the loss of water (-18Da, marked as -H_2O) are reported in the spectra. Spliced peptides showed similar retention times in nano-HPLC and the same fragmentation pattern in tandem mass spectra (MS/MS) of their synthetic counterparts.

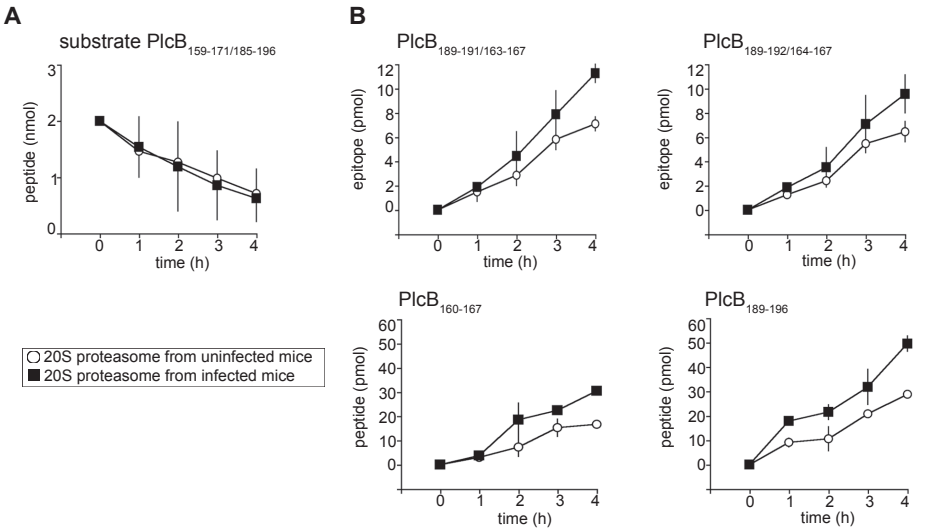

Supplementary figure 4. Quantitative kinetics of the spliced epitopes and non-spliced peptides of interest. The kinetics of (**A**) degradation of the synthetic substrate $PlcB_{159\text{-}171/185\text{-}196}$, and (**B**) generation of the spliced epitopes $PlcB_{189\text{-}191/163\text{-}167}$ and $PlcB_{189\text{-}192/164\text{-}167}$ and non-spliced peptides $PlcB_{160\text{-}167}$ and $PlcB_{189\text{-}196}$ upon proteasome–mediated processing are shown. (**A,B**) 20S proteasomes were purified from spleens of uninfected or *L. monocytogenes*-infected mice. The values are the means, and bars the SD of two independent experiments as computed by applying QME to the MS peak area.

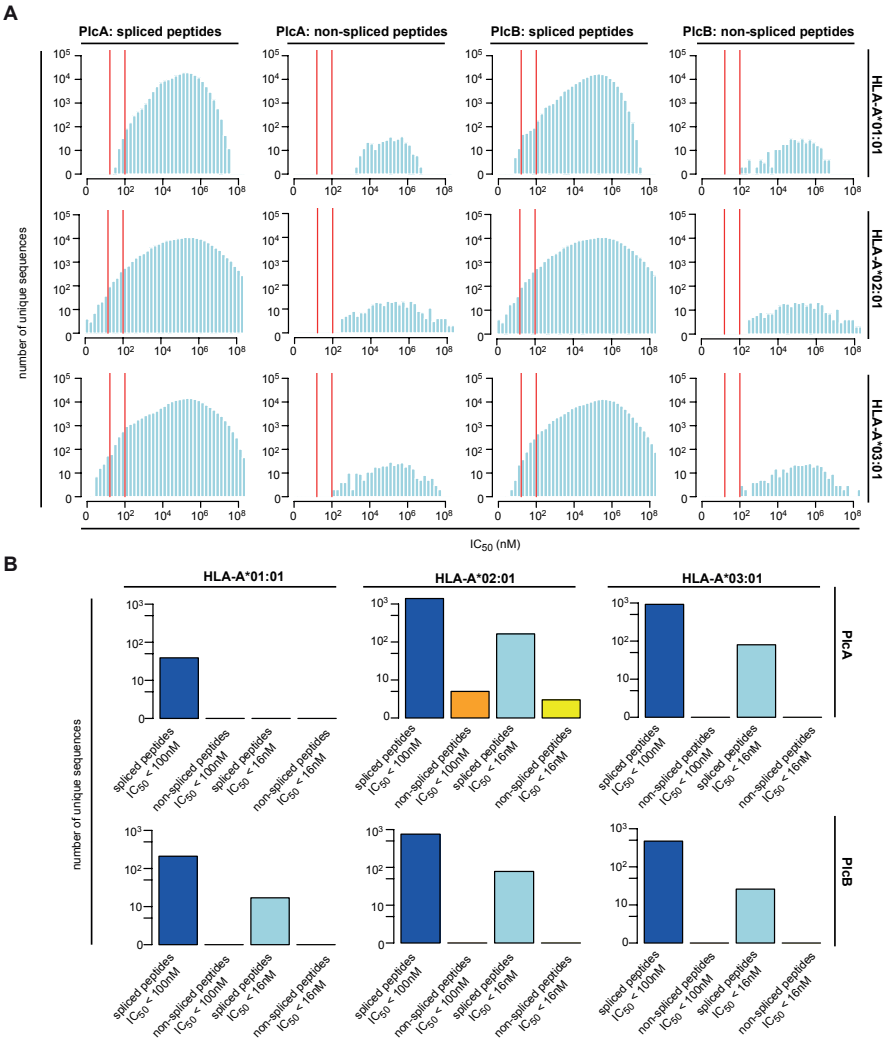

Supplementary figure 5. Prediction of PlcA and PlcB derived peptides for binding to human HLA-A haplotypes. (**A**) Shown are predicted IC_{50} distributions of spliced and non-spliced peptide candidates derived from PlcA and PlcB and selected by applying our reverse immunology approach (Fig. 1). Red lines indicate a predicted IC_{50} of 16 nM and 100 nM for some of the most frequent HLA-A haplotypes in the Caucasian population, *i.e.* HLA-A*01:01, -A*02:01, and -A*03:01. (**B**) Shown are the numbers of spliced and non-spliced peptide candidates with predicted IC_{50} smaller than 100 nM and 16 nM for the HLA-A*01:01, -A*02:01, and -A*03:01 variants.

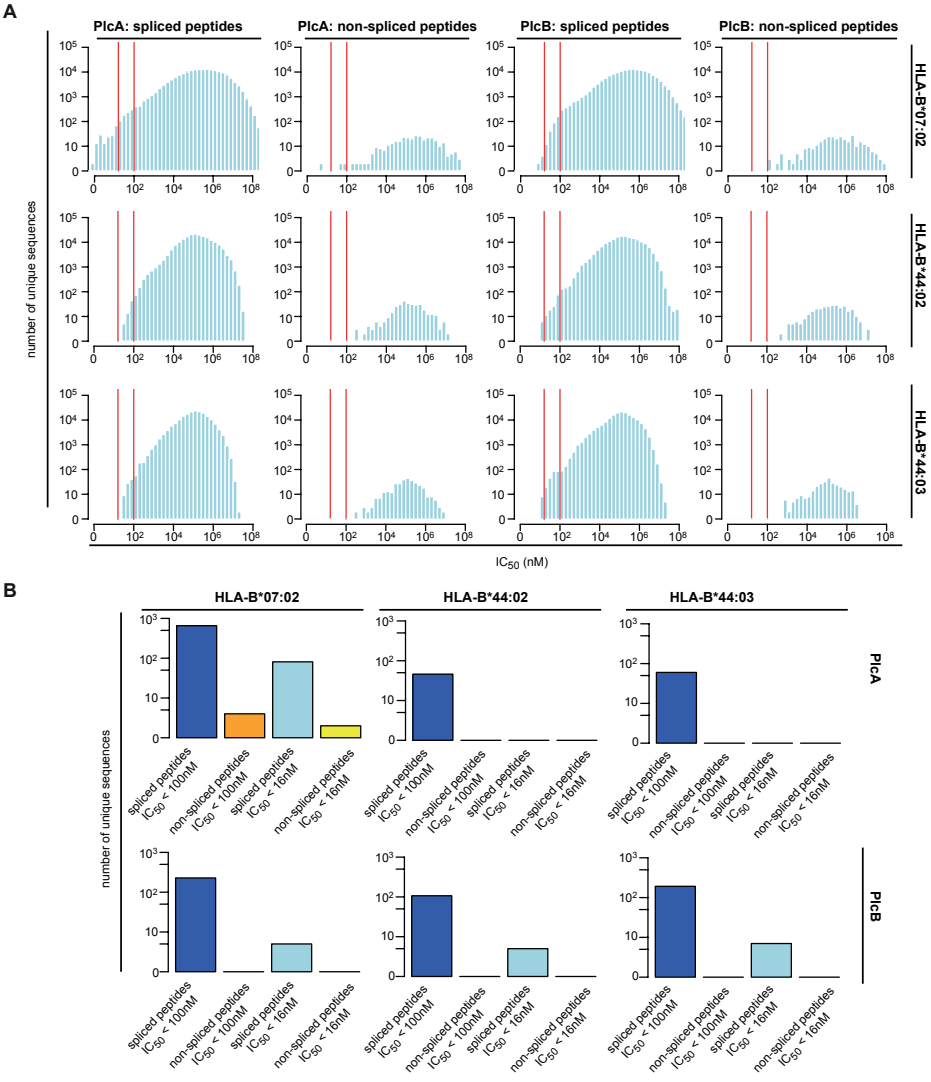

Supplementary figure 6. Prediction of PlcA and PlcB derived peptides for binding to human HLA-B haplotypes. (**A**) Shown are predicted IC_{50} distributions of spliced and non-spliced peptide candidates derived from PlcA and PlcB and selected by applying our reverse immunology approach (Fig. 1). Red lines indicate a predicted IC_{50} of 16 nM and 100 nM for some of the most frequent HLA-A haplotypes in the Caucasian population, *i.e.* HLA-B*07:02, -B*44:02, and -B*44:03. (**B**) Shown are the numbers of spliced and non-spliced peptide candidates with predicted IC_{50} smaller than 100 nM and 16 nM for HLA-B*07:02, B*44:02, B*44:03.

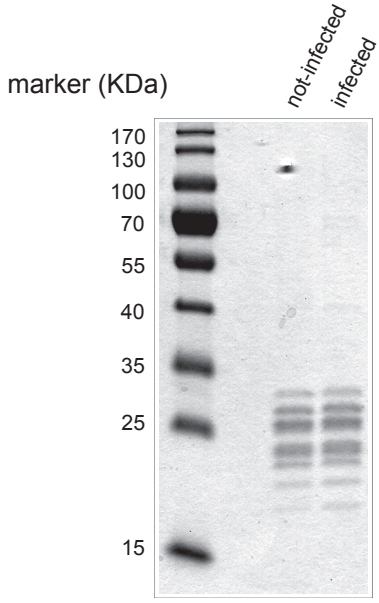

Supplementary figure 7. Purity of 20S proteasome preparation. 5 μg of 20S proteasomes purified from spleens of uninfected or *L. monocytogenes*-infected mice were stained by coomassie blue. Only the characteristic bands of the proteasome are visible, confirming the high purity of the 20S proteasome preparation.

References

1. Sijts, E. J. A. M. & Kloetzel, P. -. The role of the proteasome in the generation of MHC class I ligands and immune responses. Cellular and Molecular Life Sciences **68,** 1491-1502 (2011).
2. Cascio, P., Hilton, C., Kisselev, A. F., Rock, K. L. & Goldberg, A. L. 26S proteasomes and immunoproteasomes produce mainly N-extended versions of an antigenic peptide. EMBO J. **20,** 2357-2366 (2001).
3. Rock, K. L. et al. Inhibitors of the proteasome block the degradation of most cell proteins and the generation of peptides presented on MHC class I molecules. Cell **78,** 761-771 (1994).
4. Groettrup, M., Kirk, C. J. & Basler, M. Proteasomes in immune cells: More than peptide producers? Nat. Rev. Immunol. **10,** 73-78 (2010).
5. Aki, M. et al. Interferon-γ induces different subunit organizations and functional diversity of proteasomes. J. Biochem. **115,** 257-269 (1994).
6. Mishto, M. et al. Proteasome isoforms exhibit only quantitative differences in cleavage and epitope generation. Eur. J. Immunol. **44,** 3508-3521 (2014).
7. Liepe, J. et al. Quantitative time-resolved analysis reveals intricate, differential regulation of standard- and immuno-proteasomes. eLife 2015;4:e07545 (2015).
8. Ruschak, A. M. & Kay, L. E. Proteasome allostery as a population shift between interchanging conformers. Proc. Natl. Acad. Sci. U. S. A. **109**(50):E3454-62 (2012).
9. Arciniega, M., Beck, P., Lange, O. F., Groll, M. & Huber, R. Differential global structural changes in the core particle of yeast and mouse proteasome induced by ligand binding. Proc. Natl. Acad. Sci. U. S. A. **111,** 9479-9484 (2014).
10. Sijts, A. J. A. M. et al. Efficient generation of a hepatitis B virus cytotoxic T lymphocyte epitope requires the structural features of immunoproteasomes. J. Exp. Med. **191,** 503-513 (2000).
11. Vigneron, N. et al. An Antigenic Peptide Produced by Peptide Splicing in the Proteasome. Science **304,** 587-590 (2004).

12. Rammensee, H. -. Protein surgery. Nature **427,** 203-204 (2004).
13. Berkers, C. R., de Jong, A., Ovaa, H. & Rodenko, B. Transpeptidation and reverse proteolysis and their consequences for immunity. International Journal of Biochemistry and Cell Biology **41,** 66-71 (2009).
14. Dalet, A. et al. An antigenic peptide produced by reverse splicing and double asparagine deamidation. Proc. Natl. Acad. Sci. U. S. A. **108,** E323-E331 (2011).
15. Hanada, K. -., Yewdell, J. W. & Yang, J. C. Immune recognition of a human renal cancer antigen through post-translational protein splicing. Nature **427,** 252-256 (2004).
16. Michaux, A. et al. A spliced antigenic peptide comprising a single spliced amino acid is produced in the proteasome by reverse splicing of a longer peptide fragment followed by trimming. Journal of Immunology **192,** 1962-1971 (2014).
17. Warren, E. H. et al. An antigen produced by splicing of noncontiguous peptides in the reverse order. Science **313,** 1444-1447 (2006).
18. Ebstein, F. et al. Proteasomes generate spliced epitopes by two different mechanisms and as efficiently as non-spliced epitopes. Sci. Rep. **6,** 24032 (2016).
19. Liepe, J. et al. A large fraction of HLA class I ligands are proteasome-generated spliced peptides. Science **354,** 354-358 (2016).
20. Platteel, A. C. M. et al. CD8+ T cells of Listeria monocytogenes-infected mice recognize both linear and spliced proteasome products. Eur. J. Immunol. **46,** (5):1109-18 (2016).
21. Pamer, E. G. Immune responses to Listeria monocytogenes. Nat. Rev. Immunol. **4,** 812-823 (2004).
22. Bielecki, J., Youngman, P., Connelly, P. & Portnoy, D. A. Bacillus subtilis expressing a haemolysin gene from Listeria monocytogenes can grow in mammalian cells. Nature **345,** 175-176 (1990).
23. Portnoy, D. A., Chakraborty, T., Goebel, W. & Cossart, P. Molecular determinants of Listeria monocytogenes pathogenesis. Infect. Immun. **60,** 1263-1267 (1992).
24. Geginat, G., Schenk, S., Skoberne, M., Goebel, W. & Hof, H. A novel approach of direct ex vivo epitope mapping identifies dominant and subdominant CD4 and CD8 T cell epitopes from Listeria monocytogenes. Journal of Immunology **166,** 1877-1884 (2001).
25. Dalet, A., Vigneron, N., Stroobant, V., Hanada, K. -. & Van Den Eynde, B. J. Splicing of distant peptide fragments occurs in the proteasome by transpeptidation and produces the spliced antigenic peptide derived from fibroblast growth factor-5. Journal of Immunology **184,** 3016-3024 (2010).
26. Peters, B. & Sette, A. Integrating epitope data into the emerging web of biomedical knowledge resources. Nature Reviews Immunology **7,** 485-490 (2007).
27. Falk, K., Rötzschke, O., Stevanovic, S., Jung, G. & Rammensee, H. -. Allele-specific motifs revealed by sequencing of self-peptides eluted from MHC molecules. Nature **351,** 290-296 (1991).
28. Busch, D. H., Pilip, I. M., Vijh, S. & Pamer, E. G. Coordinate regulation of complex T cell populations responding to bacterial infection. Immunity **8,** 353-362 (1998).
29. Berkers, C. R. et al. Peptide splicing in the proteasome creates a novel type of antigen with an isopeptide linkage. J. Immunol. **195,** 4075-4084 (2015).
30. Van Der Burg, S. H., Visseren, M. J. W., Brandt, R. M. P., Kast, W. M. & Melief, C. J. M. Immunogenicity of peptides bound to MHC class I molecules depends on the MHC-peptide complex stability. J. Immunol. **156,** 3308-3314 (1996).

31. Sijts, A. J. A. M. & Pamer, E. G. Enhanced intracellular dissociation of major histocompatibility complex class I-associated peptides: A mechanism for optimizing the spectrum of cell surface-presented cytotoxic T lymphocyte epitopes. J. Exp. Med. **185**, 1403-1411 (1997).
32. Watson, A. M., Mylin, L. M., Thompson, M. M. & Schell, T. D. Modification of a tumor antigen determinant to improve peptide/MHC stability is associated with increased immunogenicity and cross-priming a larger fraction of CD8+ T cells. J. Immunol. **189**, 5549-5560 (2012).
33. Mishto, M. et al. Driving forces of proteasome-catalyzed peptide splicing in yeast and humans. Molecular and Cellular Proteomics **11**, 1008-1023 (2012).
34. Chapiro, J. et al. Destructive cleavage of antigenic peptides either by the immunoproteasome or by the standard proteasome results in differential antigen presentation. Journal of Immunology **176**, 1053-1061 (2006).
35. Platteel, A. C. M. et al. Strategies to enhance immunogenicity of cDNA vaccine encoded antigens by modulation of antigen processing. Vaccine **34**(42):5132-40 (2016).
36. Berkers, C. R. et al. Definition of proteasomal peptide splicing rules for high-efficiency spliced peptide presentation by MHC class I molecules. J. Immunol. **195**, 4085-4095 (2015).
37. Liepe, J. et al. The 20S proteasome splicing activity discovered by SpliceMet. PLoS computational biology **6**(6):e1000830 (2010).
38. Deol, P., Zaiss, D. M. W., Monaco, J. J. & Sijts, A. J. A. M. Rates of processing determine the immunogenicity of immunoproteasome-generated epitopes. Journal of Immunology **178**, 7557-7562 (2007).
39. Textoris-Taube, K. et al. The T210M substitution in the HLA-A*02:01 gp100 epitope strongly affects overall proteasomal cleavage site usage and antigen processing. J Biol Chem. **290**(51):30417-28 (2015).

2

CD8+ T CELLS OF *LISTERIA MONOCYTOGENES*-INFECTED MICE RECOGNIZE BOTH LINEAR AND SPLICED PROTEASOME PRODUCTS

3

Anouk C.M. Platteel[1], Michele Mishto[2,3], Kathrin Textoris-Taube[2], Christin Keller[2], Juliane Liepe[4], Dirk H. Busch[5], Peter M. Kloetzel[2] and Alice J.A.M. Sijts[1]

[1] Department of Infectious Diseases and Immunology, Faculty of Veterinary Medicine, Utrecht University, Utrecht, The Netherlands.
[2] Institut für Biochemie, Charité - Universitätsmedizin Berlin, Berlin, Germany.
[3] Interdepartmental Centre "Luigi Galvani" for Bioinformatics, Biophysics and Bio-complexity (CIG), Alma Mater Studiorum, University of Bologna, Bologna, Italy.
[4] Centre for Integrative Systems Biology and Bioinformatics, Department of Life Sciences, Imperial College London, London, UK.
[5] Institute for Medical Microbiology, Immunology and Hygiene, TU Munich, Munich, Germany.

European Journal of Immunology
2016, May;46(5):1109-18

Graphical abstract

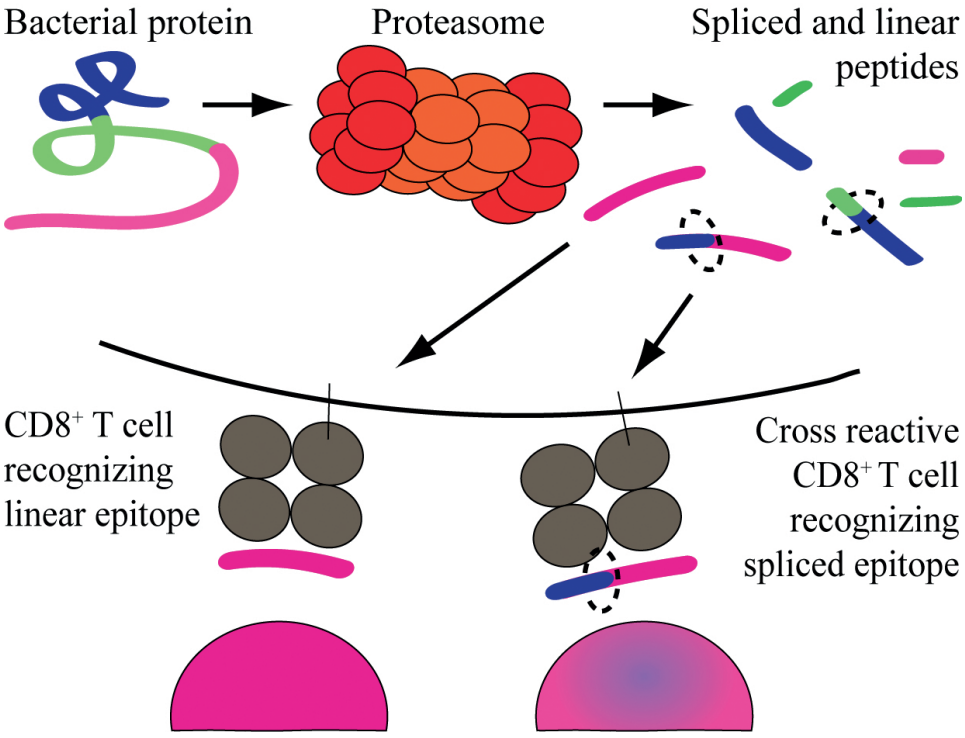

3

Abstract

CD8+ T cells responding to infection recognize pathogen-derived epitopes presented by MHC class I molecules. While most of such epitopes are generated by proteasome-mediated antigen cleavage, analysis of tumor antigen processing has revealed that epitopes may also derive from proteasome-catalyzed peptide splicing (PCPS). To determine whether PCPS contributes to epitope processing during infection, we analyzed the fragments produced by purified proteasomes from a *Listeria monocytogenes* polypeptide. Mass spectrometry identified a known H-2K^b–presented linear epitope ($LLO_{296-304}$) in the digests, as well as four spliced peptides that were trimmed by ERAP into peptides with *in silico* predicted H-2K^b binding affinity. These spliced peptides, which displayed sequence similarity with $LLO_{296-304}$, bound to H-2K^b molecules in cellular assays and one of the peptides was recognized by CD8+ T cells of infected mice. This spliced epitope differed by one amino acid from $LLO_{296-304}$ and double staining with $LLO_{296-304}$- and spliced peptide-folded MHC multimers showed that $LLO_{296-304}$ and its spliced variant were recognized by the same CD8+ T cells. Thus, PCPS multiplies the variety of peptides that is processed from an antigen and leads to the production of epitope variants that can be recognized by cross-reacting pathogen-specific CD8+ T cells. Such mechanism may reduce the chances for pathogen immune evasion.

Introduction

$CD8^+$ T cells recognize antigenic peptides that are presented by MHC class I molecules on the cell surface. These epitopes mainly derive from proteasome-mediated processing of intracellular proteins, which produces both final sized epitopes and N-terminally extended epitope precursor fragments that are trimmed to final size by cytosolic or ER-localized amino- and endopeptidases [1, 2]. Epitopes or their precursors are translocated into the ER by TAP and there are loaded into the antigen binding cleft of MHC class I molecules [3].

Although proteasomes are present in all eukaryotic cells, their subunit composition may vary. Proteasomes consist of four stacked rings, formed of seven subunits each. The two inner rings are composed of β-subunits, of which the three subunits β1, β2 and β5 are constitutively expressed and display catalytic activity. Exposure of cells to inflammatory cytokines, such as IFNγ, induces the expression of the facultative subunits β1i/LMP2, β2i/MECL-1 and β5i/LMP7 that are preferentially incorporated by newly assembled proteasome complexes, leading to the formation of immunoproteasomes [4]. Cells of the immune system express different combinations of the facultative subunits in a constitutive manner.

Proteasomes generate epitopes by simple peptide-bond cleavage as well as by proteasome-catalyzed peptide splicing (PCPS), which involves the linkage of fragments originally distant in the parental protein [5-9]. Cleavage by the proteasome is the result of a nucleophilic attack on peptide bonds by the catalytic threonines of the β1, β2 and β5 subunits in constitutive proteasomes, or of the β1i, β2i and β5i subunits in immunoproteasomes. This attack results in the formation of an acyl-enzyme intermediate. These peptides are released from the proteasome by rapid hydrolysis, giving rise to linear proteasome-generated products. However, when the acyl-enzyme intermediate is stabilized at the active site for an extended time span, the N-termini of released peptide fragments may outcompete hydrolysis and make a nucleophilic attack on the ester bond of the acyl-enzyme intermediate, forming a new peptide bond and producing a proteasome-catalysed spliced product [10]. Quantitative differences in catalytic activity between proteasome isoforms have been shown to strongly affect antigen presentation of both linear- and spliced epitopes [10-18].

One theoretical outcome of PCPS is to enhance the variety of antigenic epitopes that is presented during infection, which would have implications for the ability

of our immune system to tackle pathogens [19, 20]. While PCPS has been proven to generate MHC class I-presented tumor epitopes [5-7, 9, 12], its relevance in immunity is still controversial and no evidence for its involvement in pathogen-specific immune responses has been found so far. In this study, applying a SpliceMet-facilitated reverse immunology approach [21], we identified both spliced and linear H-2K^b-presented epitopes generated by mouse proteasomes from a *Listeria monocytogenes*-derived model antigen, Listeriolysin O $(LLO)_{291-317}$. Our studies show that PCPS broadens the peptide repertoire derived from a single antigen.

Materials and methods

Peptides and peptide synthesis.

The *Listeria monocytogenes* Listeriolysin O polypeptide $LLO_{291-317}$ (AYISSVAYGRQVYLKLSTNSHSTKVKA) and epitope candidates derived from this sequence were synthesized using Fmoc solid phase chemistry as previously described [22]. The purity of synthetic peptides was tested by amino acid analysis [10].

20S proteasome purification

20S proteasomes were purified from spleens of: (i) control or *Listeria monocytogenes*-infected C57BL/6 mice kept in animal facilities of the Utrecht University and used at 8 weeks of age (Fig. 2C); (ii) wild type or β1i (N2 C57BL/6x129SvJ) [23] or β5i (N6 C57BL/6) [24] gene-targeted C57BL/6 mice, which had been kept in animal facilities of the Charité and were used at 8 weeks of age (Fig. 2D). To purify the 20S proteasome we modified the earlier described protocol [25] as follows: mouse spleens were homogenized and centrifuged, the supernatant was fractionated by ammonium sulphate precipitation, chromatography on DEAE-Sephacel, 10-40 % sucrose gradient and anion exchange chromatography on Mono Q. In each step the fractions were monitored by degradation assays of standard short fluorogenic peptides. Proteasome concentration was measured by Bradford staining and verified by coomassie staining in a SDS-Page gel as previously shown [26]. Spleens from 5 mice were pooled prior to proteasome purification. The purity of these proteasome preparations has been shown elsewhere [21].

In vitro digestion of synthetic polypeptide by proteasomes and peptide quantification by QME

The synthetic $LLO_{291-317}$ polypeptide (20 µM) was digested with 2 µg 20S proteasomes in 100 µl TEAD buffer (Tris 20 mM, EDTA 1 mM, NaN_3 1 mM, DTT 1

mM, pH 7.2) for the time intervals specified in the figure legends, at 37°C. Liquid-chromatography mass spectrometry analyses of polypeptide digestion products were performed as previously described [21] with the ESI-ion trap instrument DECA XP MAX (ThermoFisher Scientific, USA). Database searching was performed using the SpliceMet's ProteaJ algorithm [21]. Quantification of proteasome-generated linear and spliced peptides was carried out by applying the QME method to the liquid-chromatography-mass-spectrometry analyses as previously described [10].

ERAP1-mediated N-terminal trimming of the epitope precursors and product identification

In vitro digestion of the spliced peptides $LLO_{291\text{-}298/300\text{-}304}$, $LLO_{291\text{-}300/302\text{-}304}$, $LLO_{291\text{-}294/297\text{-}304}$ and $LLO_{291\text{-}298/291\text{-}293}$ by recombinant ERAP1 was carried out as described elsewhere [27]. Briefly, 50 µM peptide was digested *in vitro* by 3 ng recombinant ERAP 1 (R&D systems) in 20 µl buffer (25 mM Tris pH 7.5, 150 mM NaCl, 0,5 µg/ml albumin) at 37°C. Reactions were stopped by addition of 0.5% TFA after 4 hours. As a control, to test whether observed trimming was mediated by ERAP1, 3 ng ERAP1 was incubated with 30 µM leucinethiol [28] at room temperature for 20 min and then used in the *in vitro* experiments as described above. No production of trimmed peptides was observed (data not shown) thereby confirming the specific trimming by recombinant ERAP1.

For identification of the trimming products, 10 µl samples of ERAP1-mediated digestion were analyzed directly by nanoscale LC-MS/MS using an Ultimate 3000 and LTQ Orbitrap XL mass spectrometer (both Thermo Fisher Scientific). The system comprises a 5 mm × 300 µm, 100 Å trapping column (PepMap C18, 5 µm; Dionex) and a PicoChip analytical column (Reprosil-pur, 3 µm; New Objective). The mobile phase (A) was 0.1% (v/v) formic acid in water, and (B) was 80:20 (v/v) acetonitrile/water containing 0.1% (v/v) formic acid. The elution was carried out using a gradient 15-50% B in 34′ with a flow rate of 300 nl / min. Full MS spectra (*m/z* 200–2000) were acquired in an Orbitrap instrument at a resolution of 60000 (FWHM). The 10 most abundant precursor ions were selected for either data-dependent CID fragmentation (TOP10) with parent list (1+ charge state included). Fragment ions were detected in an ion trap instrument. Dynamic exclusion was enabled with a repeat count of 1- and 60-s exclusion duration. The maximum ion accumulation time for MS scans was set to 200 ms and for MS/MS scans to 500 ms. Background ions at *m/z* 391.2843 and 445.1200 act as lock mass. Trimmed products were identified by comparing retention time and tandem mass spectra (MS/MS) of their synthetic counterparts (Supporting Information Fig.1).

Western blot

Protein homogenates were extracted from one spleen or liver of uninfected or infected mice, three days after administration of *Listeria monocytogenes* as previously described [29]. Proteasome subunits were revealed by Western blot assays as follows: 20 µg protein homogenates were separated in a 12.5% polyacrilamide SDS gel and transferred on a polyvinylidene difluoride filter (Immobilon-P Transfer Membrane, Millipore). Unspecific sites on the membrane were blocked for 1 h in a 5% non-fat dry milk (AppliChem) - PBS solution. Mouse proteasome subunits were detected by staining the membrane overnight at 4°C with the following primary antibodies: anti-β1 (1:10000; custom), anti-β2 (1:1000; Enzo Life Science), anti-β5 (1:1000; Abcam), anti-β1i (1:10000; Thermo Fisher Scientific), anti-β2i (1:2000; custom) and anti-β5i (1:1000; Thermo Fisher Scientific). As secondary anti-mouse or anti-rabbit HRP-conjugated Ab (1:5000; Calbiochem) was used for 2 h at room temperature followed by ECL detection (Amersham).

Cell culture

RMA-S cells were cultured in IMDM (Invitrogen Life Technologies), supplemented with 10% FBS (LONZA), 2 mM L-glutamine, 30 µM 2-mercaptoethanol, and penicillin/streptomycin.

MHC class I stability assays

RMA-S off rate assays were performed in serum-free medium as described [30]. In short, RMA-S cells were incubated overnight in the presence or absence of 100 µM synthetic peptide, at 37 °C. The next day, cells were harvested, washed 3 times with PBS, and chased in the absence of peptide, at 37 °C. Samples of the cells were taken at t: 0, 0.5, 1 and 2 hours, stained for H-2K^b class I expression with a conformation-sensitive, biotin-conjugated mouse antibody (AF6-88.5; BD Bioscience) and PE-conjugated streptavidin (eBioscience). FACS Canto II (BD Bioscience) and FlowJo software (Tree Star) were used for the analysis.

Mice and infection

Listeria monocytogenes strain 10403S was grown in brain-heart infusion medium (Sigma-Aldrich) and harvested while in log phase. Six to eight weeks old female C57BL/6 J mice were purchased from Charles River. For primary infection, mice were inoculated intravenously in the tail vain with 2000 bacteria in 200 µl PBS. Re-infection was performed 21 days later with 2x10^5 CFU. All *in vivo* animal experiments were approved by the Animal Ethics Committee of Utrecht University (DEC 2014.II.11.081 and DEC 2014.II.01.003).

Analysis of specific CD8+ T cell responses

Intracellular cytokine staining

2.5 x 10^6 erythrocyte depleted splenocytes were incubated with or without 1 µg/ml synthetic peptide for 6 h in 1 ml RPMI Medium 1640 (Life Technologies) containing 50 µg/ml gentamycin (GIBCO) and 10 µM monensin (eBioscience), at 37 °C. Subsequently, cells were stained with an APC-conjugated anti-mouse CD8 antibody (53-6.7; eBioscience) in the presence of anti-mouse CD16/CD32 (clone 2.4G2). Cells were fixed with 2% paraformaldehyde and then stained with PE-conjugated anti-mouse IFNγ mAb (XMG1.2; eBioscience) in the presence of 0.5% saponin and analyzed on a FACS Canto II (BD Biosciences) using FlowJo software (Tree Star).

Multimer staining

PE or APC labelled MHC class I multimers were prepared by refolding H-2K^b heavy chains and murine β2m in the presence of synthetic *Listeria monocytogenes*-derived $LLO_{296-304}$ or $LLO_{294/297-304}$. Splenocytes were incubated with either one or both tetramers simultaneously for 20 minutes at 4 °C. Cells were washed, cell surface stained with a V500 conjugated anti-mouse CD8 antibody (53 - 6.7; eBioscience) and analyzed on a FACS Canto II (BD Biosciences) using FlowJo software (Tree Star).

Statistical Analysis

Data was tested for normality by Levene's test and for homoscedasticity by Shapiro-Wilk's test. Independent *in vitro* experiments were performed with different proteasome preparations, therefore the SD also represents variability between different proteasome preparations. To compare responses to different peptides within infected mice a paired One-way ANOVA followed by Dunnet's post hoc test was used. Independent student t-test was used to compare differences between infected and non-infected mice. P values < 0.05 were considered significant.

Results

Digestion of $LLO_{291-317}$ by purified proteasomes produces $LLO_{296-304}$ and spliced epitope variants

In previous *in vitro* studies, digestion of polypeptide substrates by purified 20S proteasomes was shown to lead to the production of both linear- and spliced peptide products [10, 21, 27]. To determine whether PCPS contributes to proteasome-

mediated production of MHC class I-presented antigenic peptides, we analyzed the products generated by mouse 20S proteasomes from the polypeptide $LLO_{291-317}$ by mass spectrometry [10] and evaluated them for their MHC class I binding affinity using the online available NetMHC3.4/ANN prediction software. As expected, this approach identified $LLO_{296-304}$, a well-known H-2K^b-presented epitope [31] (Table 1). By applying the mass spectrometry-based method (SpliceMet) [21] we further identified four putative epitope precursors in the *in vitro* digests that were generated by PCPS (Table 1), hereby confirming our previous identifications obtained with 20S human and yeast proteasomes [10]. From these precursors, six spliced peptides (Fig. 1), with *in silico* predicted binding affinity for H-2K^b, were generated by N-terminal trimming with recombinant ERAP1 *in vitro* (Fig. 2A and Supporting Information Fig.1). The predicted IC50 values showed that two of these spliced peptides might bind the MHC class I H-2K^b with similar affinity as $LLO_{296-304,}$ while the other four spliced peptides were predicted to bind the H-2K^b complex with an IC50 > 100 nM (Table 1).

$LLO_{291-317}$-derived spliced peptide products are produced by different proteasome types

Listeria monocytogenes infection evokes vigorous innate immune responses, leading to the release of large quantities of pro-inflammatory cytokines and, consequently, to different degrees of modification of proteasome subunit composition in the infected tissues, in favor of larger contents of immunoproteasomes. Because such differences in proteasome subunit composition may strongly affect the generation of linear epitopes [30, 32-36], we determined whether the increased expression of immunosubunits in spleens of mice infected by *Listeria monocytogenes* (Fig 2B) affected the *in vitro* generation kinetics of the spliced peptides / putative epitope precursors, derived from the polypeptide $LLO_{291-317}$. The quantitative method QME was applied, which estimates the absolute content of spliced and linear peptide products based on their mass spectrometry ion strength measured in the digestion probe, as used before [10, 15, 27]. As shown in Fig 2C, 20S proteasomes derived from spleens of *Listeria monocytogenes* infected or from uninfected control mice produced similar amounts of the four spliced peptides, and only a marginal alteration in frequency of cleavages along the polypeptide was observed (data not shown). Thus, the increased immunosubunit content in infected mouse spleens compared to regular spleen tissue (Fig. 2B) did not lead to a change in quantities of spliced peptides generated. These observations can be explained by the fact that for example dendritic cells, macrophages and B cells in the spleen constitutively express large amounts of proteasomes

Table 1. $LLO_{291-317}$ - derived spliced epitope candidates.

Potential epitope[a]	Sequence	Predicted IC50 (nM)[b]	$t_{1/2}$ (min)[c]	Peptide identified *in vitro*[d]	Sequence
$LLO_{296-304}$	[VAYGRQVYL]	8	120	$LLO_{296-304}$	[VAYGRQVYL]
$LLO_{294/297-304}$	[S][AYGRQVYL]	10	35	$LLO_{291-294/297-304}$	[AYIS][AYGRQVYL]
$LLO_{294-298/291-293}$	[SSVAY][AYI]	4	62	$LLO_{291-298/291-293}$	[AYISSVAY][AYI]
$LLO_{293-298/291-293}$	[ISSVAY][AYI]	117	55		
$LLO_{296-298/300-304}$	[VAY][RQVYL]	169	22	$LLO_{291-298/300-304}$	[AYISSVAY][RQVYL]
$LLO_{295-298/300-304}$	[SVAY][RQVYL]	169	20		
$LLO_{296-300/302-304}$	[VAYGR][VYL]	197	14	$LLO_{291-300/302-304}$	[AYISSVAYGR][VYL]

[a] epitope candidates, identified by in silico analysis of proteasome-generated peptides products for MHC class I binding affinity.

[b] NetMHC 3.4/ANN predicted H-2K[b] binding affinities (IC50). Only peptides with predicted IC50 smaller than 500 nM were included in this study [47].

[c] half live of H-2K[b]-peptide complexes on the cell surface of RMA-S cells, calculated from Fig. 3B.

[d] linear and spliced peptides identified by SpliceMet 21 in 20S proteasome digests of the synthetic substrate $LLO_{291-317}$.

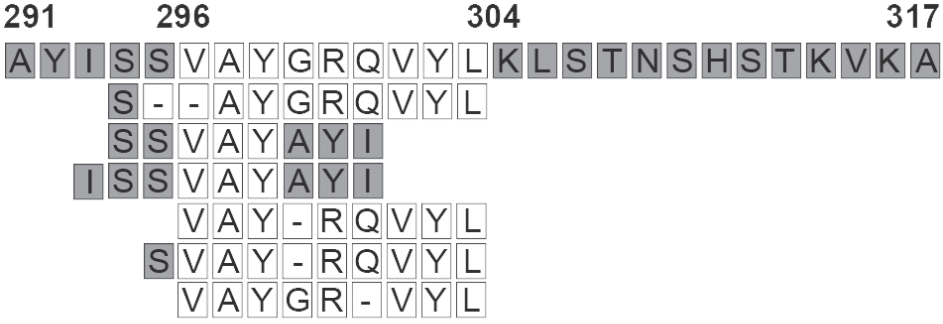

Figure 1. Overview of the different peptides derived by PCPS from $LLO_{291-317}$ and used in this study. All common residues between spliced antigenic peptides and the linear epitope $LLO_{296-304}$ (VAYGRQVYL) are depicted in white whereas the amino acids that originate from flanking residues are grey. Dashes indicate that the original residues are not present in the spliced peptides.

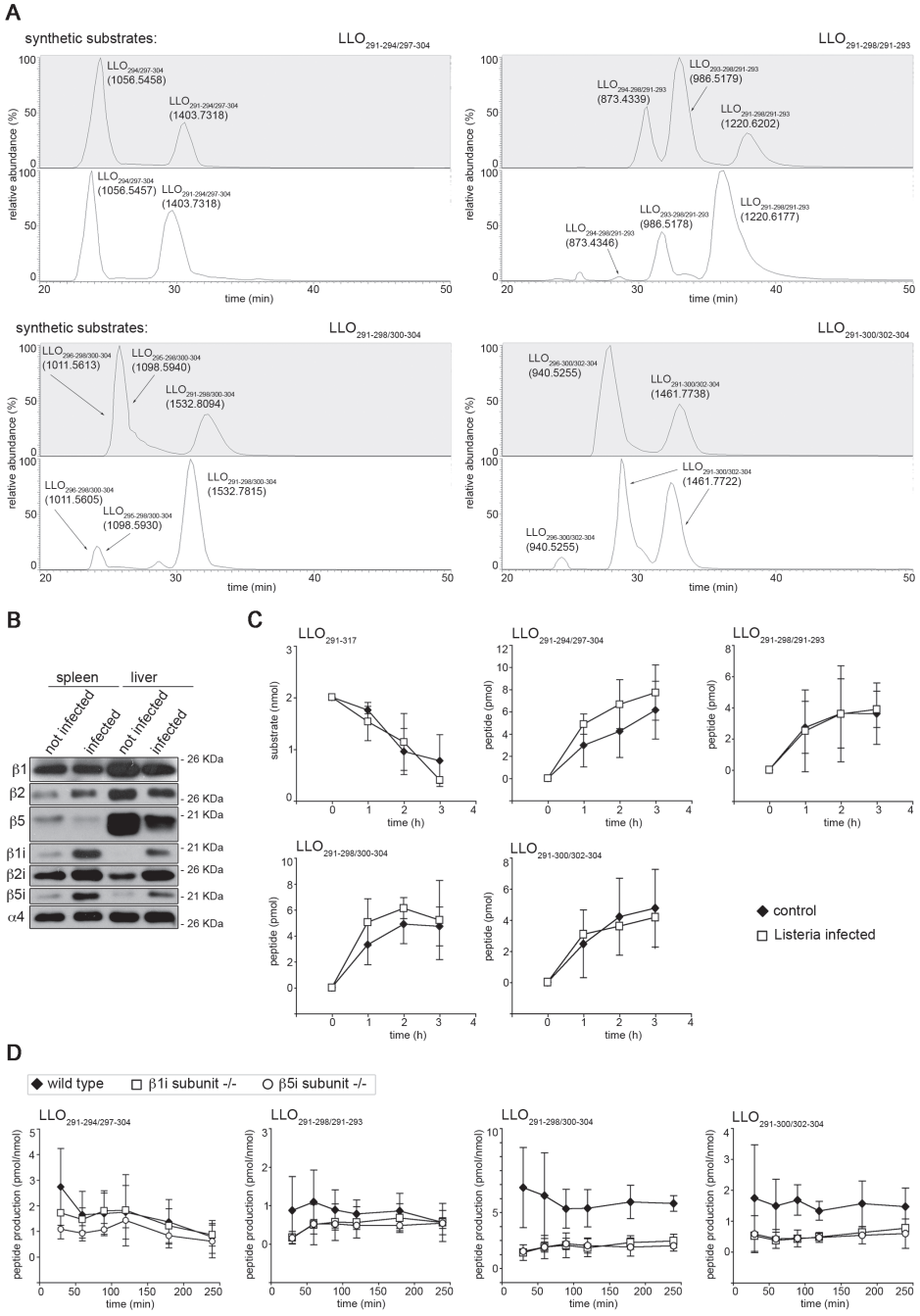
A
synthetic substrates:
LLO291-294/297-304
LLO294/297-304 (1056.5458)
LLO291-294/297-304 (1403.7318)
LLO294/297-304 (1056.5457)
LLO291-294/297-304 (1403.7318)
LLO291-298/291-293
LLO294-298/291-293 (873.4339)
LLO293-298/291-293 (986.5179)
LLO291-298/291-293 (1220.6202)
LLO294-298/291-293 (873.4346)
LLO293-298/291-293 (986.5178)
LLO291-298/291-293 (1220.6177)
synthetic substrates:
LLO291-298/300-304
LLO296-298/300-304 (1011.5613)
LLO295-298/300-304 (1098.5940)
LLO291-298/300-304 (1532.8094)
LLO296-298/300-304 (1011.5605)
LLO295-298/300-304 (1098.5930)
LLO291-298/300-304 (1532.7815)
LLO291-300/302-304
LLO296-300/302-304 (940.5255)
LLO291-300/302-304 (1461.7738)
LLO291-300/302-304 (1461.7722)
LLO296-300/302-304 (940.5255)
relative abundance (%)
time (min)
B
spleen
liver
not infected
infected
not infected
infected
β1
β2
β5
β1i
β2i
β5i
α4
26 KDa
21 KDa
C
LLO291-317
LLO291-294/297-304
LLO291-298/291-293
LLO291-298/300-304
LLO291-300/302-304
substrate (nmol)
peptide (pmol)
time (h)
control
Listeria infected
D
wild type
β1i subunit -/-
β5i subunit -/-
peptide production (pmol/nmol)
time (min)

Figure 2. Generation of $LLO_{291-317}$-derived spliced epitopes and epitope precursors by mouse spleen 20S proteasomes and recombinant ERAP1. (**A**) Products of the *in vitro* degra-dation of the spliced peptides $LLO_{291-294/297-304}$, $LLO_{291-298/291-293}$, $LLO_{291-298/300-304}$, $LLO_{291-300/302-304}$ by recombinant ERAP1. Educts and enzymatically processed products were separated by reversed phase HPLC (lower panels) and identified by MS/MS (Supporting Information Fig.1). Extracted ion chromatograms of the single and double protonated peptides versus time are displayed. The syn-thetic counterparts are shown in the upper panels. All peptides are detected by mass spectrometry with almost the same ionization products [M+H] + and by chromatography with similar retention times of their synthetic analogous. The spliced peptides produced by recombinant ERAP1 are re-ported in Table 1. Data are representative of one experiment. (**B**) Western blot assays performed on spleen and liver of mice infected with *Listeria monocytogenes* compared to not infected mice. The three constitutive- and three immuno-subunits as well as the α4 subunit, which is present in every proteasome isoform, were detected with proteasome subunit-specific antibodies and HRP-conjugated anti-rabbit or anti-mouse IgG secondary Ab. Blots are representative of one experiment. (**C**) Degradation kinetics of the synthetic substrate $LLO_{291-317}$ and the generation kinetics of the spliced peptides $LLO_{291-294/297-304}$, $LLO_{291-298/291-293}$, $LLO_{291-298/300-304}$ and $LLO_{291-300/302-304}$. (**D**) The efficiency of generation of the spliced peptides $LLO_{291-294/297-304}$, $LLO_{291-298/291-293}$, $LLO_{291-298/300-304}$ and $LLO_{291-300/302-304}$ is here depicted as pmol peptide produced per nmol of cleaved substrate over time. Digestions of the synthetic substrate $LLO_{291-317}$ were carried out by wild type, β1i subunit$^{-/-}$ or β5i subunit$^{-/-}$ mouse spleen 20S proteasomes. (**C-D**) Quantitation of the digestion products was carried out by applying the QME method. Data are shown as mean ± SD and are representative of two independent experiments, each performed in triplicate.

containing the immunosubunits [15], thus, uninfected spleen tissue already contains considerable quantities of immunoproteasomes (Fig. 2B).

To understand the specific role of the individual immunosubunits in the generation of the spliced LLO peptide products, we further compared the digests of proteasomes purified from wildtype mouse spleens with those from spleens of gene-deficient mice that lacked either β1i or β5i [10, 15]. We found that both immunosubunit-deficient proteasomes generated the spliced peptides $LLO_{291-298/300-304}$ and $LLO_{291-300/302-304}$ less efficiently than proteasomes of *wt* mice (Fig. 2D). These two spliced products are the N-terminally extended precursors of the H-2K^b-restricted $LLO_{295-298/300-304}$, $LLO_{296-298/300-304}$ and $LLO_{296-300/302-304}$ epitope candidates (Fig. 2A and Table 1). The generation efficiency of the other spliced peptides $LLO_{291-294/297-304}$ and $LLO_{291-298/291-293}$ was not affected by the complete depletion of immunosubunits (Fig. 2D). No significant variation in the $LLO_{291-317}$ degradation rate was observed comparing digests of proteasomes of wildtype, β1i- and β5i-deficient mice (data not shown), as shown before [15]. Of note, the average amount of $LLO_{296-304}$ generated *in vitro* by wildtype spleen 20S proteasomes over time was higher (89.3 pmol *per* nmol of substrate processed [15]) than that of the spliced peptides $LLO_{291-294/297-304}$ (1.7 pmol *per* nmol of substrate processed), $LLO_{291-298/291-293}$ (0.8 pmol *per* nmol of substrate processed), $LLO_{291-298/300-304}$ (4.7 pmol *per* nmol of substrate processed) and $LLO_{291-300/302-304}$ (1.5 pmol *per* nmol of substrate processed) (Fig. 2D).

Taken together, while the absence of specific immunosubunits diminished the generation of two spliced peptide products, all proteasome types generated all four spliced, putative epitope precursors, with no significant differences observed between proteasome preparations that varied in immunosubunit contents. Furthermore, the amount of linear epitope generated over time was larger than those of spliced peptide products, for all 20S proteasomes used, independent of subunit composition (data not shown).

Six putative spliced LLO epitopes bind the H-2K^b molecule

$LLO_{296-304}$ is presented to CD8+ T cells by the MHC class I H-2K^b molecule [31]. To verify that the predicted spliced epitope candidates are MHC class I H-2K^b binders, their ability to stabilize MHC class I molecules on RMA-S cells was tested. Incubation with the spliced epitope candidates $LLO_{294/297-304}$, $LLO_{293-298/291-293}$, $LLO_{294-298/291-293}$, $LLO_{296-298/300-304}$ upregulated H-2K^b levels on RMA-S cells to a similar extent as incubation with $LLO_{296-304}$, while $LLO_{295-298/300-304,}$ and $LLO_{296-300/302-304}$ stabilized H-2K^b to a lesser extent (Fig. 3A). During a subsequent chase in the absence of peptide,

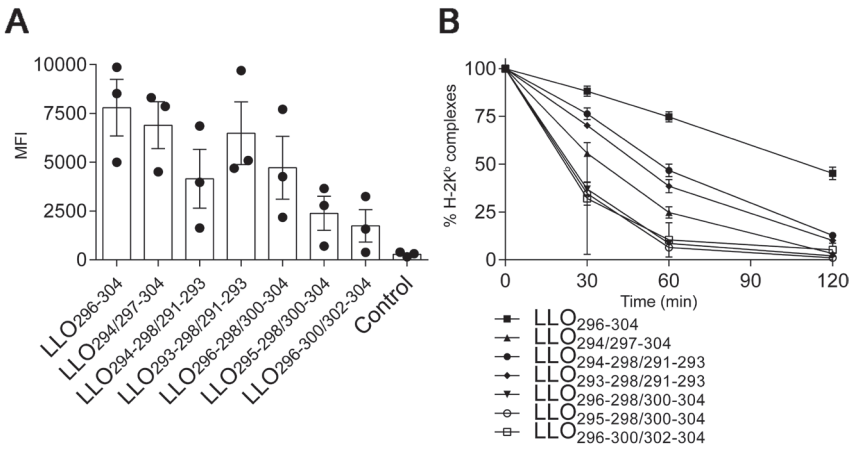

Figure 3. Binding of spliced LLO epitope candidates to H-2Kb molecules. (**A and B**) RMA-S cells were incubated overnight with or without synthetic peptide. (**A**) H-2K^b complexes (t = 0) were stained with a conformation-sensitive, biotin-conjugated anti-H-2K^b mAb and with PE-conjugated streptavidin and detected by FACS analysis. Filled circles represent stabilization of H-2K^b molecules measured in independent experiments in MFI (**B**) RMA-S cells loaded with peptide overnight were chased in the absence of peptide and at the indicated time points samples were stained for H-2K^b expression. Depicted are mean percentages of remaining MHC class I complexes (t=0 is 100%). (**A and B**) Data are shown as mean ± SEM and are representative of three independent experiments. Gating strategy is shown in Supporting Information Fig.2.

three spliced epitope candidates LLO$_{296\text{-}298/300\text{-}304,}$ LLO$_{295\text{-}298/300\text{-}304}$ and LLO$_{296\text{-}300/302\text{-}304}$ rapidly dissociated from H-2K^b molecules while the decay of the other spliced epitope candidates and LLO$_{296\text{-}304}$ was substantially slower (Fig. 3B, Supporting Information Fig.2). Corresponding half-lives ranged from 14 to 120 min for the linear epitope, which displayed the highest binding affinity (Table 1). Comparing the IC50 values predicted by the MHC3.4/ANN (Table 1) with the measured ability of the spliced epitope candidates to upregulate H-2K^b expression (Fig. 3A) and their dissociation rates (Fig. 3B, Table 1), we observed similar patterns, illustrating the accuracy of *in silico* prediction by NetMHC3.4/ANN.

We conclude that not only LLO$_{296\text{-}304,}$ but also the six putative spliced antigenic peptides can bind to H-2K^b molecules and thus could be presented by infected cells *in vivo*.

CD8+ T cells of *Listeria monocytogenes* infected mice recognize a spliced epitope candidate

To test whether the spliced epitope candidates are targeted during infection, CD8+ T cell responses to the putative $LLO_{291-317}$-derived epitopes were measured in the spleens of *Listeria monocytogenes* infected C57BL/6 mice *ex vivo*, at the peak of the response after primary infection and secondary infection [37]. Intracellular IFNγ staining (Supporting Information Fig.3) showed that both $LLO_{296-304}$ and the spliced $LLO_{294/297-304}$ epitope candidate were recognized by CD8+ T cells stimulated *ex vivo* with these peptides, in both primary (Fig. 4A) and secondary infection (Fig. 4B). None of the other spliced $LLO_{291-317}$ -derived epitope candidates induced IFNγ production in CD8+ T cells, exceeding the background measured upon incubation in the absence of peptide (Fig. 4A, Fig. 4B).

Because $LLO_{296-304}$ and $LLO_{294/297-304}$ share 8 out of 9 residues, the detected CD8+ T cell response to $LLO_{294/297-304}$ could be due to cross-reactivity of CD8+ T cells recognizing $LLO_{296-304}$. To test this possibility, we stained splenocytes of infected mice and uninfected controls *ex vivo* with PE-labelled MHC class I H-2K^b /$LLO_{294/297-304}$ and APC-labelled MHC class I H-2K^b /$LLO_{296-304}$ multimers. CD8+ T cells specific for the linear epitope were significantly ($p = 0.007$) detected in all infected mice (Fig. 5A, Fig. 5D). In contrast, the percentages of $LLO_{294/297-304}$–specific CD8+ T cells were above the background in only 5 out of 9 infected mice (Fig. 5B, Fig. 5D). In double staining with the two MHC/peptide multimers, CD8+ T cells specific for both $LLO_{294/297-304}$ and $LLO_{296-304}$ were significantly ($p = 0.025$) detected in all mice (Fig. 5C, Fig. 5D). While a small population of single, MHC H-2K^b/$LLO_{296-304}$ multimer-positive CD8+ T cells were detected in double stained samples (Fig. 5D, right panel), no solely $LLO_{294/297-304}$ positive cells were detected any more (Fig. 5D, right panel).

Thus, all CD8+ T cells specific for the spliced epitope candidate also recognize the linear epitope $LLO_{296-304}$. These data suggest that $LLO_{296-304}$-specific CD8+ T cells cross-react with $LLO_{294/297-304}$-presented on H-2K^b molecules, demonstrating that spliced epitopes could be recognized by pathogen-specific CD8+ T cells during infection.

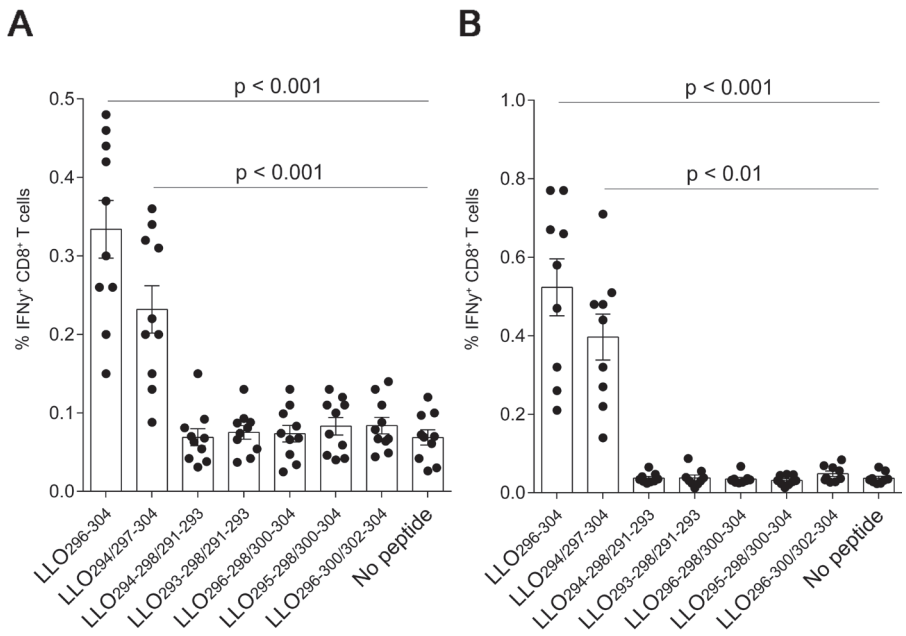

Figure 4. Recognition of LLO-derived linear and spliced peptides by CD8⁺ T cells of *Listeria monocytogenes*-infected mice. C57BL/6 mice were infected *i.v.* with (**A**) a primary dose of 2000 CFU Listeria monocytogenes, and (**B**) challenged 21 days later with a 100 fold higher bacterial dose. At day 7 following primary infection and day 26 following secondary infection, percentages of LLO peptide-specific CD8⁺ T cells in the spleen were measured *ex vivo* by re-stimulation of spleno-cytes with the indicated peptides, followed by staining of cell surface CD8 with APC-anti-CD8 and intracellular IFNγ staining with PE-anti-IFNγ antibodies. (**A and B**) Data are shown as mean ± SEM in which every dot represents an individual mouse, representative of three independent experi-ments (n > 5 animals per experiment). Data was tested for normality using Levene's test and ana-lyzed using a paired One-way ANOVA, comparing responses per peptide to the no peptide control per mouse, followed by Dunnet's post hoc test. At both time points, a significant difference ($p < 0.05$) was found between the CD8⁺ T cell responses specific for $LLO_{296-304}$ and $LLO_{294/297-304}$ compared to background responses measured in samples stimulated without peptide. Uninfected control animals did not show any response (data not shown). Gating strategy is shown in Supplementary figure 3.

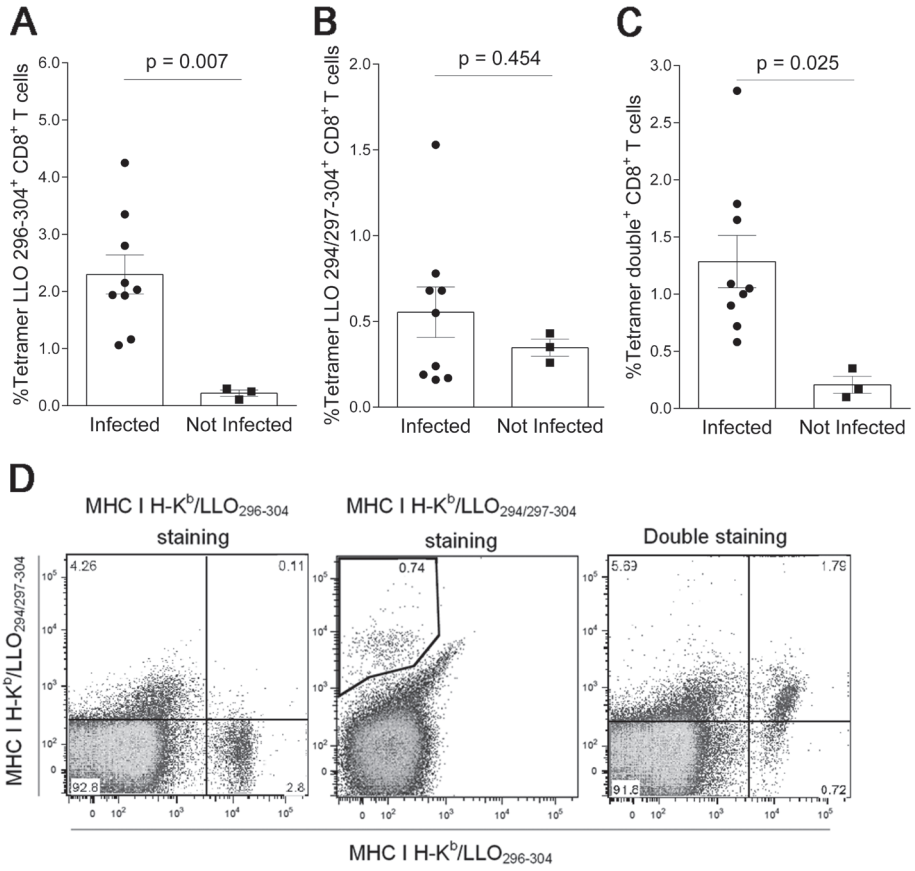

Figure 5. Recognition of $LLO_{296-304}$ and its spliced epitope variant by CD8+ T cells of *Listeria monocytogenes*-infected mice. $LLO_{296-304}$ - and $LLO_{294/297-304}$ - specific CD8+ T cell responses in the spleens of infected and control mice were measured *ex vivo* at day 7 post primary infection with 2000 CFU *Listeria monocytogenes* using V500-anti-CD8 mAb and (**A**) APC-labeled MHC multimers folded with $LLO_{296-304}$, (**B**) PE-labeled MHC multimers folded with $LLO_{294/297-304}$ or (**C**) by double staining with the two MHC multimers. (**A and B**) Data are shown as mean ± SEM in which every dot represents an individual infected (circles) or uninfected (squares) mouse. The data are representative of two independent experiments (n = 15 animals in total), tested for normality using Levene's test and analyzed using an independent student's T test comparing infected with non-infected mice. A significant difference ($p < 0.05$) was found between percentages of $LLO_{296-304}$-specific CD8+ T cells in infected versus non-infected mice. (**D**) Representative FACS plots of CD8+ T cells from the spleens of infected mice stained with V500-anti-CD8 in combination with APC conjugated MHC class I H-2K^b /$LLO_{296-304}$ multimers only (left), PE conjugated MHC class I H-2K^b /$LLO_{294/297-304}$ multimers only (middle) or both multimers (right).

Discussion

CD8$^+$ T cell responses to complex pathogens often target a relatively small number of antigenic peptides only. The parameters that influence whether a pathogen-derived peptide will elicit an immune response are still not fully understood. Nevertheless, the requirements to be fulfilled by antigenic peptides to be recognized by T cells, *e.g.* successful proteolytic liberation, TAP transport, MHC class I binding and TCR recognition, are numerous [38]. Thus, the number of epitopes that is processed from an antigen and presented by a specific MHC class I molecule is limited. It has been hypothesized that PCPS could expand the pool of antigenic peptides [19, 20] and here we report first evidence that this may happen during an infection *in vivo*. We demonstrate that, from a small portion of the *Listeria monocytogenes* LLO antigen only, proteasomes generate one linear epitope along with four spliced epitope precursors from which, by ERAP-mediated N-terminal trimming, six spliced antigenic peptides that bind to H-2K^b molecules can be generated. The generation efficiency of the spliced peptides was smaller than that of the linear epitope, as described by quantitative comparison of several linear and spliced peptides produced *in vitro* by 20S proteasomes [10]. These findings are in line with a publication by Berkers at al. [39], showing that peptide ligation even under the most optimal conditions *in vitro* occurs with at most 30% efficiency. It is worth to note, however, that spliced epitopes can be presented in similar amounts as linear epitopes on the cell surface (Ebstein et al., *personal communication*).

Of the six spliced epitope candidates, one spliced peptide, $LLO_{294/297\text{-}304}$, along with the linear epitope $LLO_{296\text{-}304}$, was recognized by CD8$^+$ T cells of mice infected with *Listeria monocytogenes,* in both primary- and secondary infection (Fig. 4). Double staining with MHC/peptide multimers folded with either $LLO_{294/297\text{-}304}$ or $LLO_{296\text{-}304}$ (Fig. 5D) showed that all CD8$^+$ T cells specific for the spliced epitope were detected also by the multimer folded with the linear epitope. Conversely, most but not all CD8$^+$ T cells stained with $LLO_{296\text{-}304}$–folded multimers were stained by the multimer folded with the spliced epitope candidate. From these data we infer that most likely, CD8$^+$ T cells primed by $LLO_{296\text{-}304}$, recognizing the C-terminal part of this peptide (residues between amino acid 297-304) cross-react to the spliced epitope candidate, while a small proportion of $LLO_{296\text{-}304}$–specific CD8$^+$ T cells recognize the peptide N-terminal amino acid and therefore fail to detect the $LLO_{204/297\text{-}304}$ peptide. Thus, based only on the data shown in Fig 5, it is unclear whether $LLO_{204/297\text{-}304}$ is presented and participates in CD8$^+$ T cell priming during infection.

Notwithstanding the above notion, the $LLO_{204/297-304}$ is generated by the MHC class I antigen processing machinery of Listeria infected mice (Fig. 2) and the H-2K^b off rate of this peptide, although higher than that of $LLO_{296-304}$ (Table 1), is within the range of off rates that we detect for CD8+ T cell epitopes in RMA-S based assays [32]. In addition, *in vivo* antigen processing of *Listeria monocytogenes* derived antigens has been shown to be highly efficient [40-42]. $LLO_{296-304}$ is the immunodominant known epitope in C57BL/6 mice [31] and LLO_{91-99} is immunodominant in BALB/c mice [31, 37], which most likely is due to the rapid degradation of LLO antigen and the very efficient liberation of these two peptides in combination with high MHC class I binding affinity [41]. Because the spliced antigenic peptides are derived from the LLO antigen, they are processed with similar rates as the described dominant epitopes (although with a lower efficiency) and therefore will appear early on MHC class I molecules. Thus, $LLO_{294/297-304}$ may well be presented over the course of *Listeria monocytogenes* infection, albeit in smaller quantities than $LLO_{296-304}$, and be recognized by CD8+ T cells primed against the linear epitope, thereby facilitating bacterial clearance.

Remarkably, it has been argued that the ability of any given TCR to recognize multiple epitopes is a strict necessity, because if every T cell recognized one epitope only, the breadth of the T cell response needed to eradicate a pathogen could not be achieved [43]. Moreover, if multiple TCR recognize multiple peptides, displaying a high degree of similarity, the chances of a diverse, broad T cell response are higher, which would make it substantially more difficult for pathogens to escape the immune system. It was shown that amino acid exchanges in the epitope- or epitope flanking residues can diminish the ability of proteasomes to efficiently liberate epitope' C-termini [44-46]. In case of presentation and concurrent recognition of proteasome cleavage and proteasome spliced products by (cross reactive) CD8+ T cells, the impact of such mutations in epitope or epitope flanking sequences of pathogens would decrease substantially.

Thus, it might be advantageous for infected cells to present linear epitopes as well as spliced epitope variants simultaneously. Such mechanism may help the host by tackling mutation-driven escape mechanisms of pathogens, which might have been one of the reasons for the preservation of PCPS along evolution.

Acknowledgments

Support was by European Union's Seventh Framework Programme [FP7/2007-2013] - Grant No. 280873 ADITEC to A.S., AICE FIRE Onlus Emilia Romagna to M.M, and Deutsche Forschungsgemeinschaft SFB 740 and SFBTR43, BIH CRG1-TP1 and Einstein Stiftung Berlin (A2013-174) to P-M.K and NC3Rs through a David Sainsbury Fellowship to JL. We thank P. Henklein, P. Kunert and B. Brecht-Jachan for technical assistance, A. Voigt for providing the gene-deficient mouse spleens and A. Marit de Groot for critical reading of the manuscript.

Abbreviations

PCPS Proteasome-catalyzed peptide splicing
LLO Listeriolysin O

A

$LLO_{294/297-304}$

synthetic peptide

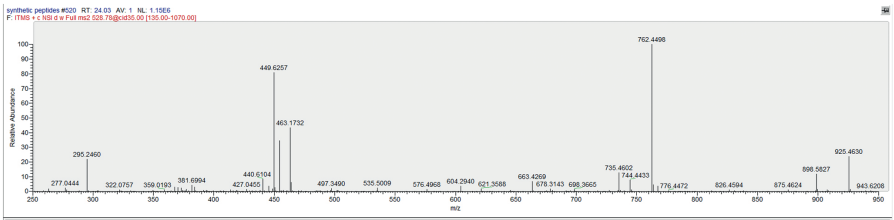

ERAP1-mediated trimming

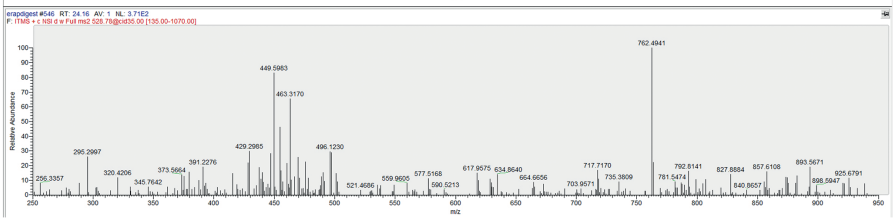

B

$LLO_{294-298/291-293}$

synthetic peptide

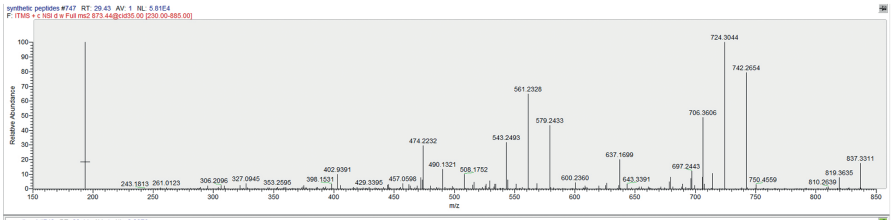

ERAP1-mediated trimming

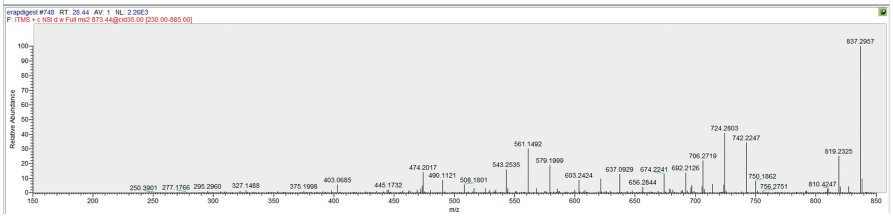

C

LLO$_{293-298/291-293}$

synthetic peptide

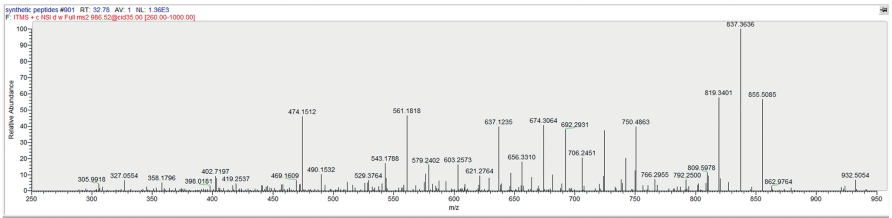

ERAP1-mediated trimming

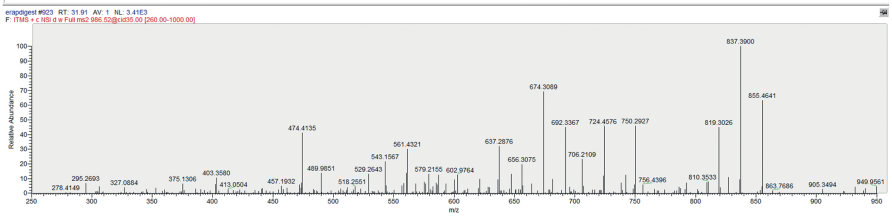

D

LLO$_{296-298/300-304}$

synthetic peptide

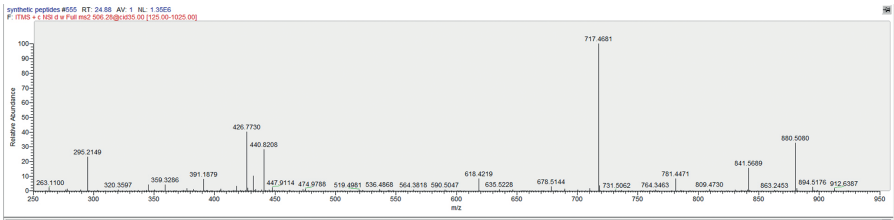

ERAP1-mediated trimming

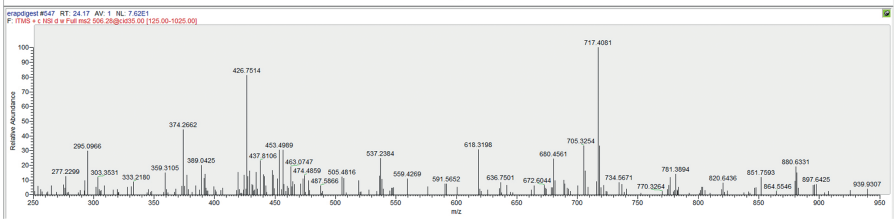

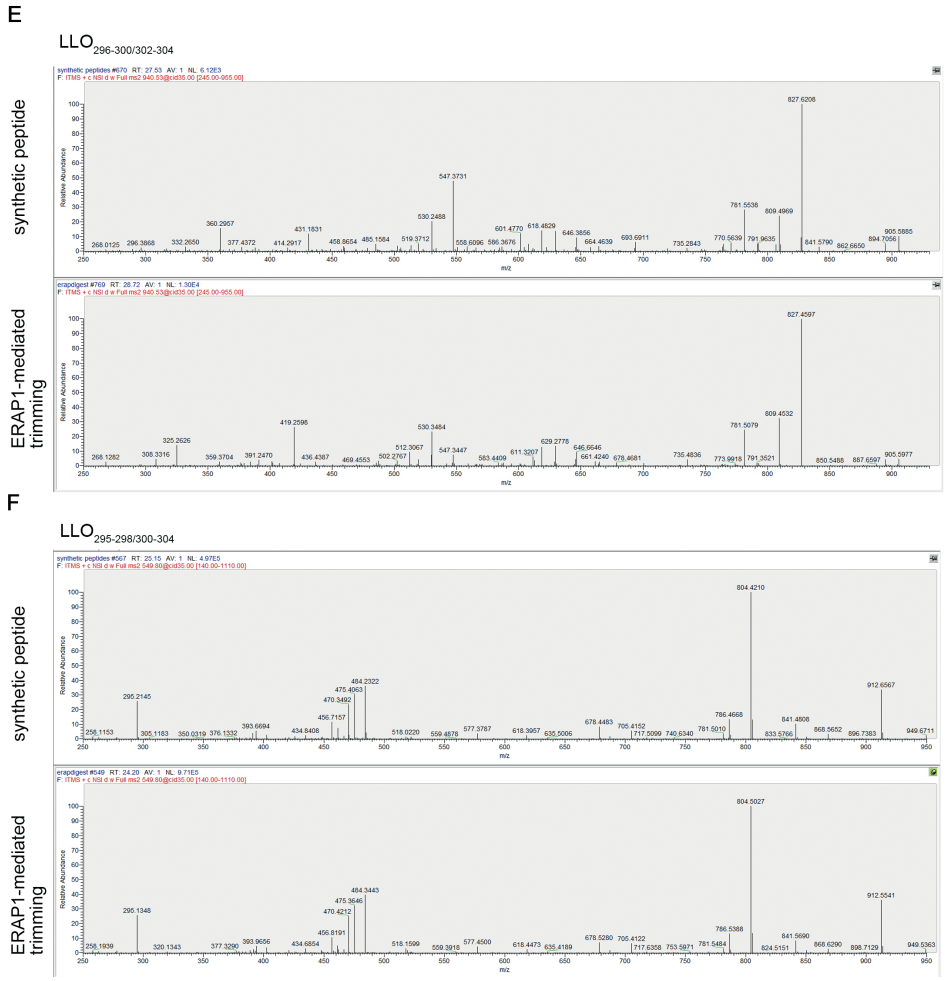

Supplementary figure 1. Orbitrap MS/MS spectra of N-terminally trimmed spliced peptides by recombinant ERAP1. A-F) Identification of products of the trimming by recombinant ERAP1 of the $LLO_{291-317}$-derived spliced N-terminal elongated precursors produced in vitro by 20S proteasomes is reported. (**A**) ESI fragment ion spectrum (MS/MS) of the doubly charged peptides $[M^{+}2H]2^{+}$ $LLO_{294/297-304}$ [S][AYGRQVYL] (*m/z* 528.78, +2) (**B**) the singly charged ions $[M^{+}H]1^{+}$ $LL_{O294-298/291-293}$ [SSVAY][AYI] (*m/z* 873.44, +1) (C) $LLO_{293-298/291-293}$ [ISSVAY][AYI] (*m/z* 986.52, +1) (D) $LLO_{296-298/300-304}$ [VAY][RQVYL] (*m/z* 506.28, +2) (E) $LLO_{296-300/302-304}$ [VAYGR][VYL] (*m/z* 940.52, +1) (F) $LLO_{295-298/300-304}$ [SVAY][RQVYL] (*m/z* 549.80, +2) in a synthetic peptide mixture (upper panels in A-F) or in a 4 h reaction with the N-terminally extended peptides (**A**) $LLO_{291-294/297-304}$ (**B, C**) $LLO_{291-298/291-293}$ (**D,F**) $LLO_{291-298/300-304}$ and (**E**) $LLO_{291-300/302-304}$ and ERAP1 (lower panels in **A-F**).

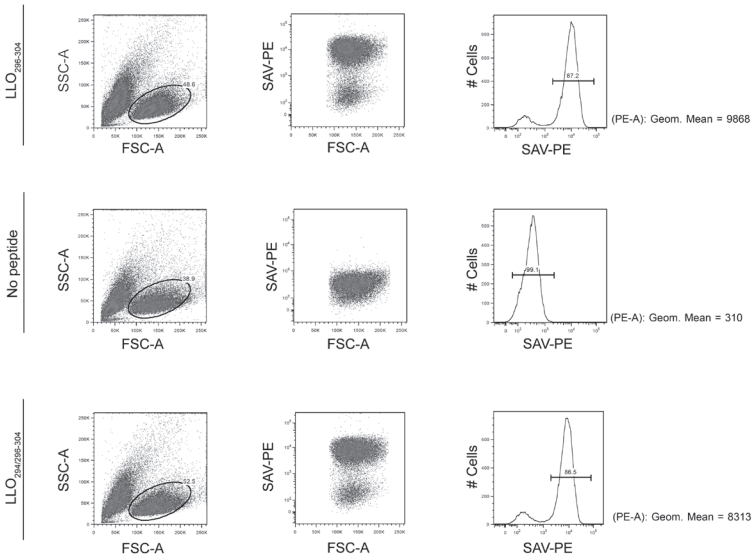

Supplementary figure 2. Gating strategy. RMA-S cells were incubated overnight with synthetic peptide or without peptide. H-2K^b complexes (t = 0) were stained with a conformation-sensitive, biotin-conjugated anti-H-2K^b mAb and with PE-conjugated streptavidin. Immunofluorescence was measured using a FACS Canto II and analyzed with FlowJo software. Representative FACS plots and histograms including the MFI are shown for RMA-S cells loaded with LLO$_{296\text{-}304}$, LLO$_{294/296\text{-}304}$ or without peptide (t = 0).

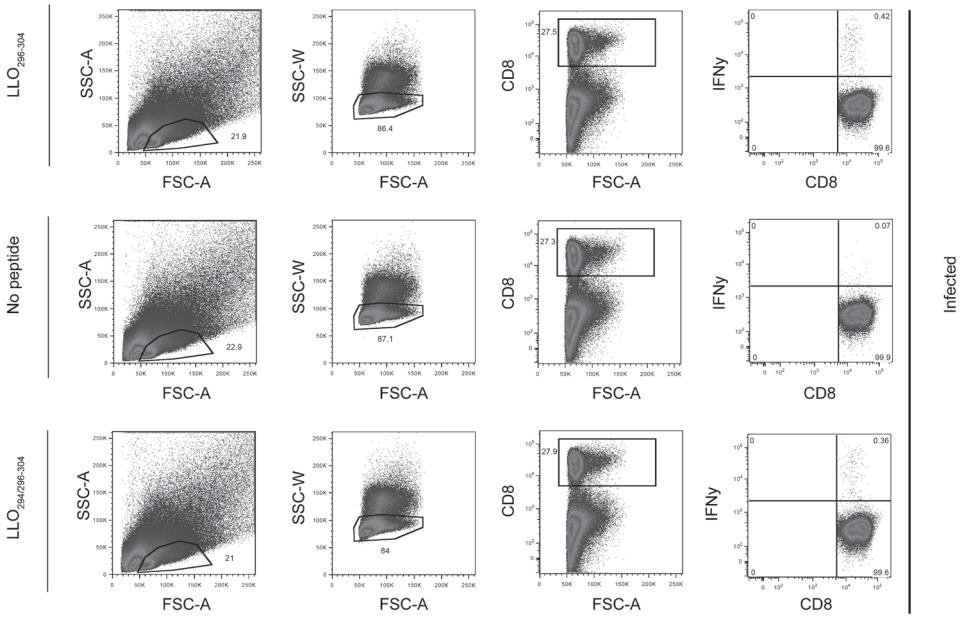

Supplementary figure 3. Gating strategy. C57BL/6 mice were intravenously infected with 2000 CFU Listeria monocytogenes. At day 7 post infection, splenocytes were harvested and re-stimulated *ex vivo* with $LLO_{296\text{-}304}$, $LLO_{294/296\text{-}304}$ or without peptide in the presence of monensin and then stained with fluorochrome-conjugated mAbs for CD8 cell surface expression and intracellular IFNγ. Representative FACS plots, analyzed with FlowJo software, including percentages of IFNγ⁺ and IFNγ- CD8⁺ T cells are shown.

3

References

1. Rock, K. L. *et al*. Inhibitors of the proteasome block the degradation of most cell proteins and the generation of peptides presented on MHC class I molecules. *Cell* **78,** 761-771 (1994).
2. Sijts, E. J. A. M. & Kloetzel, P. -. The role of the proteasome in the generation of MHC class I ligands and immune responses. *Cellular and Molecular Life Sciences* **68,** 1491-1502 (2011).
3. Cascio, P., Hilton, C., Kisselev, A. F., Rock, K. L. & Goldberg, A. L. 26S proteasomes and immunoproteasomes produce mainly N-extended versions of an antigenic peptide. *EMBO J.* **20,** 2357-2366 (2001).
4. Aki, M. *et al*. Interferon-γ induces different subunit organizations and functional diversity of proteasomes. *J. Biochem.* **115,** 257-269 (1994).
5. Dalet, A. *et al*. An antigenic peptide produced by reverse splicing and double asparagine deamidation. *Proc. Natl. Acad. Sci. U. S. A.* **108,** E323-E331 (2011).
6. Hanada, K. -., Yewdell, J. W. & Yang, J. C. Immune recognition of a human renal cancer antigen through post-translational protein splicing. *Nature* **427,** 252-256 (2004).
7. Michaux, A. *et al*. A spliced antigenic peptide comprising a single spliced amino acid is produced in the proteasome by reverse splicing of a longer peptide fragment followed by trimming. *Journal of Immunology* **192,** 1962-1971 (2014).
8. Warren, E. H. *et al*. An antigen produced by splicing of noncontiguous peptides in the reverse order. *Science* **313,** 1444-1447 (2006).
9. Vigneron, N. *et al*. An Antigenic Peptide Produced by Peptide Splicing in the Proteasome. *Science* **304,** 587-590 (2004).
10. Mishto, M. *et al*. Driving forces of proteasome-catalyzed peptide splicing in yeast and humans. *Molecular and Cellular Proteomics* **11,** 1008-1023 (2012).
11. Dalet, A., Stroobant, V., Vigneron, N. & Van Den Eynde, B. J. Differences in the production of spliced antigenic peptides by the standard proteasome and the immunoproteasome. *Eur. J. Immunol.* **41,** 39-46 (2011).

12. Vigneron, N. & Van den Eynde, B. J. Proteasome subtypes and the processing of tumor antigens: Increasing antigenic diversity. *Curr. Opin. Immunol.* **24,** 84-91 (2012).
13. Kincaid, E. Z. *et al*. Mice completely lacking immunoproteasomes show major changes in antigen presentation. *Nat. Immunol.* **13,** 129-135 (2012).
14. Sijts, A. J. A. M. *et al*. Efficient generation of a hepatitis B virus cytotoxic T lymphocyte epitope requires the structural features of immunoproteasomes. *J. Exp. Med.* **191,** 503-513 (2000).
15. Mishto, M. *et al*. Proteasome isoforms exhibit only quantitative differences in cleavage and epitope generation. *Eur. J. Immunol.* **44,** 3508-3521 (2014).
16. Zanker, D. & Chen, W. Standard and immunoproteasomes show similar peptide degradation specificities. *Eur. J. Immunol.* **44,** 3500-3503 (2014).
17. Mishto, M. *et al*. Immunoproteasome LMP2 60HH variant alters MBP epitope generation and reduces the risk to develop multiple sclerosis in Italian female population. *PLoS ONE* **5** (2010).
18. Liepe, J. *et al*. Quantitative time-resolved analysis reveals intricate, differential regulation of standard- and immuno-proteasomes. *eLife; 4:e07545* (2015).
19. Rammensee, H. -. Protein surgery. *Nature* **427,** 203-204 (2004).
20. Berkers, C. R., de Jong, A., Ovaa, H. & Rodenko, B. Transpeptidation and reverse proteolysis and their consequences for immunity. *International Journal of Biochemistry and Cell Biology* **41,** 66-71 (2009).
21. Liepe, J. et al. The 20S proteasome splicing activity discovered by SpliceMet. *PLoS computational biology* 6 (6):e1000830 (2010).
22. Textoris-Taube, K. *et al*. The N-terminal flanking region of the TRP2360-368 melanoma antigen determines proteasome activator PA28 requirement for epitope liberation. *J. Biol. Chem.* **282,** 12749-12754 (2007).
23. Van Kaert, L. *et al*. Altered peptidase and viral-specific T cell response in LMP2 mutant mice. *Immunity* **1,** 533-541 (1994).
24. Fehling, H. J. *et al*. MHC class I expression in mice lacking the proteasome subunit LMP-7. *Science* **265,** 1234-1237 (1994).
25. Gohlke, S. *et al*. Molecular alterations in proteasomes of rat liver during aging result in altered proteolytic activities. *Age* **36,** 57-72 (2014).
26. Mishto, M. *et al*. The immunoproteasome ß5i subunit is a key contributor to ictogenesis in a rat model of chronic epilepsy. *Brain Behav. Immun.* **49,** 188-196 (2015).
27. Textoris-Taube, K. *et al*. The T210M substitution in the HLA-A*02:01 gp100 epitope strongly affects overall proteasomal cleavage site usage and antigen processing. *J Biol Chem.* **290**:30417-30428 (2015).
28. Saric, T. *et al*. An IFN-γ-induced aminopeptidase in the ER, ERAP I, trims precursors to MHC class I-presented peptides. *Nat. Immunol.* **3,** 1169-1176 (2002).
29. Mishto, M. *et al*. A structural model of 20S immunoproteasomes: Effect of LMP2 codon 60 polymorphism on expression, activity, intracellular localisation and insight into the regulatory mechanisms. *Biol. Chem.* **387,** 417-429 (2006).
30. Deol, P., Zaiss, D. M. W., Monaco, J. J. & Sijts, A. J. A. M. Rates of processing determine the immunogenicity of immunoproteasome-generated epitopes. *Journal of Immunology* **178,** 7557-7562 (2007).
31. Geginat, G., Schenk, S., Skoberne, M., Goebel, W. & Hof, H. A novel approach of direct ex vivo epitope mapping identifies dominant and subdominant CD4 and CD8 T cell epitopes from Listeria monocytogenes. *Journal of Immunology* **166,** 1877-1884 (2001).
32. Zaiss, D. M. W., Bekker, C. P. J., Gröne, A., Lie, B. A. & Sijts, A. J. A. M. Proteasome immunosubunits protect against the development of CD8 T cell-mediated autoimmune diseases. *Journal of Immunology* **187,** 2302-2309 (2011).

33. De Verteuil, D. *et al*. Deletion of immunoproteasome subunits imprints on the transcriptome and has a broad impact on peptides presented by major histocompatibility complex I molecules. *Mol. Cell. Proteomics* **9,** 2034-2047 (2010).
34. Chen, W., Norbury, C. C., Cho, Y., Yewdell, J. W. & Bennink, J. R. Immunoproteasomes shape immunodominance hierarchies of antiviral CD8+ T cells at the levels of T cell repertoire and presentation of viral antigens. *J. Exp. Med.* **193,** 1319-1326 (2001).
35. Basler, M., Moebius, J., Elenich, L., Groettrup, M. & Monaco, J. J. An altered T cell repertoire in MECL-1-deficient mice. *J. Immunol.* **176,** 6665-6672 (2006).
36. Chapiro, J. *et al*. Destructive cleavage of antigenic peptides either by the immunoproteasome or by the standard proteasome results in differential antigen presentation. *J. Immunol.* **176,** 1053-1061 (2006).
37. Busch, D. H., Pilip, I. M., Vijh, S. & Pamer, E. G. Coordinate regulation of complex T cell populations responding to bacterial infection. *Immunity* **8,** 353-362 (1998).
38. Yewdell, J. W. Confronting Complexity: Real-World Immunodominance in Antiviral CD8+ T Cell Responses. *Immunity* **25,** 533-543 (2006).
39. Berkers, C. R. *et al*. Definition of proteasomal peptide splicing rules for high-efficiency spliced peptide presentation by MHC class I molecules. *J. Immunol.* **195,** 4085-4095 (2015).
40. Villanueva, M. S., Fischer, P., Feen, K. & Pamer, E. G. Efficiency of MHC class I antigen processing: A quantitative analysis. *Immunity* **1,** 479-489 (1994).
41. Villanueva, M. S., Sijts, A. J. A. M. & Pamer, E. G. Listeriolysin is processed efficiently into an MHC class I-associated epitope in Listeria monocytogenes-infected cells. *Journal of Immunology* **155,** 5227-5233 (1995).
42. Pamer, E. G., Sijts, A. J. A. M., Villanueva, M. S., Busch, D. H. & Vijh, S. MHC class I antigen processing of Listeria monocytogenes proteins: Implications for dominant and subdominant CTL responses. *Immunol. Rev.* **158,** 129-136 (1997).
43. Mason, D. A very high level of crossreactivity is an essential feature of the T- cell receptor. *Immunol. Today* **19,** 395-404 (1998).
44. Ossendorp, F. *et al*. A single residue exchange within a viral CTL epitope alters proteasome-mediated degradation resulting in lack of antigen presentation. *Immunity* **5,** 115-124 (1996).
45. Tenzer, S. *et al*. Antigen processing influences HIV-specific cytotoxic T lymphocyte immunodominance. *Nat. Immunol.* **10,** 636-646 (2009).
46. Beekman, N. J. *et al*. Abrogation of CTL epitope processing by single amino acid substitution flanking the C-terminal proteasome cleavage site. *Journal of Immunology* **164,** 1898-1905 (2000).
47. Peters, B. & Sette, A. Integrating epitope data into the emerging web of biomedical knowledge resources. *Nature Reviews Immunology* **7,** 485-490 (2007).

3

Strategies to enhance immunogenicity of cDNA vaccine encoded antigens by modulation of antigen processing

Anouk C.M. Platteel[1], A. Marit de Groot[1], Christin Keller[2,3], Peter Andersen[4], Huib Ovaa[5], Peter M. Kloetzel[2,3], Michele Mishto[2,3] and Alice J.A.M. Sijts[1,#]

[1] Department of Infectious Diseases and Immunology, Faculty of Veterinary Medicine, Utrecht University, Utrecht, The Netherlands.
[2] Institut für Biochemie, Charité - Universitätsmedizin Berlin, Berlin, Germany. Berlin Institute of Health, Berlin, Germany.
[3] Department of Infectious Disease Immunology, Statens Serum Institut, Copenhagen, Denmark.
[4] Department of Chemical Immunology, Leiden University Medical Center, Leiden, The Netherlands.

Vaccine
2016, Sep 30;34(42):5132-40.

Graphical Abstract

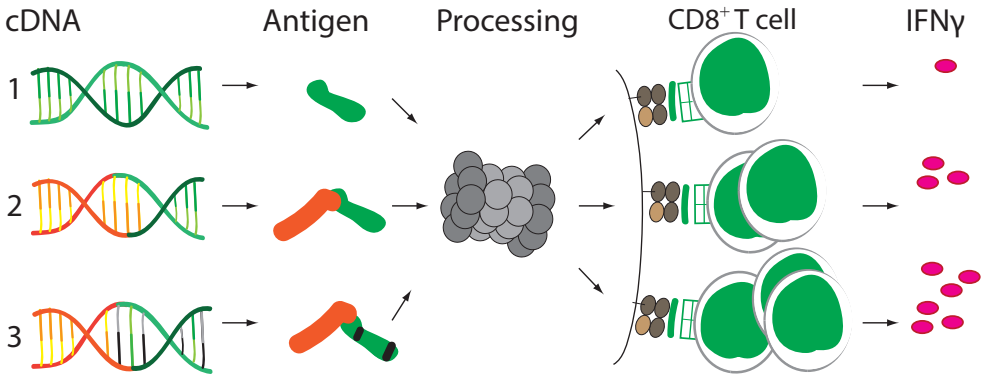

Vaccine H56 antigen cDNA (1), fused to TTFC (tetanus toxin fragment C) or UB (ubiquitin) cDNA (2) and modified to flank $CD8^+$ T cell epitope C-termini with an glutamic acid residue (3) was administered by tattoo immunization. Linkage to either TTFC or UB enhanced $CD8^+$ T cell responses to all epitopes, while replacement of C-terminal epitope flanks for a Glu residue further increased the $CD8^+$ T cell response to 4 out of 6 epitopes. These strategies can be exploited for vaccine design.

4

Abstract

Most vaccines are based on protective humoral responses while for intracellular pathogens $CD8^+$ T cells are regularly needed to provide protection. However, poor processing efficiency of antigens is often a limiting factor in $CD8^+$ T cell priming, hampering vaccine efficacy. The multistage cDNA vaccine H56, encoding three secreted Mycobacterium tuberculosis antigens, was used to test a complete strategy to enhance vaccine' immunogenicity. Potential $CD8^+$ T cell epitopes in H56 were predicted using the NetMHC3.4/ANN program. Mice were immunized with H56 cDNA using dermal DNA tattoo immunization and epitope candidates were tested for recognition by responding CD8+ T cells in ex vivo assays. Seven novel $CD8^+$ T cell epitopes were identified. H56 immunogenicity could be substantially enhanced by two strategies: (i) fusion of the H56 sequence to cDNA of proteins that modify intracellular antigen processing or provide $CD4^+$ T cell help, (ii) by substitution of the epitope's hydrophobic C-terminal flanking residues for polar glutamic acid, which facilitated their proteasome-mediated generation. We conclude that this whole strategy of in silico prediction of potential $CD8^+$ T cell epitopes in novel antigens, followed by fusion to sequences with immunogenicity-enhancing properties or modification of epitope flanking sequences to improve proteasome-mediated processing, may be exploited to design novel vaccines against emerging or 'hard to treat' intracellular pathogens.

Introduction

$CD8^+$ T cells recognize epitopes of pathogen-derived, intracellularly degraded proteins that are presented by MHC class I molecules. A major role in the generation of such epitopes is played by proteasomes. Proteasomes usually liberate the C-terminus of the epitope by cleaving after hydrophobic or basic residues [1]. The N-terminus may undergo further N-terminal trimming by cytosolic or ER-localized amino- and endopeptidases. The correctly sized ligands that contain a binding motif will bind to newly assembled MHC class I molecules and presented at the cell surface [2, 3].

Proteasomes consist of four rings composed of seven subunits each and are present in every cell of an organism. In constitutive proteasomes, the β1, β2 and β5 subunits, located in the inner rings, display catalytic activity. Upon exposure of cells to inflammatory cytokines, expression of three homologous subunits, β1i/LMP2, β2i/MECL1 and β5i/LMP7 is induced, which leads to the formation of intermediate- or immunoproteasomes [4]. The different pocket conformations and peptide transport dynamics quantitatively alter the pool of peptides produced by the proteasomes [5-9].

Multiple strategies can be used to influence epitope generation and processing by the proteasome which can enhance immunogenicity of $CD8^+$ T cell epitopes and thus could aid in designing better vaccines against intracellular pathogens. Especially for DNA vaccines, which generally elicit cellular responses in animals but show limited immunogenicity in clinical studies [10], those strategies can help to increase immunogenicity.

One strategy directly targets proteasome-mediated processing; since the proteasome usually creates the epitope' C-terminus, characteristics of the last amino acid of the epitope (positioned at P1) and the C-terminally flanking residue (positioned at P1') in the protein sequence have been shown to greatly influence epitope processing [11-16]. Although the limited size of the datasets analyzed so far does not allow generalizations, proteasomes often favor hydrolyzing the peptide bond between hydrophobic large residues at P1 and polar large residues at P1', whereas hydrophobic large residues at P1' are disfavored [17]. By for example introducing a residue at P1' that is favored by the proteasome, chances of effective processing may be increased.

A second strategy to influence epitope processing is fusion of the target cDNA to cDNA that codes for proteins with immunogenicity-enhancing properties. The underlying mechanisms differ with the characteristics of the fusion protein but both self-derived (*e.g.* HSP-70 [18], invariant chain [19]) as well as pathogen-derived proteins (*e.g*. *E.coli* β-glucoronidase [20]) have been reported to enhance immunogenicity.

We combined these strategies to study the effect of antigen processing modulation on the immunogenicity of a DNA-encoded antigen. The multistage DNA vaccine H56 was used as a model antigen, which expresses the full protein sequence of the *Mycobacterium tuberculosis (Mtb)* antigens Ag85B, ESAT-6 and Rv2660c [21]. This was delivered using dermal DNA tattoo immunization, which is a proven method to induce an effective $CD8^+$ T cell response [22]. We report seven novel $CD8^+$ T cell epitopes in H56, identified using *in silico* prediction [23]. Immunogenicity of H56 was enhanced by fusion of the H56-encoding DNA sequences to cDNA encoding ubiquitin or TTFC, and by substitution of C-terminal flanking residues of epitopes. The two proposed approaches increased the immunogenicity and such a combined strategy may be applied in vaccine design.

Materials and methods

Peptide synthesis and 20S proteasome purification

All peptides were synthesized using Fmoc solid phase chemistry. The sequence enumeration of the synthetic peptides referred to the vaccine H56 [21]. In particular, for the polypeptides $H56_{53\text{-}79}$ (WDINTPAFEWYYQSGLSIVMPVGGQSS) the residue V_{71} was substituted to E, for $H56_{137\text{-}160}$ (LAAYHPQQFIYAGSLSALLDPSQG) L_{155} to E and for $H56_{64\text{-}86}$ (YQSGLSIVMPVGGQSSFYSDWYS) Y_{81} to E. 20S proteasomes were purified from 5 pooled spleens of C57BL/6 mice [6] and purity was verified [17].

In vitro digestion of synthetic polypeptide and peptide quantification

The synthetic polypeptides (20 μM) were digested by 2 μg 20S proteasomes in 100 μl TEAD buffer (Tris 20 mM, EDTA 1 mM, NaN_3 1 mM, DTT 1 mM, pH 7.2) for a period of 1-4 hours at 37°C. Liquid-chromatography mass spectrometry (LC-MS) analyses of polypeptide digestion products was performed with the ESI-ion trap instrument DECA XP MAX and the LTQ Orbitrap XL MS (ThermoFisher Scientific) coupled with nanoUPLC Aquity (Waters) [24]. The database used for the LC-MS/MS analyses was generated by applying the SpliceMet algorithm to allow

the identification of linear and spliced peptides [25]. Quantification of peptides was carried out by applying QME to the LC-MS analyses by DECA XP MAX of the in vitro digestion kinetics [24]. QME estimates the absolute content of peptide products based on their MS ion peak area measured in the digestion probe. It makes use of the law of mass conservation and MS instrument features. The QME algorithm parameters were empirically computed in a previous study [24]. QME also estimates the site-specific cleavage strength (SCS), which describes the relative frequencies of proteasome cleavage after residues of the synthetic polypeptide [24]. The values showed in this study are the averages of SCS measured over time [24]. For the comparison of the SCS and the investigated peptides of wild type and E-substituted synthetic substrates we ran QME by including only the peptide products common to the wild type and corresponding substituted substrates [26].

Mice, DNA and dermal tattoo immunization

Six week old CB6F1 mice from Charles River were immunized at day 0, 3 and 6 with 15 µl cDNA (2 µg/µl) in TE buffer with a 9-needle bar mounted on a tattoo rotary device (Cheyenne) on 100 Hz, at 1 mm depth for 1 minute [22]. The full length H56 cDNA [21] was codon optimized and inserted 3' of tetanus toxin fragment C domain 1 (TTFC) [27, 28], ubiquitin (UB) with UB_{75} mutated to A and UB_{76} mutated to V [29], HLA-F-adjacent transcript 10 (FAT10) [29] or mouse invariant chain (mLi) [30] in pVAX1 vector (Invitrogen). In the H56_E construct (ThermoFisher Scientific), H56-V_{71}, H56-Y_{81}, H56-T_{104}, H56- L_{155}, H56-M_{170} and H56- S_{364} were changed into E (GAA). All animal experiments were approved by the Animal Ethics Committee from Utrecht University (DEC.2014.II.01.001, DEC.2014.II.08.069).

Analysis of specific $CD8^+$ or $CD4^+$ T cell responses

Intracellular cytokine staining

T cell responses were quantified as reported [6]. Briefly, 2.5 x 10^6 erythrocyte depleted splenocytes were incubated in RPMI 1640 medium supplemented with 10% FCS (Lonza), 2 mM L-glutamine, 30 µM 2-mercaptoethanol, and penicillin/streptomycin (RPMI medium) with or without 1 (CD8) or 10 µg/ml synthetic peptide (CD4) and 10 µM monensin (eBioscience), for 6 h at 37 °C. Cells were stained with an APC-conjugated anti-mouse CD8 antibody (53-6.7; eBioscience) or APC-conjugated anti-mouse CD4 (L3T4; eBioscience) in the presence of anti-mouse CD16/CD32 (2.4G2; made in house), fixed and stained with PE-conjugated anti-mouse IFNγ antibody (XMG1.2; eBioscience) and analyzed on a FACS Canto II (BD Biosciences) using FlowJo software (Tree Star).

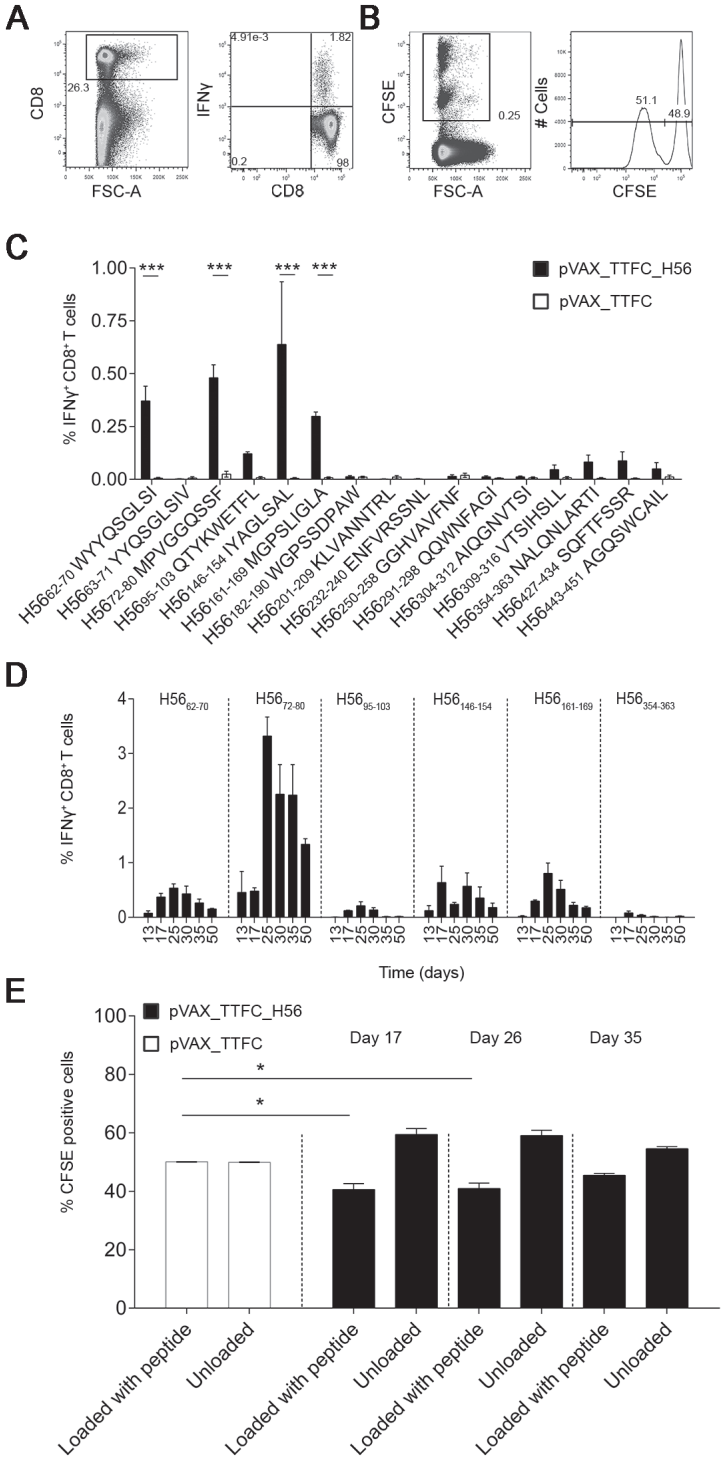
A
CD8
26.3
FSC-A
IFNγ
4.91e-3
1.82
0.2
98
CD8
B
CFSE
0.25
FSC-A
Cells
51.1
48.9
CFSE
C
% IFNγ+ CD8+ T cells
pVAX_TTFC_H56
pVAX_TTFC
***
H56 62-70 WYYQSGLSI
H56 63-71 YYQSGLSIV
H56 72-80 MPVGGQSSF
H56 95-103 QTYKWETFL
H56 146-154 IYAGLSAL
H56 161-169 MGPSLIGLA
H56 182-190 WGPSSDPAW
H56 201-209 KLVANNTRL
H56 232-240 ENFVRSSNL
H56 250-258 GGHVAVFNF
H56 291-298 QQWNFAGI
H56 304-312 AIQGNVTSI
H56 309-316 VTSIHSLL
H56 354-363 NALQNLART
H56 427-434 SQFTFSSR
H56 443-451 AGQSWCAIL
D
% IFNγ+ CD8+ T cells
H56 62-70
H56 72-80
H56 95-103
H56 146-154
H56 161-169
H56 354-363
Time (days)
E
% CFSE positive cells
pVAX_TTFC_H56
pVAX_TTFC
Day 17
Day 26
Day 35
*
Loaded with peptide
Unloaded

Figure 1. CD8T⁺ cell responses specific for novel epitopes in H56 are functional and persist 50 days after immunization. (**A, B**) CB6F1 mice were immunized with H56 cDNA using dermal DNA tattooing and percentages or killing capacity of IFNγ- producing specific CD8⁺ T cells were determined using (**A**) intracellular cytokine staining or (**B**) *in vivo* killing assays. (**C, D**) At day 17 (**C**) or indicated dates (**D**), percentages of epitope-specific CD8⁺ T cells were measured *ex vivo* from spleen. Data are shown as mean of 5-8 mice per group ± SEM per peptide corrected for IFNγ background level as measured in control samples that were incubated without peptide, and are representative of 2 independent experiments. (**E**) At indicated days, pVAX_TTFC_H56- (black bars) or pVAX_TTFC (white bars) immunized animals were injected with splenocytes labeled with CFSE and synthetic $H56_{62-70}$ WYYQSGLSI, $H56_{72-80}$ MPVGGQSSF, $H56_{95-103}$ QTYKWETFL, $H56_{146-154}$ IYAGLSAL, $H56_{161-169}$ MGPSLIGLA and $H56_{354-363}$ NALQNLARTI. Bars indicate percentages of CFSE labeled cells in the spleen after 2 hours of 5 mice per group ± SEM. (**C, E**) All data were analyzed using a two tailed independent sample T test comparing pVAX_TTFC_H56 immunized animals with pVAX_TTFC immunized control animals per peptide, combined with a Sidak-Holm correction for multiple comparisons. P values < 0.05 are depicted with * and P < 0.001 with ***.

IFNγ ELISpot

MAIP ELISPOT plates (Millipore) were coated overnight with 2 µg/ml AN18 in PBS at 4 °C. Wells were washed and blocked with RPMI medium (Life Technologies). 5 x 10^5 erythrocyte depleted splenocytes were plated with or without 2 µg/ml synthetic peptide for 6 h in RPMI medium at 37 °C. Plates were washed with PBS plus 0.01% tween 20 (PBST), and IFNγ was detected with biotinylated IFNγ antibody (XMG1.2; BD), followed by alkaline phosphatase-conjugated streptavidin (Jackson Immuno Research Laboratories), in PBST supplemented with 2% BSA. The assay was developed with the Vector blue substrate kit (Vector Laboratories) and analyzed using an ELISpot plate reader and scanner (AELVIS).

In vivo killing assay

CB6F1 splenocytes were divided into two populations and labelled with either 0.4 µM or 4 µM CFSE (Invitrogen) in PBS at room temperature for 10 minutes and quenched with FCS HI. CFSE high cells were subsequently pulsed with 1 µM of $H56_{146-154}$ IYAGLSAL, $H56_{161-169}$ MGPSLIGLA, $H56_{62-70}$ WYYQSGLSI, $H56_{72-80}$ MPVGGQSSF, $H56_{95-103}$ QTYKWETFL and $H56_{354-363}$ NALQNLARTI in PBS containing 2% FCS, for 1 h at 37 °C, and washed with PBS before *i.v.* injection.

Statistical Analysis

To compare functionality of responses or responses to individual epitopes, both between the H56 immunized group compared to the control group, epitope

specific responses of every mouse were corrected for background IFNγ level as measured in samples incubated without peptide, in both IFNγ ELISpot and IFNγ ICS. The variance homogeneity was tested using Levene's test. A two-tailed independent sample T test was used, combined with a Holm-Sidak correction for multiple comparisons. P values < 0.05 were considered significant.

Results

Identification of novel CD8$^+$ T cell epitopes in H56

Rational vaccine design aimed at inducing protective CD8$^+$ T cell responses would start with predicting the pathogen derived potential epitopes. To test this approach we used the *Mtb* vaccine candidate H56 in which we predicted potential CD8$^+$ T cell epitopes for H-2^b and H-2^d MHC class I molecules using the NetMHC3.4/ANN prediction algorithm [23]. As expected, the known epitopes *e.g.* $H56_{72\text{-}80}$ MPVGGQSSF and $H56_{146\text{-}154}$ IYAGLSAL [31-33], as well as 14 novel epitope candidates, were predicted to bind the H-2^{b,d} MHC class I molecules with IC50 < 500 nM (Table 1). To determine which of these were epitopes, peptide specific CD8$^+$ T cell responses were determined *ex vivo* in spleens of mice immunized with H56 cDNA using dermal DNA tattoo immunization [22]. Intracellular IFNγ staining (ICS) (Fig. 1A) showed that four peptides ($H56_{62\text{-}70}$ WYYQSGLSI, $H56_{72\text{-}80}$ MPVGGQSSF, $H56_{146\text{-}154}$ IYAGLSAL, $H56_{161\text{-}169}$ MGPSLIGLA), out of 16 potential epitopes, were recognized by CD8$^+$ T cells of mice immunized with a H56 containing construct when compared to mice immunized with a control construct (Fig. 1C). For five other peptides ($H56_{95\text{-}103}$ QTYKWETFL, $H56_{309\text{-}316}$ VTSIHSLL, $H56_{354\text{-}363}$ NALQNLARTI, $H56_{427\text{-}434}$ SQFTFSSR, $H56_{443\text{-}451}$ AGQSWCAIL) a trend towards recognition was visible (Fig. 1C). Of these epitopes, $H56_{309\text{-}316}$ VTSIHSLL and $H56_{354\text{-}363}$ NALQNLARTI derived from ESAT-6, $H56_{427\text{-}434}$ SQFTFSSR and $H56_{443\text{-}451}$ AGQSWCAIL from Rv2660c, and all other peptides from Ag85B. CD8$^+$ T cell responses to the identified epitopes persisted until 50 days after immunization (Fig. 1D) and dominance hierarchy of responding CD8$^+$ T cells was maintained over time, with the already known epitope $H56_{72\text{-}80}$ MPVGGQSSF [31-33] being responsible for the activation of the largest percentage of specific CD8$^+$ T cells.

To check whether the H56 cDNA vaccine-induced CD8$^+$ T cells displayed killing capacity, *in vivo* killing assays were performed at different days (Fig. 1B). At day 17 and 25, from the 1 : 1 ratio of cells that were labeled in high CFSE concentration and loaded with epitopes ($H56_{62\text{-}70}$ WYYQSGLSI, $H56_{72\text{-}80}$ MPVGGQSSF, $H56_{95\text{-}103}$ QTYKWETFL, $H56_{146\text{-}154}$ IYAGLSAL, $H56_{161\text{-}169}$ MGPSLIGLA and $H56_{354\text{-}363}$

Table 1. Predicted CD8+ T cell epitopes in H56.

Allele	Start	End	Sequence	IC50 (nM)[a]
H-2L^d	62	70	WYYQSGLSI	47.38
H-2K^d	63	71	YYQSGLSIV	13.27
H-2K^d	72	80	MPVGGQSSF	11.81
H-2K^b	95	103	QTYKWETFL	128.41
H-2K^d	146	154	IYAGSLSAL	3.88
H-2K^d	161	169	MGPSLIGLA	676.78
H-2D^d	182	190	WGPSSDPAW	47.13
H-2D^d	201	209	KLVANNTRL	303.29
H-2K^b	232	240	ENFVRSSNL	264
H-2K^d	250	258	GGHNAVFNF	63.73
H-2K^b	291	298	QQWNFAGI	180.79
H-2L^d	304	312	AIQGNVTSI	558.05
H-2K^b	309	316	VTSIHSLL	477.84
H-2D^b	354	363	NALQNLARTI	280.87
H-2K^b	427	434	SQFTFSSR	395.10
H-2D^d	443	451	AGQSWCAIL	392.12

[a] NetMHC 3.4/ANN [23] predicted H-2^b and H-2^d binding affinities (IC50). All peptides were included in this study [58].

NALQNLARTI) versus unloaded cells that were labeled in low CFSE concentration, we found less CFSE high cells back in the H56 immunized mice, implying specific killing of peptide loaded splenocytes by H56 specific CD8+ T cells (Fig. 1E). In the mice that were immunized with a control construct, this balance was still 1 : 1.

Thus, by applying the NetMHC3.4/ANN prediction algorithm, we identified 16 potential epitopes of which four ($H56_{62\text{-}70}$ WYYQSGLSI, $H56_{72\text{-}80}$ MPVGGQSSF, $H56_{146\text{-}154}$ IYAGLSAL, $H56_{161\text{-}169}$ MGPSLIGLA) were recognized by CD8+ T cells of H56 immunized mice. These responses could be measured up to day 50 after immunization and CD8+ T cells showed measurable killing capacity until day 26.

Fusion of H56 cDNA to cDNA of UB or TTFC in antigen construct increases immunogenicity

Fusion of antigen-encoding cDNA to cDNA, encoding specific pathogen-derived proteins or self-proteins involved in antigen processing, is known to increase immunogenicity [18, 27-30, 34-36]. To determine whether the immunogenicity of H56 could be improved likewise, different cDNA fusion constructs encoding H56 preceded by self- and non-self-derived proteins were tested. ICS for identification of specific $CD8^+$ T cells (Fig. 2A) or $CD4^+$ T cells [37, 38] (Fig. 2B) at day 17 showed that constructs with ubiquitin (UB) [29, 36] or tetanus toxin fragment C (TTFC) [27, 28] fused to the N-terminal end of H56, were capable of enhancing $CD8^+$ T cell responses to the H56 epitopes, as compared to responses elicited by immunization with H56 alone, which is poorly immunogenic in this experimental setting (Fig. 2C). The dominance hierarchy of the responses to different epitopes seemed similar for the two H56 fusion constructs, with $H56_{72-80}$ MPVGGQSSF being responsible for activation of the largest percentage of $CD8^+$ T cells. The control peptide $OVA_{257-264}$ was not recognized, illustrating specificity of the responses. Fusion of H56 to TTFC and UB also enhanced H56 specific $CD4^+$ T cell responses (Fig. 2D, Fig. 2E). HLA-F-adjacent transcript 10 (FAT10) [29, 39] and mouse invariant chain (mLi) [19, 30] did not increase H56 specific $CD8^+$ or $CD4^+$ T cell responses (Supplementary Fig.1). We conclude that TTFC and UB are able to increase immunogenicity of the H56 encoding construct.

Substitution of the C-terminal flanking residues of identified H56 epitopes generally increases immunogenicity

The substitution of C-terminal flanking residues of epitopes in the parental antigen sequence can affect proteasome-mediated cleavage and therefore have major consequences for epitope generation [11-16]. In 5 out of 6 epitopes used in the current study, P1 contains a hydrophobic large residue with the exception of $H56_{161-169}$ MGPSLIGLA (Table 2). Of those 6 epitopes, 3 have a hydrophobic large residue at P1' as well, thereby creating a peptide bond that has been shown to be infrequently hydrolyzed by proteasomes [17]. In order to further enhance immunogenicity of the vaccination, we adopted a second strategy in which the flanking residues of the H56 peptides $H56_{62-70}$ WYYQSGLSI, $H56_{72-80}$ MPVGGQSSF, $H56_{95-103}$ QTYKWETFL, $H56_{146-154}$ IYAGLSAL, $H56_{161-169}$ MGPSLIGLA, and $H56_{354-363}$ NALQNLARTI were changed to glutamic acid (E) [17]. As proof of principle we also included the weakly immunogenic epitopes in our experimental set up, since especially their immunogenicity may be enhanced by introduction of novel COOH-terminal flanking residues that facilitate proteasome-mediated epitope generation. Reponses of mice immunized with the modified H56 construct were

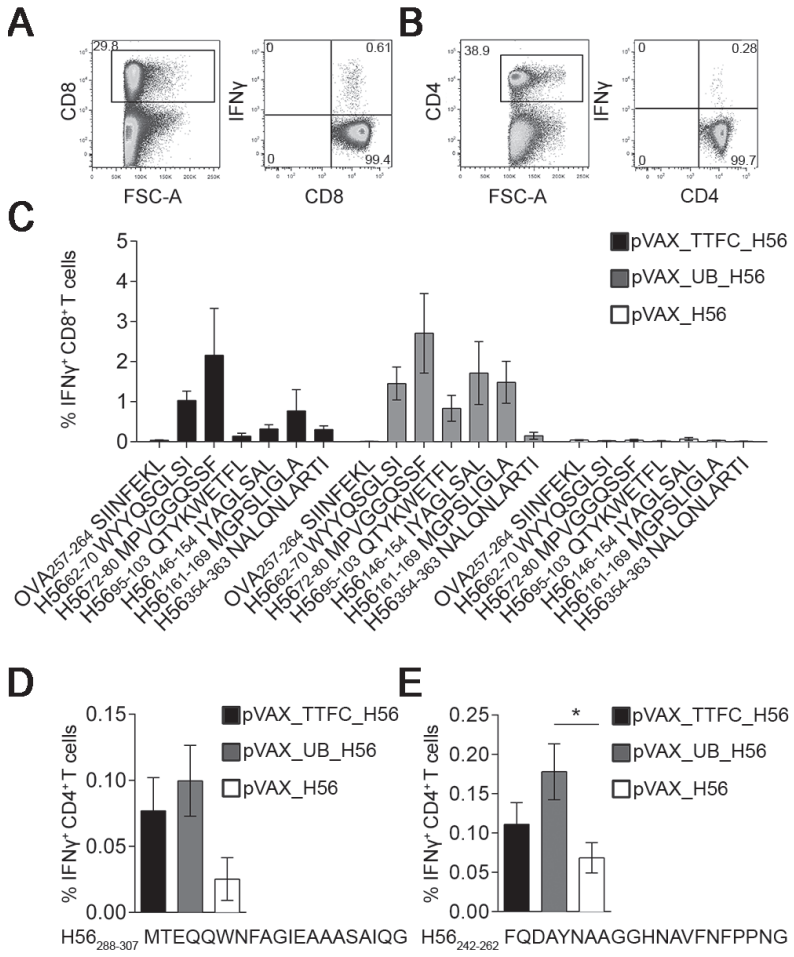

Figure 2. Fusion of H56 cDNA to cDNA of UB and TTFC enhances immunogenicity. (**A, B**) CB6F1 mice were immunized with H56 cDNA using dermal DNA tattooing and percentages of (**A**) specific $CD8^+$ T cells and (**B**) $CD4^+$ T cells were determined using intracellular cytokine staining at day 17. (**C**) Data of $CD8^+$ T cells are shown as mean of 4-5 mice per group ± SEM per peptide corrected for IFNγ background level as measured in control samples that were incubated without peptide. (**D, E**) Data of $CD4^+$ T cells are shown as mean of 4-5 mice per group ± SEM per peptide corrected for IFNγ background level as measured in control samples that were incubated without peptide. P values < 0.05 are depicted with *.

Table 2. Characteristics of last amino acid of epitope or first C-terminal flanking residue of different CD8⁺ T cell epitopes in H56

Epitope	Characteristics P1[a]	Residue at P1′	Characteristics P1′[a]
$H56_{62-70}$ WYYQSGLSI	HL	V	HS
$H56_{72-80}$ MPVGGQSSF	HL	Y	HL
$H56_{95-103}$ QTYKWETFL	HL	T	PS
$H56_{146-154}$ IYAGLSAL	HL	L	HL
$H56_{161-169}$ MGPSLIGLA	HS	M	HL
$H56_{354-363}$ NALQNLARTI	HL	S	PS

[a] Amino acid characteristics of last residue of epitope (P1) and C-terminal flanking residue (P1′). Amino acid characteristic acronyms are the following: HS, hydrophobic small; HL, hydrophobic large; PS, polar small.

Figure 3. C-terminal flanking residue modulation of epitopes from hydrophobic- to polar residues enhances immunogenicity. (**A-D**) CB6F1 mice were immunized with H56 cDNA using dermal DNA tattooing. (**A, C**) At day 17 IFNγ ELISpot was used to measure IFNγ secreting T cells in spleen. Data are shown as mean ± SEM of 5 mice per group per peptide corrected for IFNγ background level as measured in control samples that were incubated without peptide, and are representative of pooled data of 2 independent experiments out of 4 independent experiments. (**B, D**) Additionally at day 17 using, intracellular cytokine staining, percentages of epitope specific CD8⁺ T cells in the spleen were measured *ex vivo*. Data are shown as mean ± SEM of 5 mice per group measured in triplicate per corrected for IFNγ background level as measured in control samples that were incubated without peptide, and are representative of 3 independent experiments. (**E,F**) Data of $CD4^+$ T cells are shown as mean of 4 mice per group ± SEM per peptide corrected for IFNγ background level as measured in control samples that were incubated without peptide. (**A-D**) All data were analyzed using a two tailed independent sample T test comparing pVAX_TTFC_H56 immunized animals with pVAX_TTFC_H56_E immunized animals per peptide, combined with a Sidak-Holm correction for multiple comparisons. P values < 0.05 were considered significant and marked by *.

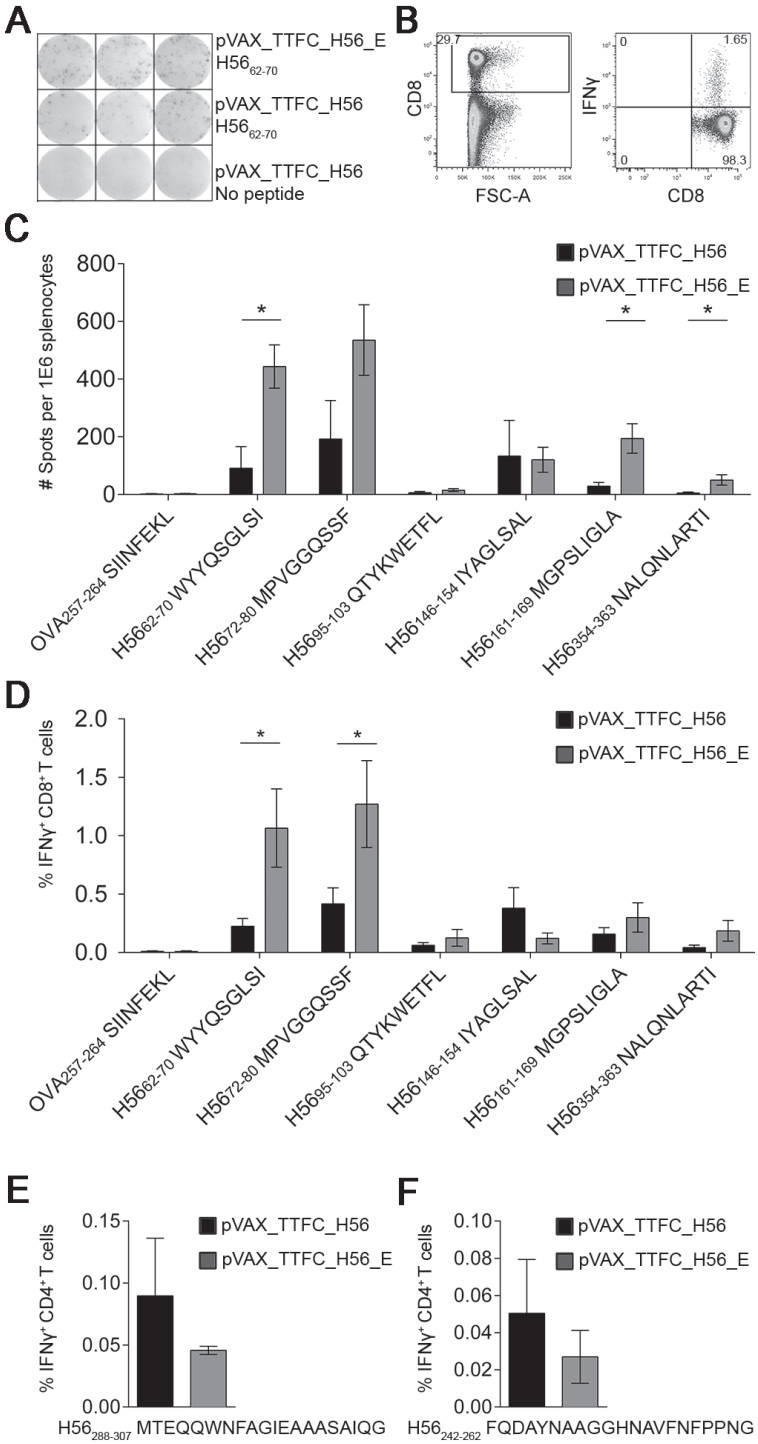
A
pVAX_TTFC_H56_E
H56 62-70
pVAX_TTFC_H56
H56 62-70
pVAX_TTFC_H56
No peptide
B
29.7
CD8
FSC-A
0
1.65
0
98.3
IFNγ
CD8
C
Spots per 1E6 splenocytes
pVAX_TTFC_H56
pVAX_TTFC_H56_E
OVA257-264 SIINFEKL
H5662-70 WYYQSGLSI
H5672-80 MPVGGQSSF
H5695-103 QTYKWETFL
H56146-154 IYAGLSAL
H56161-169 MGPSLIGLA
H56354-363 NALQNLARTI
D
% IFNγ+ CD8+ T cells
pVAX_TTFC_H56
pVAX_TTFC_H56_E
OVA257-264 SIINFEKL
H5662-70 WYYQSGLSI
H5672-80 MPVGGQSSF
H5695-103 QTYKWETFL
H56146-154 IYAGLSAL
H56161-169 MGPSLIGLA
H56354-363 NALQNLARTI
E
% IFNγ+ CD4+ T cells
pVAX_TTFC_H56
pVAX_TTFC_H56_E
H56288-307 MTEQQWNFAGIEAAASAIQG
F
% IFNγ+ CD4+ T cells
pVAX_TTFC_H56
pVAX_TTFC_H56_E
H56242-262 FQDAYNAAGGHNAVFNFPPNG

compared to those triggered by the wildtype H56 version using IFNγ ELISpot (Fig. 3A) and IFNγ ICS (Fig. 3B). Both assays showed the same pattern of $CD8^+$ T cell responses that were enhanced to E-flanked epitopes. IFNγ ELISpot showed 3 out of 6 E-flanked epitopes to be enhanced (Fig. 3C) and ICS 2 out of 6 (Fig. 3D). The overall results of these two assays, despite inter-experimental differences, were similar and combining these two assays, we found that 4 epitopes ($H56_{62-70}$ WYYQSGLSI, $H56_{72-80}$ MPVGGQSSF, $H56_{161-169}$ MGPSLIGLA, $H56_{354-363}$ NALQNLARTI) showed an enhanced immunogenicity following substitution of their C-terminal flanking residue for E, whereas immunogenicity of $H56_{146-154}$ IYAGLSAL seemed mildly diminished. The control peptide $OVA_{257-264}$ was not recognized, illustrating specificity of the responses. The substitutions at the P1′ site were not in the regions encoding the H56 $CD4^+$ T cell epitopes $H56_{242-262}$ FQDAYNAAGGHNAVFNFPPNG and $H56_{288-307}$ MTEQQWNFAGIEAAASAIQG [37, 38] and they did not influence the $CD4^+$ T cell response to these epitopes (Fig. 3E, Fig. 3F). Thus, C-terminal flanking residue substitution to E, where the hydrophobic epitope C-terminus is followed by a hydrophobic large or small residue in the wildtype sequence, can increase the $CD8^+$ T cell response independent of the $CD4^+$ T cell response.

The substitution of the C-terminal flanking residue of H56 derived epitopes alters their generation dynamics by the proteasome

To investigate the biochemical effects of substitution of the C-terminal flanking residues of the H56-derived epitopes into E, we performed *in vitro* digestions of the synthetic substrates $H56_{137-160}$, $H56_{64-86}$, and $H56_{53-79}$ with mouse spleen 20S proteasomes. In the digestions of the first two substrates we identified the epitopes $H56_{146-154}$ IYAGLSAL and $H56_{72-80}$ MPVGGQSSF and their potential N-extended precursors, for the latter substrate we neither identified the epitope $H56_{62-70}$ WYYQSGLSI nor its potential precursors (data not shown). The inability of MS to identify epitopes in *in vitro* proteasome-mediated digestions, which are generated *in vivo* in a proteasome-dependent fashion, has been reported [24, 40, 41] and is likely due to the limited sensitivity of the MS methods used.

By using the quantitative analytical approach based on QME method [24], for comparison of $H56_{137-160}$ and $H56_{64-86}$ wild type and mutated substrates, we observed that the H56 $L_{155}E$ and the $Y_{81}E$ substitutions did not improve the relative frequency of cleavage after the preceding residues L_{154} and F_{80}, respectively (Supplementary Fig. 2). The substitutions however modified the peptide pool produced by the proteasome (data not shown) and altered the overall substrate degradation rate and the proteasome preference of hydrolysis of peptide bonds

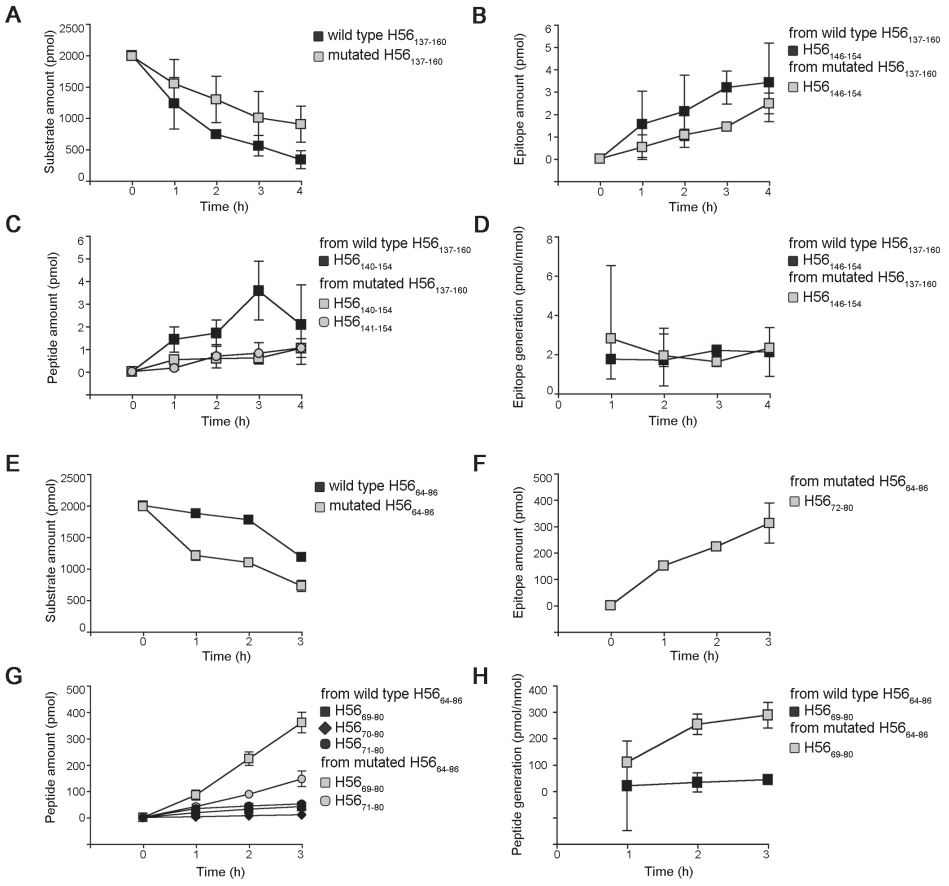

Figure 4. Substitution at the C-terminal flanking epitope residue affects the epitope production by 20S proteasomes. (**A, E**) Quantitative kinetics of substrate degradation and (**B-D, F-H**) generation of the immuno-relevant peptides of the synthetic wild type and mutated (**A-D**) $H56_{137-160}$ and (**E-H**) $H56_{64-86}$ substrates by mouse spleen 20S proteasomes. Peptide quantification was carried out by applying QME to the LC-MS analyses. Data are the mean and bars the SD of repeated measurements of a representative kinetics of two independent experiments. (**D, H**) The generation efficiency for the epitopes $H56_{146-154}$ and the potential precursor $H56_{69-80}$, measured as pmol peptide *per* nmol of substrate consumed over time, was compared between wild type and mutated substrates.

distant from the H56 $L_{155}E$ or the $Y_{81}E$ substitutions (Fig. 4 and Supplementary Fig. 2).

The H56 $L_{155}E$ substitution decelerated the degradation of the synthetic substrate (Fig. 4A), which partially hampered the amount of the epitope $H56_{146\text{-}154}$ IYAGLSAL (Fig. 4B) and its potential precursor $H56_{140\text{-}154}$ (Fig. 4C), which was also produced *in vitro*. The altered substrate degradation was likely the only factor influencing the epitope and precursor generation since the epitope generation efficiency was unaffected (Fig. 4D). On the contrary, the $Y_{81}E$ substitution enhanced the substrate degradation rate (Fig. 4E), the amount of the epitope $H56_{72\text{-}80}$ MPVGGQSSF (identified only in the mutated substrate $H56_{64\text{-}86}$ digestion; Fig. 4F) and of its N-extended potential precursors $H56_{69\text{-}80}$ and $H56_{71\text{-}80}$ (Fig. 4G). In contrast to the other epitopes the substitution in this case directly improved not only the absolute amount of the N-extended potential precursor but also its generation efficiency (Fig. 4H). Of note, N-extended versions of other self and virus epitopes have been demonstrated to be able to trigger a $CD8^+$ T cell response even in absence of N-terminal trimming [26, 42]. This *in vitro* quantitative analysis could thus explain the enhanced *in vivo* responses to E-flanked $H56_{72\text{-}80}$ MPVGGQSSF.

Discussion

Most vaccines aim to induce humoral responses, with immune protection mediated by neutralizing antibodies. In a number of diseases caused by intracellular pathogens, such vaccines provide insufficient protection. Because $CD8^+$ T cells can provide protection in these cases, novel vaccination strategies are developed allowing the induction of effective $CD8^+$ T cell responses. Modulation of antigen processing represents a strategy to enhance vaccine efficacy and here we report its applicability. In the model antigen H56 seven epitopes ($H56_{62\text{-}70}$ WYYQSGLSI, $H56_{95\text{-}103}$ QTYKWETFL, $H56_{161\text{-}169}$ MGPSLIGLA, $H56_{309\text{-}316}$ VTSIHSLL, $H56_{354\text{-}363}$ NALQNLARTI, $H56_{427\text{-}434}$ SQFTFSSR, $H56_{443\text{-}451}$ AGQSWCAIL) were discovered. Among them one – *i.e.* the epitope $H56_{62\text{-}70}$ WYYQSGLSI - was found as an epitope presented by HLA-A*24:02 MHC class I molecules [43]. The processing of H56 was altered in order to increase immunogenicity. We report that fusion of H56 cDNA to cDNA encoding TTFC or UB (Fig. 2) alone or in combination with a change of the (hydrophobic) C-terminal epitope flanking residues to polar residues, improves the vaccine-induced epitope specific $CD8^+$ T cell response (Fig. 3 and Fig. 4).

Numerous methods to enhance DNA vaccine potency have been reported in recent years, either by co-delivery of chemokines [44], TLR agonists [45] or co-stimulatory genes [46]. In the current study we report fusion to UB or TTFC to enhance immunogenicity. TTFC domain 1 has been shown to increase immunogenicity [27, 28, 47] and was therefore used in the current study to discover novel epitopes since H56 in itself is poorly immunogenic in cDNA tattoo immunization (Fig. 2C). We have no indications that TTFC affects the specificity of induced $CD8^+$ T cell responses, since (i) the known epitopes $H56_{146\text{-}154}$ IYAGLSAL and $H56_{72\text{-}80}$ MPVGGQSSF [31-33] were confirmed in our study, and (ii) immunization with the pVAX_H56 construct induced similar responses as immunization with the pVAX_TTFC_H56 fusion construct, but percentages of epitope specific $CD8^+$ T cells were very low. The immunogenicity enhancing properties of TTFC is likely due to peptide P30 ($TTFC_{91\text{-}111}$) which contains multiple DR- and DP presented $CD4^+$ T cell epitopes [34, 48] as well as mouse MHC class II presented epitopes [28]. $CD4^+$ T cell help is crucial for $CD8^+$ T cell responses in DNA vaccination [27, 28, 49]. In our study, we even found TTFC to be able to enhance the H56 specific $CD4^+$ T cell response. UB naturally does not contain $CD4^+$ T cell epitopes but was able to enhance H56 specific $CD4^+$ T cells in the current study, as shown before for viral antigens [36]. This immunogenicity enhancement might be due to modified degradation kinetics when an antigen is fused to UB [29] but also to a different antigen routing in cross-presenting professional antigen presentation cells, thereby leading to improved $CD4^+$ and $CD8^+$ T cell priming.

Besides by linkage to immunogenicity-enhancing sequences, a more immediate way of modulating antigen processing is directly influencing the cleavage by the proteasome by alteration of C-terminal flanking residues of epitopes. This can be tested accurately *in vitro*. Correlations between quantitative analysis of *in vitro* proteasome-mediated digestions and *in vivo* data have been shown [6, 41, 50] and are confirmed in this study. Noteworthy however, the E-substitutions in the mutated version had unpredictable effects on the usage of substrate cleavage-sites distant to the substitution and the substrate turnover as demonstrated in other examples [26, 51]. This can be caused by substitution-dependent alterations of the substrate transport in the proteasome cavity or the regulation of non-catalytic modifier sites, which have been described as driving factors of proteasomal dynamics [5].

In the current study an *Mtb* antigen was used as a model vaccine antigen but the proven strategies could be of help in vaccination against actual *Mtb* infection as well. Super immunogenic epitopes derived from conserved antigens, that induce vigorous responses associated with inflammation, immunopathology, and lung

cavitation can be crucial for existence and transmission of *Mtb* [52-54]. It was therefore suggested to focus on variable antigens and target cryptic- or subdominant epitopes [54]. In mice a reduction in *Mtb* bacterial load has already been shown following vaccination with different subdominant antigens in glucopyranosyl lipid adjuvant in stable emulsion [55]. $CD8^+$ T cells specific for a selection of the novel (subdominant) epitopes showed killing capacity until day 26 in this study. Whether these $CD8^+$ T cell populations are effectively reactivated upon exposure with the pathogen remains to be determined. It should be noted however that, contrary to mice in which, depending on the strain, $CD4^+$ or $CD8^+$ T cells control infection [31], in humans multifunctional $CD4^+$ T cells seem to be more important than $CD8^+$ T cells, as illustrated by findings that *Mtb*-infected HIV patients that lack $CD4^+$ but still possess $CD8^+$ T cells rapidly succumb to infection [56, 57]. When, as is the case in the current study, sufficient $CD4^+$ T cell help is provided to the $CD8^+$ T cells by successful vaccine design, vaccine improvement by eliciting $CD8^+$ T cell responses specific for subdominant epitopes could increase *Mtb* vaccine efficacy.

Acknowledgments

Support was by European Union's Seventh Framework Program [FP7/2007-2013] - Grant No. 280873 ADITEC to A.S., BIH CRG1-TP1 and Einstein Stiftung Berlin (A2013-174) to P-M.K. We thank dr. I. Ludwig, D. Janssen, and K. Textoris-Taube for technical assistance. The codon optimized version of H56 and mouse invariant chain were kindly provided by Dr. A. Cara, UB and FAT10 by Dr. F. Ebstein, TTFC by Prof. T.N.M. Schumacher and the peptides by Dr. P. Henklein, P. Kunert and B. Brecht-Jachan.

Abbreviations

FAT10	HLA-F-adjacent transcript 10
LC-MS	Liquid-chromatography mass spectrometry
mLi	Mouse invariant chain
Mtb	*Mycobacterium tuberculosis*
TTFC	Tetanus toxin fragment C
UB	Ubiquitin

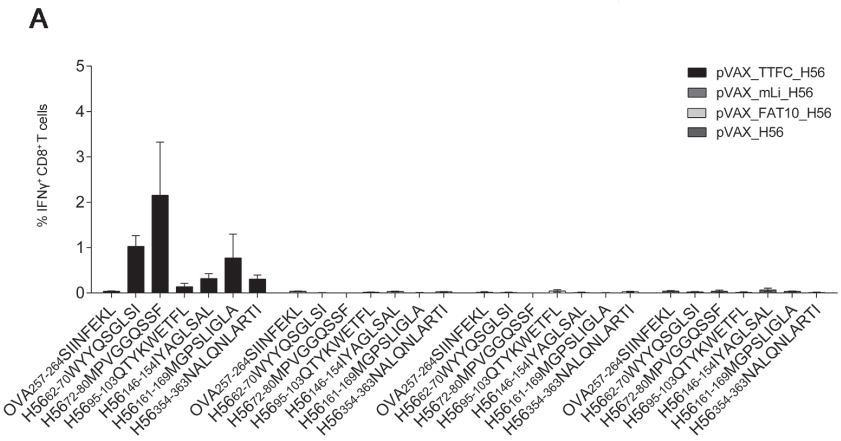

Supplementary figure 1. H56-specific CD8⁺ and CD4⁺ T cell responses in tattoo-immunized mice. (**A, B**) Groups of 5 female CB6F1 mice were immunized with the indicated constructs using dermal DNA tattoo immunization and at day 17 splenocytes were harvested and re-stimulated *ex vivo* with (**A**) $H56_{95\text{-}103}$ QTYKWETFL, $H56_{354\text{-}363}$ NALQNLARTI, $H56_{146\text{-}154}$ IYAGLSAL, $H56_{161\text{-}169}$ MGPSLIGLA, $H56_{62\text{-}70}$ WYYQSGLSI, $H56_{72\text{-}80}$ MPVGGQSSF or without peptide or (**B**) $H56_{288\text{-}307}$ MTEQQWNFAGIEAAASAIQG or $H56_{2428\text{-}262}$ FQDAYNAAGGHNAVFNFPPNG and then stained with fluorochrome-conjugated mAbs to detect CD8 and CD_4 cell surface expression and intracellular IFNγ. Representative FACS plots, analyzed with FlowJo software, including percentages of IFNγ⁺ CD8⁺ and IFNγ⁺ CD_4⁺ T cells are shown in Fig. 2A and Fig. 2B, respectively.

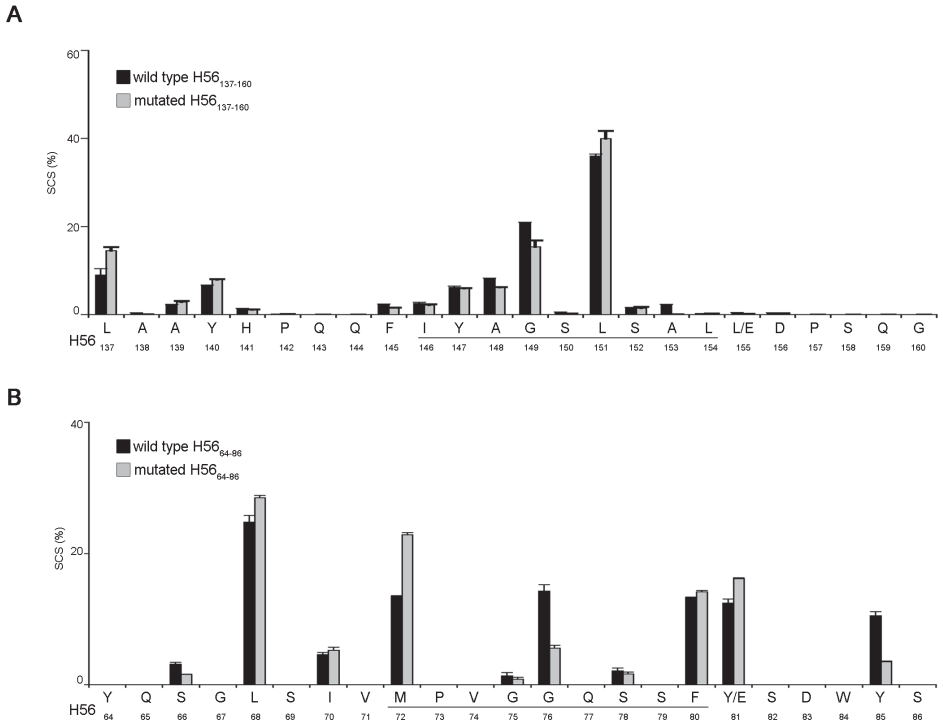

Supplementary figure 2. Relative frequency of proteasome-mediated cleavages in wild type and mutated $H56_{137-160}$ and $H56_{64-86}$ substrates. (**A, B**) The site-specific cleavage strength (SCS), which describes the relative frequency of proteasome-mediated cleavage after any given residue of the synthetic polypeptide substrate 24, in wild type and mutated (**A**) $H_{56137-160}$ and (**B**) $H56_{64-86}$ substrates detected following *in vitro* digestion with purified mouse 20S proteasomes is shown. For the SCS computation we applied the QME method to the pool of peptides common to the wild type and mutated substrates as explained elsewhere [26]. The values are the average and bars the SD of 2 measurements and of 4 time points of a representative assay. The epitopes $H56_{146-154}$ and $H56_{72-80}$ are marked by a line.

4

References

1. Kloetzel, P. -. Antigen processing by the proteasome. *Nat. Rev. Mol. Cell Biol.* **2**, 179-187 (2001).
2. Rock, K. L., York, I. A., Saric, T. & Goldberg, A. L. Protein degradation and the generation of MHC class I-presented peptides. *Advances in Immunology* **80**, 1-70 (2002).
3. Sijts, E. J. A. M. & Kloetzel, P. -. The role of the proteasome in the generation of MHC class I ligands and immune responses. *Cellular and Molecular Life Sciences* **68**, 1491-1502 (2011).
4. Aki, M. *et al*. Interferon-γ induces different subunit organizations and functional diversity of proteasomes. *J. Biochem.* **115**, 257-269 (1994).
5. Liepe, J. *et al*. Quantitative time-resolved analysis reveals intricate, differential regulation of standard- and immuno-proteasomes. *eLife; **4**:e07545* (2015).
6. Platteel, A. C. M. *et al*. CD8+ T cells of Listeria monocytogenes-infected mice recognize both linear and spliced proteasome products. *Eur. J. Immunol.* **46**(5):1109-18 (2016).
7. Arciniega, M., Beck, P., Lange, O. F., Groll, M. & Huber, R. Differential global structural changes in the core particle of yeast and mouse proteasome induced by ligand binding. *Proc. Natl. Acad. Sci. U. S. A.* **111**, 9479-9484 (2014).
8. Ruschak, A. M. & Kay, L. E. Proteasome allostery as a population shift between interchanging conformers. *Proc. Natl. Acad. Sci. U. S. A.* **109**(50):E3454-62 (2012).
9. Mishto, M. *et al*. Immunoproteasome LMP2 60HH variant alters MBP epitope generation and reduces the risk to develop multiple sclerosis in Italian female population. *PLoS ONE* **5**:e9287 (2010).
10. Tregoning, J. S. & Kinnear, E. Using plasmids as DNA vaccines for infectious diseases. *Microbiol. Spectr.* **2**(6)0028-2014 (2014).
11. Le Gall, S., Stamegna, P. & Walker, B. D. Portable flanking sequences modulate CTL epitope processing. *J. Clin. Invest.* **117**, 3563-3575 (2007).

12. Mo, A. X. Y., Van Lelyveld, S. F. L., Craiu, A. & Rock, K. L. Sequences that flank subdominant and cryptic epitopes influence the proteolytic generation of MHC class I-presented peptides. *J. Immunol.* **164,** 4003-4010 (2000).
13. Beekman, N. J. *et al*. Abrogation of CTL epitope processing by single amino acid substitution flanking the C-terminal proteasome cleavage site. *Journal of Immunology* **164,** 1898-1905 (2000).
14. Ossendorp, F. *et al*. A single residue exchange within a viral CTL epitope alters proteasome-mediated degradation resulting in lack of antigen presentation. *Immunity* **5,** 115-124 (1996).
15. Del Val, M., Schlicht, H. -., Ruppert, T., Reddehase, M. J. & Koszinowski, U. H. Efficient processing of an antigenic sequence for presentation by MHC class I molecules depends on its neighboring residues in the protein. *Cell* **66,** 1145-1153 (1991).
16. Seifert, U. *et al*. Hepatitis C virus mutation affects proteasomal epitope processing. *J. Clin. Invest.* **114,** 250-259 (2004).
17. Mishto, M. *et al*. Proteasome isoforms exhibit only quantitative differences in cleavage and epitope generation. *Eur. J. Immunol.* **44,** 3508-3521 (2014).
18. Qazi, K. R. *et al*. Enhancement of DNA vaccine potency by linkage of Plasmodium falciparum malarial antigen gene fused with a fragment of HSP70 gene. *Vaccine* **23,** 1114-1125 (2005).
19. Karwacz, K. *et al*. Nonintegrating lentivector vaccines stimulate prolonged T-cell and antibody responses and are effective in tumor therapy. *J. Virol.* **83,** 3094-3103 (2009).
20. Šmahel, M., Pokorná, D., Macková, J. & Vlasák, J. Enhancement of immunogenicity of HPV16 E7 oncogene by fusion with E. coli ß-glucuronidase. *J. Gene Med.* **6,** 1092-1101 (2004).
21. Aagaard, C. *et al*. A multistage tuberculosis vaccine that confers efficient protection before and after exposure. *Nat. Med.* **17,** 189-195 (2011).
22. Bins, A. D. *et al*. A rapid and potent DNA vaccination strategy defined by in vivo monitoring of antigen expression. *Nat. Med.* **11,** 899-904 (2005).
23. Mishto, M. *et al*. Driving forces of proteasome-catalyzed peptide splicing in yeast and humans. *Molecular and Cellular Proteomics* **11,** 1008-1023 (2012).
24. Liepe, J. *et al*. The 20S proteasome splicing activity discovered by SpliceMet. *PLoS computational biology* **6**(6):e1000830 (2010).
25. Textoris-Taube, K. *et al*. The T210M substitution in the HLA-A*02:01 gp100 epitope strongly affects overall proteasomal cleavage site usage and antigen processing. *J Biol Chem.* **290**(51):30417-28 (2015).
26. Woodworth, J.S., Cohen, S.B., Moguche, A.O., Plumlee, C.R., Agger, E.M., Urdahl, K.B., & Andersen,P. Subunit vaccine H56/CAF01 induces a population of circulating CD4 T cells that traffic into the *Mycobacterium tuberculosis*-infected lung. *Mucosal Immunol.* (**4**) 1933-0219 (2016)
27. Oosterhuis, K. *et al*. Preclinical development of highly effective and safe DNA vaccines directed against HPV 16 E6 and E7. *International Journal of Cancer* **129,** 397-406 (2011).
28. Oosterhuis, K., Aleyd, E., Vrijland, K., Schumacher, T. N. & Haanen, J. B. Rational design of DNA vaccines for the induction of human papillomavirus type 16 E6- and E7-specific cytotoxic T-cell responses. *Hum. Gene Ther.* **23,** 1301-1312 (2012).
29. Ebstein, F., Lehmann, A. & Kloetzel, P. -. The FAT10- and ubiquitin-dependent degradation machineries exhibit common and distinct requirements for MHC class I antigen presentation. *Cell Mol. Life Sci.* **69,** 2443-2454 (2012).
30. Rowe, H. M. *et al*. Immunization with a lentiviral vector stimulates both CD4 and CD8 T cell responses to an ovalbumin transgene. *Mol. Ther.* **13,** 310-319 (2006).

31. Radoševic, K. *et al*. Protective immune responses to a recombinant adenovirus type 35 tuberculosis vaccine in two mouse strains: CD4 and CD8 T-cell epitope mapping and role of gamma interferon. *Infect. Immun.* **75,** 4105-4115 (2007).
32. Denis, O. *et al*. Vaccination with Plasmid DNA Encoding Mycobacterial Antigen 85A Stimulates a CD4+ and CD8+ T-Cell Epitopic Repertoire Broader than That Stimulated by Mycobacterium tuberculosis H37Rv Infection. *Infect. Immun.* **66,** 1527-1533 (1998).
33. D'Souza, S. *et al*. CD4+ T cells contain Mycobacterium tuberculosis infection in the absence of CD8+ T cells in mice vaccinated with DNA encoding Ag85A. *Eur. J. Immunol.* **30,** 2455-2459 (2000).
34. Stevenson, F. K., Rice, J., Ottensmeier, C. H., Thirdborough, S. M. & Zhu, D. DNA fusion gene vaccines against cancer: From the laboratory to the clinic. *Immunol. Rev.* **199,** 156-180 (2004).
35. Brulet, J. -. *et al*. DNA vaccine encoding endosome-targeted human papillomavirus type 16 E7 protein generates CD4+ T cell-dependent protection. *Eur. J. Immunol.* **37,** 376-384 (2007).
36. Rodriguez, F., Zhang, J. & Whitton, J. L. DNA immunization: Ubiquitination of a viral protein enhances cytotoxic T-lymphocyte induction and antiviral protection but abrogates antibody induction. *J. Virol.* **71,** 8497-8503 (1997).
37. Brandt, L., Oettinger, T., Holm, A., Andersen, Å B. & Andersen, P. Key Epitopes on the ESAT-6 Antigen Recognized in Mice during the Recall of Protective Immunity to Mycobacterium tuberculosis. *J. Immunol.* **157,** 3527-3533 (1996).
38. Huygen, K. *et al*. Mapping of TH1 helper T-cell epitopes on major secreted mycobacterial antigen 85A in mice infected with live Mycobacterium bovis BCG. *Infect. Immun.* **62,** 363-370 (1994).
39. Basler, M., Buerger, S. & Groettrup, M. The ubiquitin-like modifier FAT10 in antigen processing and antimicrobial defense. *Mol. Immunol.* **68,** 129-132 (2015).
40. Chapiro, J. *et al*. Destructive cleavage of antigenic peptides either by the immunoproteasome or by the standard proteasome results in differential antigen presentation. *Journal of Immunology* **176,** 1053-1061 (2006).
41. Ebstein, F. *et al*. Proteasomes generate spliced epitopes by two different mechanisms and as efficiently as non-spliced epitopes. *Sci. Rep.* **6,** 24032 (2016).
42. Tenzer, S. *et al*. Antigen processing influences HIV-specific cytotoxic T lymphocyte immunodominance. *Nat. Immunol.* **10,** 636-646 (2009).
43. Weichold, F. F. *et al*. Impact of MHC class I alleles on the M. tuberculosis antigen-specific CD8+ T-cell response in patients with pulmonary tuberculosis. *Genes Immun.* **8,** 334-343 (2007).
44. Kutzler, M. A. *et al*. Plasmids encoding the mucosal chemokines CCL27 and CCL28 are effective adjuvants in eliciting antigen-specific immunity in vivo. *Gene Ther.* **17,** 72-82 (2010).
45. Schneeberger, A. *et al*. CpG motifs are efficient adjuvants for DNA cancer vaccines. *J. Invest. Dermatol.* **123,** 371-379 (2004).
46. Iwasaki, A., Stiernholm, B. J. N., Chan, A. K., Berinstein, N. L. & Barber, B. H. Enhanced CTL Responses Mediated by Plasmid DNA Immunogens Encoding Costimulatory Molecules and Cytokines. *J. Immunol.* **158,** 4591-4601 (1997).
47. Oosterhuis, K., Van Den Berg, J. H., Schumacher, T. N. & Haanen, J. B. A. G. DNA vaccines and intradermal vaccination by DNA tattooing. *Curr. Top. Microbiol. Immunol.* **351,** 221-250 (2012).
48. Panina-Bordignon, P. *et al*. Universally immunogenic T cell epitopes: Promiscuous binding to human MHC class II and promiscuous recognition by T cells. *Eur. J. Immunol.* **19,** 2237-2242 (1989).

49. Wolkers, M. C., Toebes, M., Okabe, M., Haanen, J. B. A. G. & Schumacher, T. N. M. Optimizing the efficacy of epitope-directed DNA vaccination. *J. Immunol.* **168**, 4998-5004 (2002).
50. Deol, P., Zaiss, D. M. W., Monaco, J. J. & Sijts, A. J. A. M. Rates of processing determine the immunogenicity of immunoproteasome-generated epitopes. *Journal of Immunology* **178**, 7557-7562 (2007).
51. Tenzer, S. *et al*. Antigen processing influences HIV-specific cytotoxic T lymphocyte immunodominance. *Nat. Immunol.* **10**, 636-646 (2009).
52. Coscolla, M. *et al*. M. tuberculosis T cell epitope analysis reveals paucity of antigenic variation and identifies rare variable TB antigens. *Cell Host and Microbe* **18**, 538-548 (2015).
53. Dorhoi, A. & Kaufmann, S. H. E. Pathology and immune reactivity: understanding multidimensionality in pulmonary tuberculosis. *Semin. Immunopathol.* **38**(2):153-66 (2015).
54. Woodworth, J. S. & Andersen, P. Reprogramming the T Cell Response to Tuberculosis. *Trends Immunol.* **37** 81-83 (2016).
55. Orr, M. T. *et al*. Immune subdominant antigens as vaccine candidates against Mycobacterium tuberculosis. *J. Immunol.* **193**, 2911-2918 (2014).
56. Burman, W. J. & Jones, B. E. Clinical and Radiographic Features of HIV-Related Tuberculosis. *Semin. Respir. Infect.* **18**, 263-271 (2003).
57. Geldmacher, C. *et al*. Preferential infection and depletion of Mycobacterium tuberculosis-specific CD4 T cells after HIV-1 infection. *J. Exp. Med.* **207**, 2869-2881 (2010).
58. Peters, B. & Sette, A. Integrating epitope data into the emerging web of biomedical knowledge resources. *Nature Reviews Immunology* **7**, 485-490 (2007).

Efficacy of heterologous prime-boost vaccination using dermal H56 cDNA tattoo immunization and subcutaneous injection of BCG *::H56* against *Mycobacterium tuberculosis*

5

Anouk C.M. Platteel[1,*], Natalie Nieuwenhuizen[2,*], Teresa Domaszewska[2], Alexis Vogelzang[2], Stefanie Scheurer[2], Ulrike Zedler[2], January Weiner[2], Martin Gengenbacher[3], Alice J.A.M. Sijts[1] and Stefan H.E. Kaufmann[2]

[1] Department of Infectious Diseases and Immunology, Faculty of Veterinary Medicine, Utrecht University, Utrecht, The Netherlands.
[2] Department of Immunology, Max Planck Institute for Infection Biology, Berlin, Germany.
[3] Department of Microbiology, National University of Singapore, Singapore.

* These authors contributed equally

Abstract

Tuberculosis (TB), caused by *Mycobacterium tuberculosis* (*Mtb*), remains a global health threat. *Mycobacterium bovis* bacillus Calmette-Guérin (BCG) was introduced as a vaccine in 1924 but lacks efficacy. Several antigens can be used to boost the effect of BCG, such as the multistage vaccine H56, which encodes Ag85B, ESAT-6 and Rv2660c of *Mtb*. In this study we tested different heterologous and homologous prime-boost strategies, based on subcutaneous injection of BCG and dermal H56 cDNA tattoo immunization, for their ability to boost *Mtb*-specific immune protection. We measured cellular- and humoral immune responses and correlated this to protective efficacy in a challenge model. Dermal H56 cDNA tattoo immunization induced mainly H56-specific $CD4^+$ and $CD8^+$ T cell responses, H56-specific IgG1 and expanded the $CD4^+ T_{CM}$ cell population. BCG immunization resulted in a broad cellular response, with increased frequencies of $CD4^+ T_{EM}$ cells, as well as an *Mtb* lysate-specific IgG1 and IgG2c responses. When combining these immunizations we found that the order in which the immunizations are given is important. The most promising reduction in bacterial loads in spleens was measured in mice primed by H56 cDNA *i.d.* and boosted with BCG *::H56 s.c.*, while immunizations in reverse order were less effective. Additionally, this H56 cDNA *i.d.*/BCG *::H56 s.c.* prime-boost group, as well as mice vaccinated with homologous BCG *::H56* in prime-boost showed a slight trend towards decreased bacterial loads compared to the standard, BCG vaccination. These results will contribute to successful vaccination against *Mtb*.

Introduction

Tuberculosis (TB) remains a global health threat, with 9.6 million infections and 1.5 million deaths reported in 2014 [1, 2]. An attenuated form of the causative agent of bovine tuberculosis known as *M. bovis* bacillus Calmette-Guérin (BCG) was introduced as a live vaccine in 1924 and is widely administered in TB endemic countries [3]. BCG has contributed to a reduction in childhood mortality [4] and provides protection against TB meningitis and other forms of disseminated TB. However, it is clear that BCG fails to adequately protect against the pulmonary form of disease [5]. As BCG is given at birth throughout the developing world, a new TB vaccine for children should take into account the fact that the majority of the population has already been BCG-vaccinated. For these reasons, new vaccine strategies aim to improve the efficacy of BCG by modifying it, combining it with boosting vaccines, administering it with different adjuvants or altering the route of vaccination [6-11].

A crucial starting point in improving vaccine strategies is knowledge of immune responses that correlate with protection in *Mycobacterium tuberculosis (Mtb)* infection. However, the precise mechanisms of *Mtb* control are not known. Nevertheless, it is known that the cellular response is important, as shown in reports studying the efficacy of recombinant BCG strains expressing the *hly* gene encoding for listeriolysin O (LLO) from *Listeria monocytogenes,* in combination with the deletion of urease C, which provides a pH closer to that optimal for LLO activity [12-14]. It was shown in vaccination studies with this BCG Δ*ureC::hly* that central memory $CD4^+$ T cells (T_{CM}), which secrete cytokines such as IFNγ, IL-2 and TNFα, are important in protecting against infection [13]. Additionally, BCG Δ*ureC::hly*Δ*nuoG* vaccinated mice, which were more protected than BCG Δ*ureC::hly* vaccinated mice, had relatively increased effector memory $CD4^+$ T cells (T_{EM}), T follicular helper cells (T_{FH}) and germinal center B cells [14]. In other studies, Ag85B-specific $CD4^+$ T_{EM} were also shown to control infection in the lungs [15]. Next to the $CD4^+$ T cells, $CD8^+$ T cells also appeared to protect against *Mtb* [16-19]. Additionally, there are studies that report about the role of B cells and antibodies in tuberculosis [20, 21]. However, although vaccination with the more protective BCG Δ*ureC::hly* strain leads to increased antibody responses in mice, passive transfer of serum from mice vaccinated with BCG Δ*ureC::hly* into naive mice did not increase protection to tuberculosis in initial studies [13].

Next to genetic modification by insertion of *hly* or deletion of *ureC* or *nuoG*, efficacy of BCG can also be increased by use of adjuvants or boosting with

antigens encoding *Mtb* proteins [6, 7, 9, 11]. Aagaard et al. [22] created the multistage vaccine H56, which is composed of three antigens of *Mtb*: Ag85B, ESAT-6 and Rv2660c. Ag85B and ESAT-6 are both immunogenic proteins (with Ag85B also being present in BCG) and are secreted early in infection [23], while Rv2660c is a latency-associated secretory protein[24]. As part of the ADITEC vaccine consortium [25], H56 was chosen as a model antigen for testing of different vector vaccines, adjuvants and vaccination strategies. When administered with adjuvant CAF01[26, 27, 28] or IC31[28, 29], vaccination with H56 or H56-derived antigens, protected against *Mtb* infection in mice. Recently, Platteel et al. [30] showed that dermal tattoo administration [31] of H56 cDNA fused to tetanus toxin fragment C (TTFC) cDNA elicited vigorous antigen-specific $CD4^+$ T cell and $CD8^+$ T cell responses targeted to H56, without the need for adjuvants.

In the present study we aimed to compare the efficacy of dermal DNA tattoo immunization to that of BCG immunization, and of different heterologous and homologous prime-boost strategies using dermal H56 cDNA tattoo immunization in combination with subcutaneous injection of BCG or BCG *::H56* [32] *in vivo*. Protective capacity in *M. tuberculosis* infection, and correlates of the induced, specific immune responses were determined.

Materials and methods

Mice

Six to eight weeks old CB6F1 mice were purchased from Charles River. All animal studies were ethically approved by the State Office for Health and Social Services, Berlin, Germany. We designed two protocols, one for single vaccination and one for prime-boost vaccination, each consisting of twenty mice divided into two groups of ten for manageability and performed in two separate experiments.

DNA and dermal DNA tattoo vaccination

The full length H56 cDNA [22] was codon optimized and consists of tetanus toxin fragment C domain 1 (TTFC) [33, 34] in pVAX1 vector (Invitrogen) as described before [30]. DNA tattoo immunization was performed with 15 µl cDNA (2 µg/µl) in TE buffer with a 9-needle bar mounted on a tattoo rotary device (Cheyenne) on 100 Hz, at 1 mm depth for 1 minute [31] under isoflurane anesthesia.

BCG vaccination and *M. tuberculosis* challenge

The *M. tuberculosis* H37Rv (American Type Culture Collection; catalog no. 27294), BCG Danish 1331 (BCG SSI) (American Type Culture Collection; catalog no. 35733) and BCG *::H56* [32] (made in house, on BCG SSI background), were grown in Middlebrook 7H9 broth (BD) supplemented with albumin-dextrose-catalase enrichment (BD), 0.2% glycerol, and 0.05% Tween 80 or on Middlebrook 7H11 agar (BD) containing 10% (vol/vol) oleic acid-albumin-dextrose-catalase enrichment (BD) and 0.2% glycerol. BCG and BCG *::H56* were grown to mid-log phase, washed with phosphate-buffered saline (PBS) and stored at 80°C in PBS-10% glycerol until vaccination for which they were administered with a dose of 10^6 CFU in PBS for both subcutaneous and dermal routes. Aerosol challenge with *M. tuberculosis* was performed using a dose of 20-50 CFU.

Vaccine efficacy studies

For measurements of the bacterial load, lungs and spleens were harvested and serial dilutions were performed in PBS-0.05% Tween 80 (PBST) and plated on Middlebrook 7H11 agar.

Peptides

All peptides were synthesized using Fmoc solid phase chemistry. The sequence enumeration of the synthetic peptides referred to the vaccine H56 [22]. The eighty-five 15mer peptides used as pool to measure the total amount of H56-specific T cells (provided as a kind gift from Dr Donatella Negri) spanned the entire amino-acid sequence of H56, overlapping by 10 amino acid residues, and were synthesized by PRIMM srl.

Analysis of specific $CD8^+$ and $CD4^+$ T cell responses using intracellular cytokine staining

For intracellular cytokine production, splenocytes were plated overnight with or without 1 µg/ml peptide at 37°C. During the last 4 hrs, brefeldin (5µg/ml, Sigma) was added to wells incubated with peptide or phorbal myristate acetate (50 ng/mL, Sigma) and ionomycin (250 ng/mL, Sigma) or to cells incubated with medium alone. Cells then were stained for the cell surface markers named below, fixed with 2% paraformaldehyde, permeabilized with saponin buffer (saponin, 1 g/liter; CaCl 2, 0.11 g/liter; $MgSO_4$, 0.125 g/liter; NaN_3 , 0.5 g/liter; bovine serum albumin [BSA] 1 g/liter; 10 mM HEPES in PBS, pH 7.4), and stained for intracellular cytokine production as described [30]. The cell surface- and intracellular cytokine panel consisted of TCRβ-A700 (Biolegend; clone H57-597), CD_4-Pacific Blue (Biolegend; clone GK1.5), CD8-PerCP (Biolegend; clone 53-6.7), IL2-APC (Biolegend; clone

JES6-5H4), IFNγ-PE-Cy7 (Biolegend; clone XMG1.2), IL17-PE (Biologend; clone TC11-18H10.1), TNFα-FITC (homemade; clone YT-22). Samples were acquired on a LSR II cytometer (BD Biosciences) with BD FACS Diva software and analyzed using FlowJo v10 (TreeStar).

Analysis of specific CD8$^+$ T cell responses by IFNγ ELISpot

Multiscreen ELISPOT plates (Millipore) were coated with 2 µg/ml AN18 in PBS overnight at 4 °C. Wells were washed and blocked with 5% BSA/PBS. 5 x 10^5 erythrocyte depleted lymph node cells were plated with or without 1 µg/ml synthetic peptide overnight in IMDM with 10% fetal calf serum (FCS) Pen-Strep at 37 °C. Plates were washed with PBS plus 0.01% Tween 20 (PBS-T), and IFNγ was detected with biotinylated IFNγ (homemade; clone XMG1.2), followed by alkaline phosphatase-conjugated streptavidin (home-made), in PBS-T supplemented with 2% BSA. The assay was developed with NBT/BCIP substrate (Thermo fisher scientific) and analyzed using an Immunopost S6 Ultra-V Analyzer (CTL).

Analysis of T and B cell sub-populations

Spleens were collected and single-cell suspensions were generated in Iscove's modified Dulbecco's medium (IMDM) 10% fetal calf serum (FCS) Pen-Strep. Cells were surface stained to quantify cell populations. T cell panel: CD3-Alexa 700 (BioLegend; clone 17A2), CD4-PE-Cy7 (BioLegend; clone RM4-5), CD8-V500 (BD Horizon, clone 53-6.7), CD62L-APC (BD Pharmingen; clone MEL-14), CD44-Pacific Blue (homemade, clone IM7), CXCR5-PE (BioLegend; clone J252D4), CCR7-PerCP (BioLegend; clone 4B12), PD-1-FITC (BioLegend; clone 29F.1A12), KLRG1-CF594 (BD, clone 2F1). B cell panel: B220-PE (BioLegend; clone RA3-6B2), CD38 APC (BioLegend; clone 90), Fas-PE-Cy7 (BioLegend; clone Jo2), GL7-FITC (BioLegend; clone GL7), MHC II-Pacific Blue (BioLegend; clone M5/114.15.2), CD19-A700 (BioLegend; clone 6D5), CD138-Percp (BioLegend; clone 281-2). Central memory CD4$^+$ T cells were CD3$^+$ CD4$^+$ CD44^{high} CD62^{high}, effector memory CD4$^+$ T cells were CD3$^+$ CD4$^+$ CD44^{high} CD62L^{low}, T follicular helper cells were CD3$^+$ CD4$^+$ CXCR5$^+$ PD-1$^+$, germinal center B cells were B220$^+$ CD19$^+$ GL7$^+$ Fas$^+$ and plasma cells CD138$^+$ CD38$^+$.

Specific antibody responses

Mycobacterium-, Ag85B- and ESAT-6-specific antibodies in serum were measured by indirect enzyme-linked immunosorbent assay (ELISA) using *M. tuberculosis* H37Rv lysate (BEI Resources), Ag85B (BEI Resources), or ESAT-6 (BEI Resources) to coat and alkaline-phosphatase (AP) labelled anti-mouse IgG1 and IgG2c for detection (SouthernBiotech).

Heat maps

The scripts for figures 1, 4, S1 and S4 are available upon request. FACS data visualization was designed using R-package ggplot2 (v2.1.0; Springer-Verlag New York, 2009.) in R programming language (v3.2.3; R Development Core Team (2008)). The mean values of percentages of $CD4^+$ or $CD8^+$ T cells producing cytokines after peptide stimulation were normalized to control samples stimulated with medium and visualized using heat maps. ELISpot data visualization was designed using R-package ggplot2 (v2.1.0; Springer-Verlag New York, 2009) in R programming language (v3.2.3; R Development Core Team (2008)). The mean numbers of IFNγ producing cells per million cells after peptide stimulation were normalized to control samples stimulated with medium. For visualization purposes, the mean value for each experimental condition was transformed to square root of mean response signal and displayed as a heat map.

Statistics

Data were tested for normality distribution and homoscedasticity by Kolmogorov-Smirnov, Shapiro-Wilk and Levene tests. To identify differences between groups for the T- and B cell panels and humoral responses, data were analyzed using a one-way ANOVA with Tukey's post hoc correction. $P < 0.05$ was considered to be significant.

Results

Vaccination with dermal DNA tattoo immunization or subcutaneous injection with BCG induces different H56-specific T cell responses

We first measured the immune responses after a single vaccination with BCG or H56 cDNA (Fig.1A). Subcutaneous (*s.c.*) injection with BCG is known to lead to an approximately 1 log protection in mouse models [35, 36] and was included as the standard against which the efficacy of BCG *::H56* or dermal tattoo immunization (*i.d.*) with BCG or DNA were compared. The DNA vaccines included the canonical versions of H56 and H56_E, in which six $CD8^+$ T cell epitopes have been optimized to enhance proteasome-mediated processing [30], and were administered at day 0, 3 and 6. The two BCG strains were administered by *s.c.* injection at day 0 (Fig. 1A). One group of mice was also vaccinated by tattoo immunization with BCG (day 0 only), in order to compare *s.c.* and *i.d.* administration of BCG. Immune responses were measured at day 21 and the efficacy of the methods was tested by subjecting the mice to an aerosol challenge with *Mtb* at day 60 (Fig. 1A).

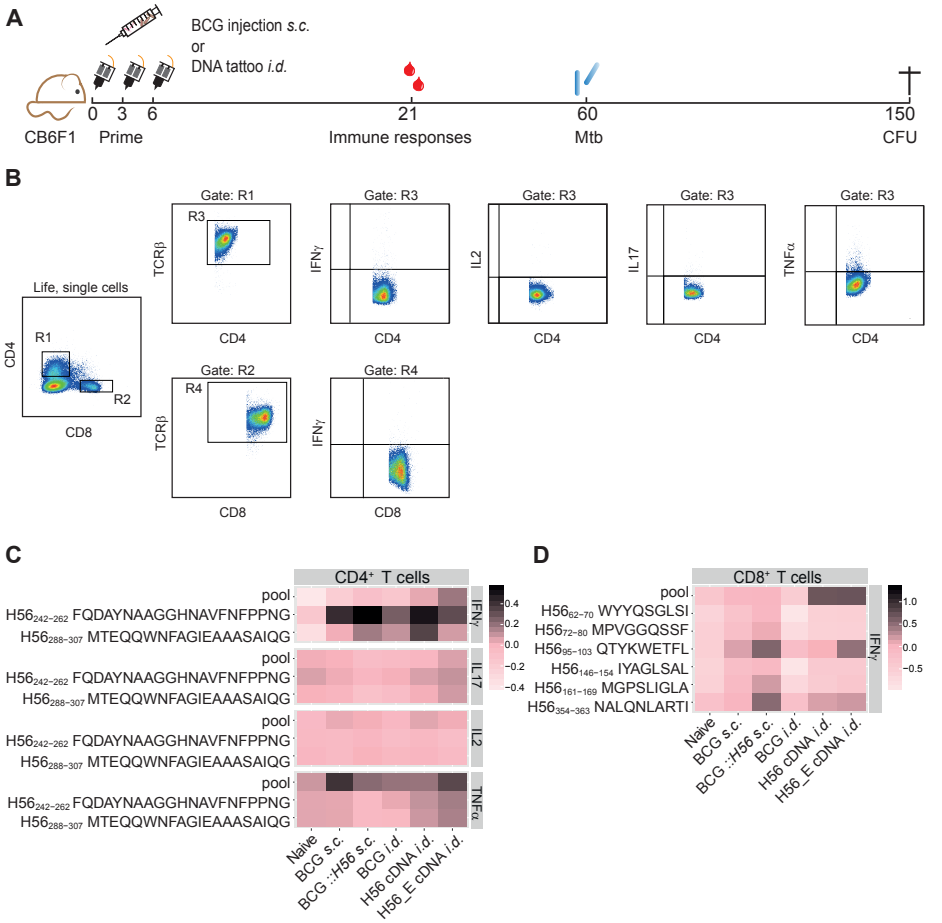

Fig. 1. Vaccination with dermal H56 or H56_E cDNA tattoo immunization or subcutaneous injection with BCG induces different H56 specific $CD4^+$ and $CD8^+$ T cell responses. Intracellular cytokine staining was performed on splenocytes harvested at day 21 post vaccination and re-stimulated with different H56 peptides. The peptide pools consisted of eighty-five 15-mer peptides spanning the entire sequence of H56, as a measure of the total percentage of H56-antigen specific cells. $CD4^+$ T cell epitopes included $H56_{242-262}$ (Ag85B derived) and $H56_{288-307}$ (ESAT-6 derived). The $CD8^+$ T cell epitopes included $H56_{354-363}$ (ESAT-6 derived) and five epitopes of Ag85B. Analysis was done using FACS. The results show pooled data from two independent experiments (n=10 in total). (**A**) Immunization scheme. (**B**) Gating strategy for FACS analysis. After gating on live, single cells, cells were gated on $CD4^+$ (R1) or $CD8^+$ (R2). Both R1 and R2 were gated on $TCR\beta^+$ cells (R3) and (R4). (**C**) Heat maps showing mean frequency of $CD4^+$ T cells secreting IFNγ, IL-17, IL-2 or TNFα after peptide stimulation, normalized to medium incubated cells. (**D**) Heat maps showing mean frequency of $CD8^+$ T cells secreting IFNγ, IL-17, IL-2 or TNFα after peptide stimulation, normalized to medium incubated cells.

To study H56-specific cellular responses, splenocytes or lymphocytes from vaccinated mice were re-stimulated *ex vivo* with Ag85B- and ESAT6-derived $CD8^+$ [30] and $CD4^+$ [37, 38] T cell epitopes and responses in the spleen were measured using ICS and flow cytometry (Fig. 1B) or in the draining lymph nodes by IFNγ ELISpot (Fig. S1). The mean values of percentages of $CD4^+$ or $CD8^+$ T cells producing cytokines after peptide stimulation were normalized to control samples stimulated with medium and were visualized using heat maps (Fig 1C-D). Incubation of splenocytes with the pool of 15-mers overlapping the H56 sequence mostly induced IFNγ production by $CD4^+$ T cells from H56 and H56_E *i.d.* vaccinated mice which illustrates the total amount of H56-specific $CD4^+$ T cells. When looking to single epitope specific cells, we found that $CD4^+$ T cells from all vaccinated mice responded to the Ag85B-derived $H56_{242-262}$ epitope, mainly by production of IFNγ (Fig. 1C). ESAT-6-derived $H56_{288-307}$ was recognized by cells from the H56 cDNA *i.d.* and BCG *::H56 s.c.* vaccinated mice while dermal tattoo immunization or subcutaneous injection with BCG did not generate $CD4^+$ T cells recognizing this epitope because it is derived from ESAT-6, which is not present in BCG. A strong H56-specific response in H56 or H56_E cDNA *i.d.* vaccinated mice was also observed in IFNγ ELISpot analyses of lymph node cells (Fig. S1). No differences in IL-17 and IL-2 secretion by spleen $CD4^+$ T cells were detected between the groups (Fig 1C). TNFα production was strongest in $CD4^+$ T cells of mice vaccinated with H56_E DNA *i.d.* Since most TNFα production was measured after *ex vivo* incubation with the pool of 15-mers derived from H56, the two individual epitopes studied were not responsible for the activation of the majority of specific $CD4^+$ T cells. In agreement to IFNγ production as a result of incubation with the pool of peptides by $CD4^+$ T cells (Fig. 1C) and IFNγ ELISpot (Fig. S1), the H56 and H56_E *i.d.* vaccination regimens induced the highest percentages of total H56-specific cells (Fig.1D). Single H56 epitope specific $CD8^+$ T cells were activated by all the vaccines containing H56 (Fig. 1D), *i.e.* BCG *::H56*, H56 cDNA and H56_E cDNA. All $CD8^+$ T cell epitopes were derived from Ag85B except for $H56_{354-363}$ which was derived from ESAT-6 and hence was not recognized by $CD8^+$ T cells from mice vaccinated *s.c.* or *i.d.*, with BCG. Taken together these results show that dermal H56 cDNA tattoo immunization mainly induces H56-specific $CD4^+$ and $CD8^+$ T cells while BCG activates T cells specific for Ag85B in H56 because ESAT-6 and Rv2660c are not present.

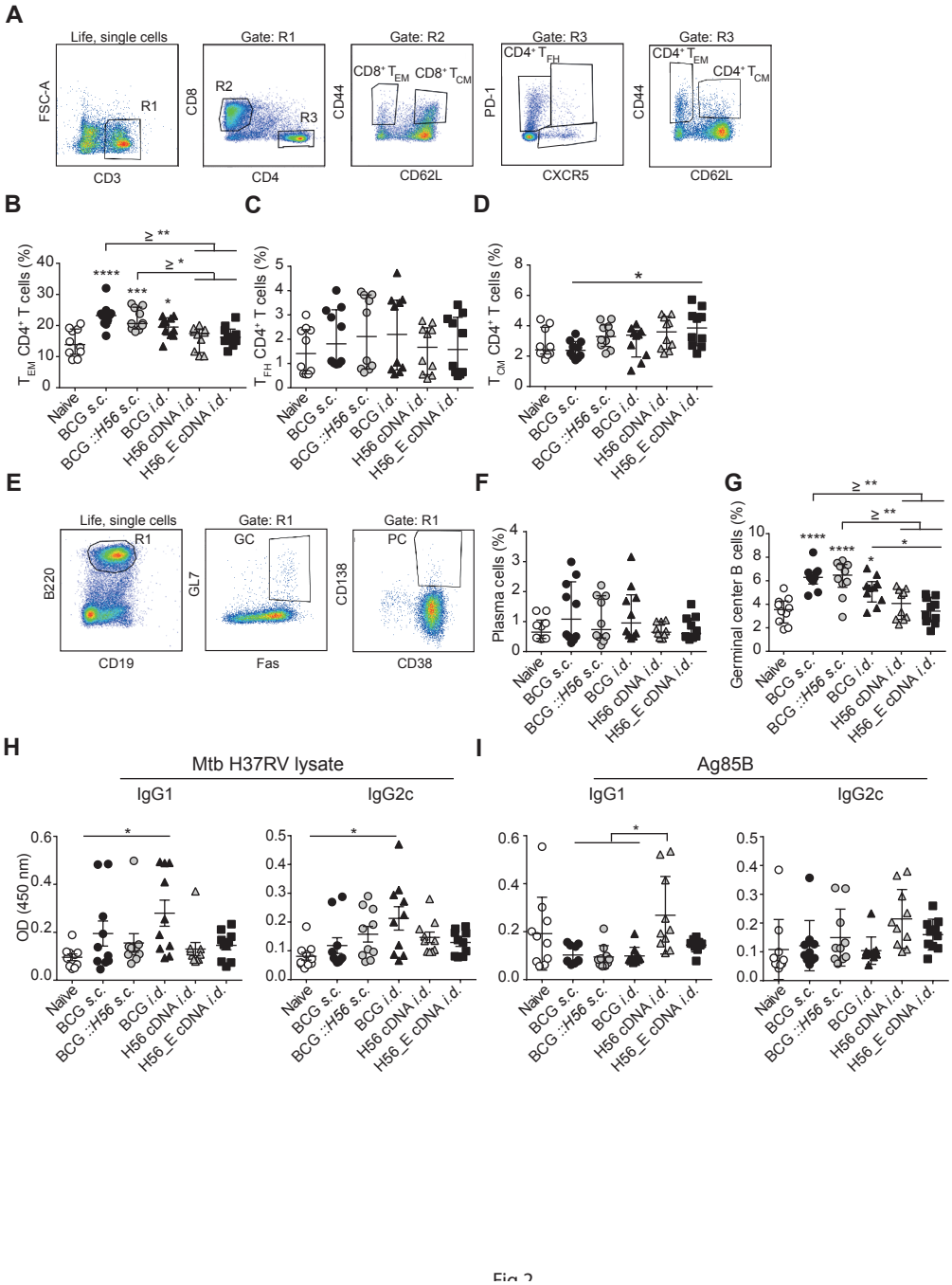
A
Life, single cells
FSC-A
R1
CD3
Gate: R1
CD8
R2
R3
CD4
Gate: R2
CD44
CD8+ TEM
CD8+ TCM
CD62L
Gate: R3
PD-1
CD4+ TFH
CXCR5
Gate: R3
CD44
CD4+ TEM
CD4+ TCM
CD62L
B
TEM CD4+ T cells (%)
C
TFH CD4+ T cells (%)
D
TCM CD4+ T cells (%)
Naive
BCG s.c.
BCG ::H56 s.c.
BCG i.d.
H56 cDNA i.d.
H56_E cDNA i.d.
E
Life, single cells
R1
B220
CD19
Gate: R1
GC
GL7
Fas
Gate: R1
PC
CD138
CD38
F
Plasma cells (%)
G
Germinal center B cells (%)
H
Mtb H37RV lysate
IgG1
IgG2c
OD (450 nm)
I
Ag85B
IgG1
IgG2c

Fig 2

Fig. 2. BCG vaccination induces most $CD4^+$ T_{EM} cells and *Mtb* specific antibodies while H56 cDNA dermal tattoo immunization induces $CD4^+$ T_{CM} cells and Ag85B specific antibodies. Splenocytes or serum collected at day 21 post vaccination and splenocytes were stained for different surface markers and analyzed by FACS and antibodies in serum were analyzed by ELISA. Pooled data of two experiments with (n = 10 in total) is shown ± SEM. (**A**) Gating strategy for FACS analysis for T cell sub-populations. After gating on live, single cells, cells were gated on $CD3^+$ (R1). R1 was gated on $CD8^+$ (R2) or $CD4^+$ (R3). (**B**) Percentage of $CD4^+$ T effector memory (T_{EM}) cells in $CD4^+$ T cell population (**C**) Percentage of $CD4^+$ T follicular helper (T_{FH}) cells in $CD4^+$ T cell population (**D**) Percentage of $CD4^+$ T central memory (T_{CM}) cells in $CD4^+$ T cell population. (**E**) Gating strategy for FACS analysis for B cell sub-populations. After gating on live, single cells, cells were gated on $B220^+$ (R1). (**F**) Percentage of plasma cells in B cell population. (**G**) Percentage of germinal center cells in B cell population. (**H**) *Mtb* lysate specific IgG1 and IgG2c antibody titers. (**I**) Ag85B lysate specific IgG1 and IgG2c antibody titers. (**A-I**) Significant differences between T- or B cell populations or antibody titers of treatment groups compared to the naive group are marked as * and significant differences between the groups with lines (ANOVA with Tukey's multiple comparison test; * $p < 0.05$; ** $p < 0.01$; *** $p < 0.001$; **** $p < 0.0001$; ≥ minimum amount of * for combined indicated groups).

Differential immune responses after vaccination by dermal H56 cDNA tattoo immunization or subcutaneous injection with BCG or BCG *::H56*

In order to gain more information on the type of responses elicited by the different immunization strategies, we measured the T cell memory populations and B cell responses by flow cytometry (Fig. 2A). Compared too naive, and especially H56 cDNA *i.d.* vaccinated mice, *s.c.* vaccination with BCG or BCG *::H56* resulted in the highest percentages of $CD4^+$ T_{EM} cells in the total $CD4^+$ T cell population (Fig. 2B). $CD4^+$ T_{FH} cell showed similar trends (Fig. 2C), while frequencies of $CD4^+$ T_{CM} cells were higher in the DNA *i.d.* vaccinated mice (Fig. 2D). There were no significant differences in frequencies of $CD8^+$ T_{EM} or $CD8^+$ T_{CM} populations between the groups (data not shown).

Humoral responses may contribute towards protection against TB [20, 21]. We measured the frequencies of plasma cells and germinal center cells among the B cells by flow cytometry (Fig. 2E) and specific antibodies by ELISA (Fig. 2H-I). There was a trend towards more plasma cells in mice that were vaccinated with BCG or BCG *::H56* either *s.c.* or *i.d*. (Fig. 2F), and an elevation in the percentages of germinal center B cells in these groups compared to naive animals or mice of other groups (Fig. 2G). In accordance, levels of specific IgG antibodies against

Mtb H37RV lysate (*Mycobacterium* specific antibodies) were increased in these groups (Fig. 2H), suggesting that BCG elicits a broader response as it contains many mycobacterial proteins whereas the DNA vaccines only encode H56. BCG *::H56* appeared to preferentially induce IgG2c rather than IgG1, whereas BCG induced both IgG2c and IgG1. Highest Ag85B specific titers were measured in the groups that had been immunized with H56 cDNA *i.d.* (Fig 2I). ESAT-6 specific antibodies were not detectable (data not shown). Thus, profound differences in T cell populations resulting from the different vaccinations can be measured in which *s.c.* BCG vaccination induces $CD4^+ T_{EM}$ cells while *i.d.* H56 cDNA vaccination induces $CD4^+ T_{CM}$ cells. *Mtb* specific humoral responses are induced by BCG *s.c.* while H56 cDNA *i.d.* induces H56-specific humoral responses, mainly IgG1.

Subcutaneous BCG vaccination has higher protective efficacy than dermal H56 cDNA tattoo immunization

To score the protective efficacy of the different immunization strategies, bacterial loads were measured in lungs and spleens at day 90 following subcutaneous vaccination with BCG or BCG *::H56*, or dermal tattoo immunization with BCG, H56 cDNA or H56_E cDNA. Mice vaccinated with BCG or BCG *::H56 s.c.* tended to have lower bacterial burdens in the lung (Fig. 3A) and spleen (Fig. 3B) than naive mice, with BCG *::H56 s.c.* vaccinated mice tending to have the lowest bacterial loads. H56 or H56_E cDNA *i.d.* vaccination did not protect mice, as there was no difference in bacterial loads compared to naive mice. From these data we infer that the broad responses elicited by BCG has higher protective efficacy than H56 cDNA tattoo immunization.

Heterologous prime-boost vaccination with dermal H56 or H56_E cDNA tattoo immunization and subcutaneous BCG *::H56* injection induces the broadest T cell responses

Although dermal DNA tattoo vaccination did not protect against tuberculosis, we hypothesized that it may increase the efficacy of the BCG vaccine in a prime-boost system, by specifically enhancing the cellular immune response. Therefore, we tested different homologous and heterologous prime-boost vaccination regimens to determine the combination that offers optimal vaccine efficacy (Fig 4A). Two groups of mice were subcutaneously vaccinated with BCG or BCG *::H56* at day 0 and then boosted by dermal H56_E DNA tattoo immunization at day 40. In other heterologous prime-boost regimens, mice were primed by dermal DNA tattoo with H56 cDNA or H56_E cDNA, and then boosted with subcutaneous BCG *::H56* injection. In homologous prime-boost vaccination, mice received subcutaneous BCG *::H56* or H56_E cDNA tattoo twice. Immune responses were

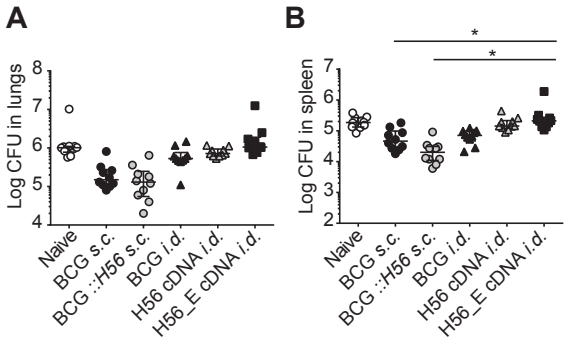

Fig. 3. BCG protects in *Mtb* infection while dermal H56 or H56_E cDNA tattoo is not protective. Lungs and spleens collected at day 90 post *Mtb* challenge were plated in serial dilution. Pooled data of two experiments with (n = 10 in total) is shown ± SEM. (**A**) Bacterial loads in lungs and (**B**) spleen (30-70 CFU). (**A-B**) Significant differences between the groups are shown with * (ANOVA with Tukey's multiple comparison test; * $p < 0.05$).

measured two weeks after the booster vaccination. H56-specific $CD4^+$ (Fig. 4B) and $CD8^+$ T cells (Fig. 4C) were measured by flow cytometry and IFNγ ELISpot (Fig. S2). Relatively high frequencies of H56-specific $CD4^+$ T cells were detected in mice that had received heterologous prime-boost with H56 cDNA/BCG *::H56* or H56_E cDNA/BCG *::H56*, both specific to single epitopes, as activated by the pool of 15-mers (Fig. 4B). In comparison, mice that received homologous prime-boosts with H56_E cDNA showed substantially weaker H56 peptide specific $CD4^+$ T cell responses to the individual epitopes although the total amount of H56 $CD4^+$ T cells, as measured with the pool of peptides, was still present. Mice which had been primed with BCG *::H56* and boosted with DNA *i.d.* as well as mice immunized by homologous *BCG::H56* vaccination also showed weak responses. A similar pattern was observed in the analyses of $CD8^+$ T cell responses. Mice primed with DNA *i.d.* and boosted with BCG *::H56 s.c.* showed the highest frequencies of H56-specific $CD8^+$ T cells, followed by the mice that had received homologous DNA *i.d.* vaccination (Fig. 4C). Using IFNγ ELISpot, we detected similar patterns in lymph nodes, except for BCG *::H56 s.c.* homologous vaccination, in which similar $CD8^+$ T cell responses were similar to those in H56 cDNA *i.d.*/BCG *::H56 s.c.* vaccination (Fig. S2).

Analysis of T cell subsets by flow cytometry indicated that the order of priming and boosting determined which type of immune responses generated. We

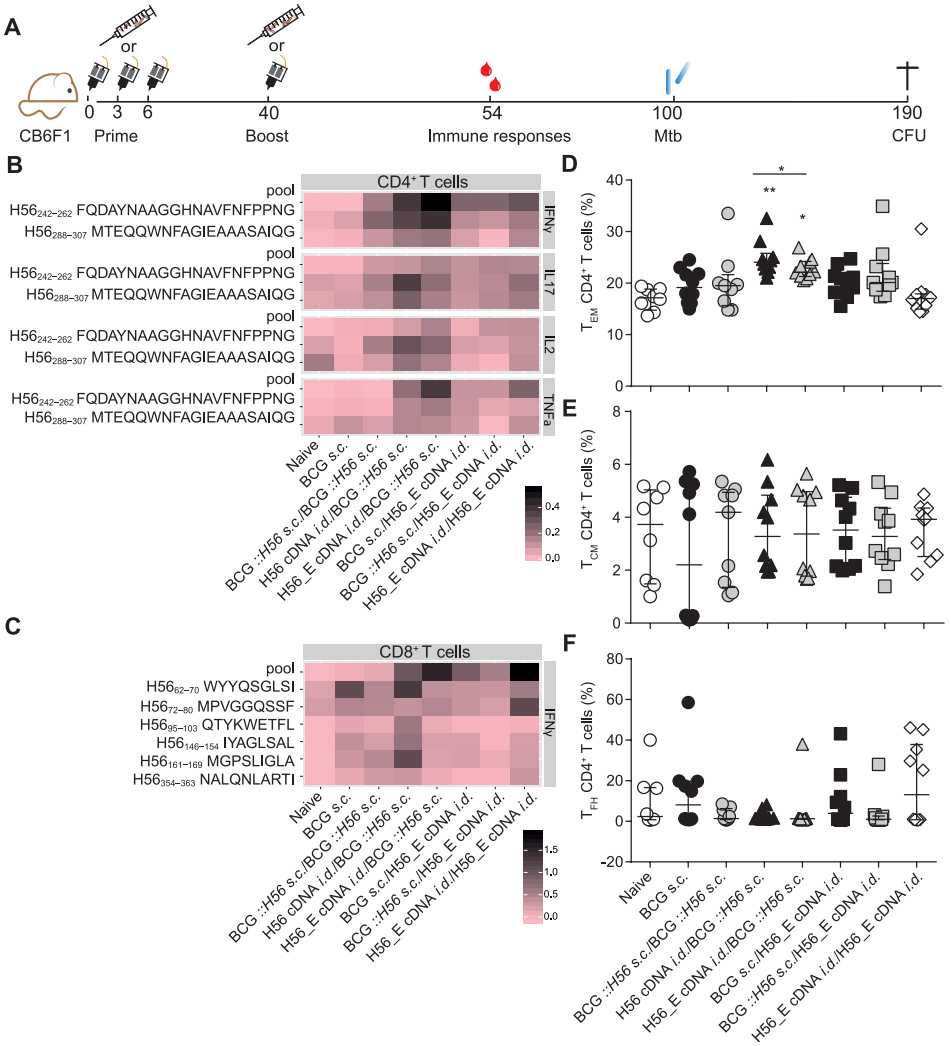
A
or
or
0 3 6
40
54
100
190
CB6F1
Prime
Boost
Immune responses
Mtb
CFU
B
CD4+ T cells
pool
H56242–262 FQDAYNAAGGHNAVFNFPPNG
H56288–307 MTEQQWNFAGIEAAASAIQG
IFNγ
IL17
IL2
TNFα
Naive
BCG s.c.
BCG ::H56 s.c./BCG ::H56 s.c.
H56 cDNA i.d./BCG ::H56 s.c.
H56_E cDNA i.d./BCG ::H56 s.c.
BCG s.c./H56_E cDNA i.d.
BCG ::H56 s.c./H56_E cDNA i.d.
H56_E cDNA i.d./H56_E cDNA i.d.
0.4
0.2
0.0
C
CD8+ T cells
pool
H5662–70 WYYQSGLSI
H5672–80 MPVGGQSSF
H5695–103 QTYKWETFL
H56146–154 IYAGLSAL
H56161–169 MGPSLIGLA
H56354–363 NALQNLARTI
IFNγ
1.5
1.0
0.5
0.0
D
TEM CD4+ T cells (%)
40
30
20
10
0
*
**
*
E
TCM CD4+ T cells (%)
8
6
4
2
0
F
TFH CD4+ T cells (%)
80
60
40
20
0
-20

Fig. 4. Broadest H56-specific T cell responses are induced by heterologous prime-boost with H56 or H56_E cDNA *i.d.*/BCG *::H56 s.c.* vaccination. (**A**) Immunization scheme. (**B, C**) Intracellular cytokine staining was performed on splenocytes harvested two weeks after the booster vaccination and re-stimulated with different H56 peptides. The peptide pools consisted of eighty-five 15-mer peptides spanning the entire sequence of H56 as a measure of the total percentage of H56-antigen specific cells. $CD4^+$ T cell epitopes included $H56_{242-262}$ (Ag85B derived) and $H56_{288-307}$ (ESAT6 derived). The $CD8^+$ T cell epitopes included $H56_{354-363}$ (ESAT6 derived) and five epitopes of the Ag85B portion. Analysis was done using FACS. The results show pooled data from two independent experiments (n=10 in total). Heat maps showing mean frequency of (**B**) $CD4^+$ T cells secreting IFNγ, IL-17, IL-2 or TNFα after peptide stimulation, normalized to medium incubated cells. (**C**) $CD8^+$ T cells secreting IFNγ after peptide stimulation, normalized to medium incubated cells. (**D**) Percentage of $CD4^+$ T effector memory (T_{EM}) cells in $CD4^+$ T cell population (**E**) Percentage of $CD4^+$ T_{CM} in $CD4^+$ T cell population (**F**) Percentage of $CD4^+$ T_{FH} in $CD4^+$ T cell population. (**A-E**) Significant differences between T cell populations of the splenocytes of treatment groups compared to the naive group are marked as * and significant differences in T cell populations between the groups with lines (ANOVA with Tukey's multiple comparison test; * $p < 0.05$; ** $p < 0.01$).

measured the highest frequencies of $CD4^+$ T_{EM} in mice primed with H56 or H56_E DNA *i.d.* and boosted with BCG *::H56 s.c.* compared to the control group (Fig. 4D), in agreement with enhanced $CD4^+$ T_{EM} populations as measured in the single BCG vaccination experiments (Fig.2B). BCG or BCG *::H56* primed mice boosted with H56_E cDNA and homologous BCG *::H56* prime- boosted mice showed lower frequencies of $CD4^+$ T_{EM}, similar to mice vaccinated with BCG only (Fig. 4D). The animals vaccinated with the homologous DNA *i.d.* regimen did not show an increase in $CD4^+$ T_{EM} compared to unvaccinated controls. While vaccinating once with H56_E cDNA *i.d.* resulted in higher percentages of $CD4^+$ T_{CM} cells compared to BCG *s.c.* vaccination (Fig. 2D), no differences between H56_E cDNA prime-boosted mice and BCG vaccinated mice were detected (Fig 4E). Groups boosted with H56_E *i.d.* tended to have elevated percentages of $CD4^+$ T_{FH} cells (Fig. 4F). Frequencies of $CD8^+$ T_{CM} cells and $CD8^+$ T_{EM} cells were not significantly different after single vaccination protocols with DNA *i.d.* or BCG *s.c.* or in different prime-boost combinations (data not shown). Thus, heterologous prime-boost immunization with H56 cDNA/BCG *::H56* or H56_E cDNA/BCG *::H56* induced the highest percentages of H56-specific $CD4^+$ and $CD8^+$ T cells, as well as profound $CD4^+$ T_{EM} populations.

Heterologous prime-boost vaccination with dermal H56 cDNA tattoo immunization and subcutaneous BCG or BCG *::H56* injection results in *Mtb*- and H56-specific humoral responses

In the single vaccination protocols, the BCG vaccinations resulted in the highest titers of *Mycobacterium* specific antibodies (Fig. 2H) and the highest frequencies of plasma cells (Fig.2F) and germinal center B cells (Fig.2G), while the DNA vaccinations induced the highest titers of H56-specific antibodies (Fig 2I). Boosting BCG or BCG *::H56* primed mice with H56_E cDNA *i.d*. led to a tendency towards the highest percentages of plasma cells (Fig. 5A). This effect was not seen after homologous prime-boost with BCG or in mice primed with H56 or H56_E cDNA *i.d.* and boosted with BCG *s.c.* While single vaccination with BCG resulted in elevated percentages of germinal center B cells (Fig 2G), in the prime-boost regimens, in particular H56 DNA-primed/BCG *::H56* boosted mice tended to have relatively high percentages of germinal center B cells (Fig. 5B). This BCG-dependent effect on *Mycobacterium*-specific antibody levels was also seen after prime-boost vaccination because all groups that received a form of BCG in either prime or boost (all heterologous vaccinations) showed elevated titers specific for *Mtb* lysate compared to the naive group (Fig. 5C). Interestingly, *Mycobacterium*-specific antibody titers in H56_E cDNA/H56_E cDNA *i.d.* prime-boosted mice remained as low as in naive controls. Similar to single H56 cDNA *i.d.* vaccination, which induced Ag85B specific antibodies (Fig. 2I), the groups that were primed with H56 or H56_E cDNA *i.d.* and boosted with BCG *s.c.* showed the highest titers of Ag85B specific antibodies (Fig. 5D). However, some of the mice receiving homologous BCG *::H56* s.c. vaccination also produced Ag85B specific IgG1 and IgG2c, while homologous vaccination with H56_E cDNA *i.d.* induced Ag85B specific IgG2c only in a few mice, and no IgG1 (Fig. 5D). Thus, heterologous prime-boost immunization in dependent on BCG as priming or booster immunization for induction of *Mtb* specific antibodies while H56-specific antibodies are mainly elicited by heterologous prime-boost immunization with H56 cDNA/BCG *::H56* or H56_E cDNA/BCG *::H56* as well as BCG *::H56* homologous immunization, and not by the other regimens.

Homologous and heterologous vaccination with BCG has better protective efficacy than homologous vaccination using dermal H56_E cDNA tattoo immunization

To determine the protective efficacy of the different homologous- and heterologous prime-boost strategies, the bacterial loads in different organs were measured after challenge. Mice vaccinated with BCG and most homologous or heterologous prime-boost strategies showed reduced bacterial burdens in lung

(Fig. 6A) and spleen (Fig. 6B) compared to naive mice. The order of immunizations was important because we measured increased bacterial loads in spleens of mice primed with BCG *::H56 s.c.* and boosted with H56_E cDNA *i.d.* compared to mice primed with H56 cDNA *i.d.* and boosted with BCG *::H56 s.c.* (Fig. 6B). The same trend was visible in the lungs, suggesting that the last vaccination (boost) had the predominant effect on the outcome. Mice vaccinated with H56 or H56_E DNA *i.d.* and boosted with BCG *::H56* as well as mice vaccinated with BCG *::H56* in prime-boost showed a slight trend towards decreased bacterial loads in both spleen and lungs. Interestingly, the group that had received H56_E cDNA *i.d.* twice had similar CFU in lung and spleen as naive animals. Thus, efficacy is dependent on BCG immunization in the vaccination regimen and the order of immunizations in a prime-boost regimen has influence on the protective capacity.

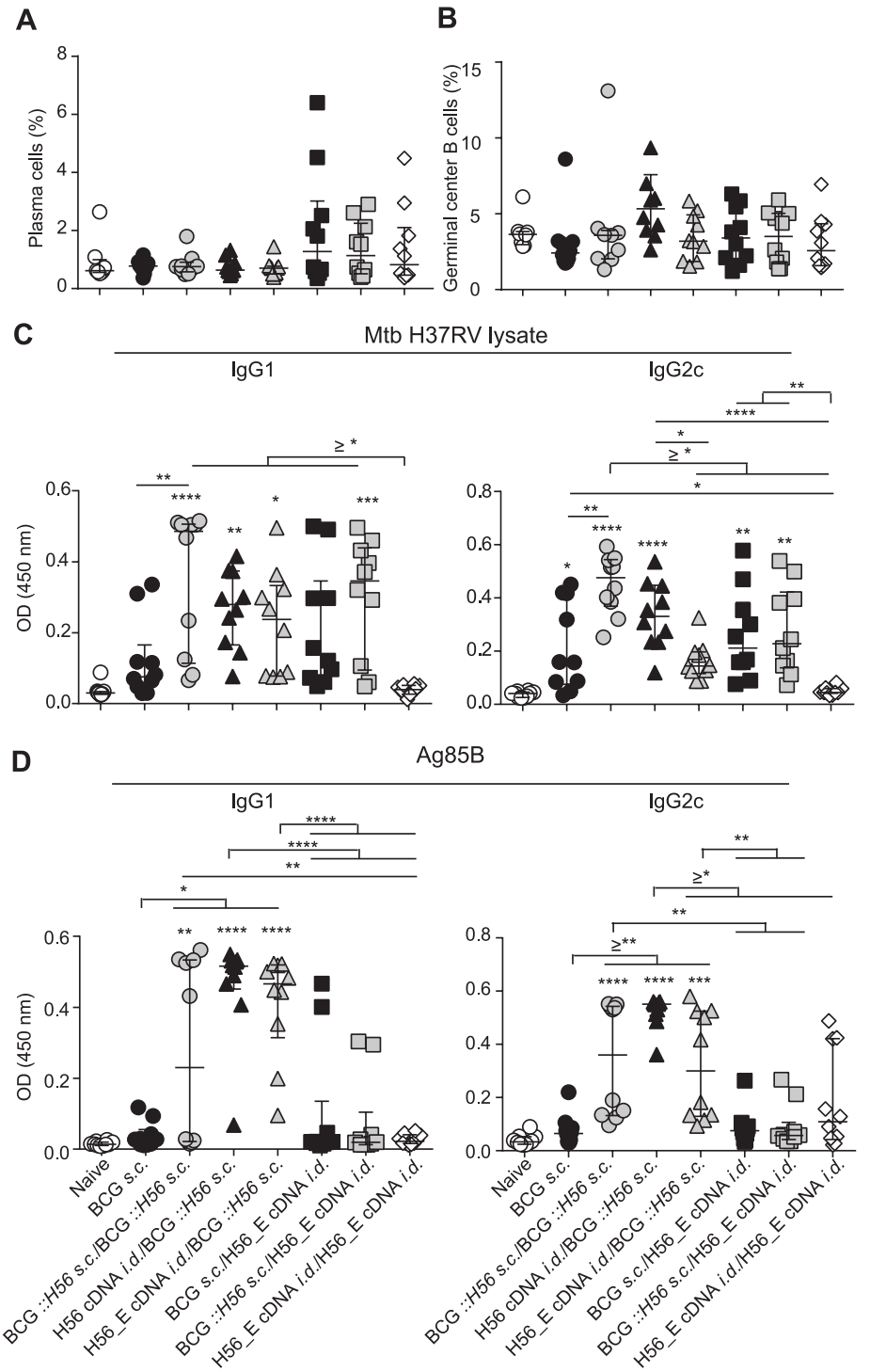
A
Plasma cells (%)
B
Germinal center B cells (%)
C
Mtb H37RV lysate
IgG1
IgG2c
OD (450 nm)
D
Ag85B
IgG1
IgG2c
OD (450 nm)
Naive
BCG s.c.
BCG ::H56 s.c.
BCG ::H56 s.c./BCG ::H56 s.c.
H56 cDNA i.d./BCG ::H56 s.c.
H56_E cDNA i.d./BCG ::H56 s.c.
BCG s.c./H56_E cDNA i.d.
BCG ::H56 s.c./H56_E cDNA i.d.
H56_E cDNA i.d./H56_E cDNA i.d.

Fig. 5. Heterologous prime-boost vaccination using H56 cDNA *i.d.* and BCG *s.c.* injection favors production of both Ag85B- and *Mycobacterium*-specific antibody production. (**A,B**) Splenocytes were stained for different surface markers 14 days after the booster vaccination and analyzed for (**A**) percentage of plasma cells in B cell population and (**B**) percentage of germinal center B cells in B cell population by FACS. (**C,D**) IgG1 and IgG2c antibodies recognizing (**C**) H37RV lysate or (**D**) Ag85B were measured in blood of immunized mice at day 40. (**A-D**) Significant differences between treatment groups and the naive group are marked as * and significant differences between groups with lines (ANOVA with Tukey's multiple comparison test; * $p < 0.05$; ** $p < 0.01$; *** $p < 0.001$; **** $p < 0.0001$; ≥ minimum amount of * for combined indicated groups).

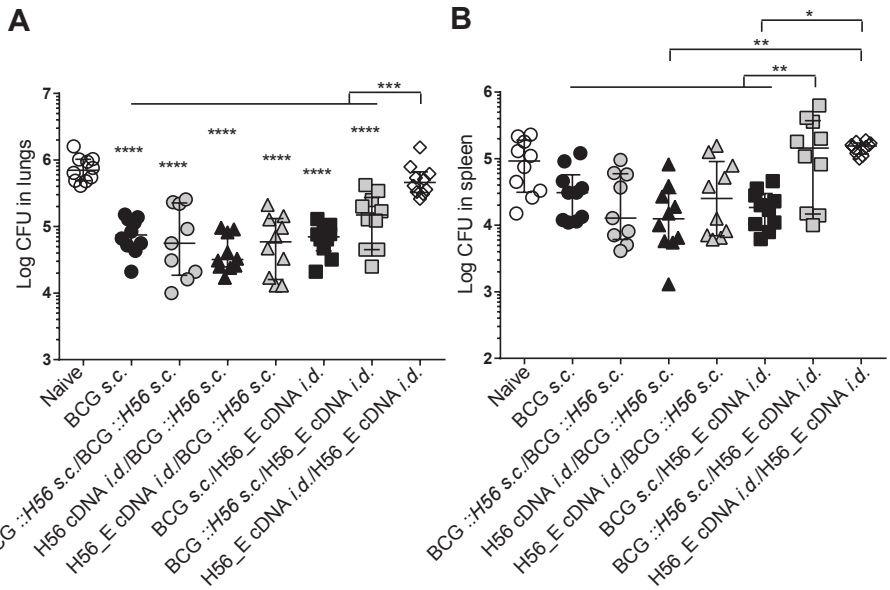

Fig. 6. Heterologous prime-boost with H56 cDNA *i.d.* and BCG *s.c.* in different combinations has protective efficacy while homologous prime-boost vaccination with H56_E cDNA does not. Lungs and spleens collected at day 90 post *Mtb* challenge were plated in serial dilution. Pooled data of two experiments with (n = 10 in total) is shown ± SEM. (**A**) Bacterial loads in lungs and (**B**) spleen (±30 CFU). One mouse in the BCG *::H56* prime-boost group died early in the experiment due to unknown reasons, therefore there were n=9 in this group. (**A-B**) Significant differences between the groups are shown with * (ANOVA with Tukey's multiple comparison test; * $p < 0.05$; ** $p < 0.01$; *** $p < 0.001$; **** $p < 0.0001$).

Discussion

BCG is the only licensed vaccine against tuberculosis, but provides inadequate protection [5]. Therefore, other types of adjuvants, different routes of vaccination and prime-boost regimens are being investigated for their ability to boost the immunogenicity and efficacy of the BCG vaccine [6-8, 10, 11, 27-29, 39]. Aagaard et al. [22] found that two times boosting of BCG vaccination with CAF01-adjuvanted *Mtb* fusion protein H56 (encompassing Ag85b, ESAT6 and Rv2660) increased BCG-induced protection against tuberculosis in a murine model. In order to test other routes of delivery and prime-boost strategies, we cloned H56 into BCG [32] and generated a H56 encoding DNA vaccine which was shown to induce H56-specific $CD4^+$ and $CD8^+$ T cell responses [30]. We determined whether vaccination by dermal H56 cDNA tattoo has protective efficacy against tuberculosis infection in mice, and whether subcutaneous injection of BCG (including BCG *::H56*) and dermal H56 cDNA tattoo could be used in a heterologous prime-boost strategy to increase protection. We found that dermal H56 cDNA dermal tattoo vaccination did not protect against tuberculosis in our model, although it enhanced immune responses in heterologous regimens when used as a prime vaccination in combination with a BCG *::H56* boost. Overall, our results suggested that the order of immunizations in prime boost regimens determines the immune response that is elicited and that T- and B cell responses with broad specificity, rather than H56-specific responses, were associated with protection.

Studying the immune responses elicited by different vaccination regimens and evaluating them in light of the resulting efficacy provides important insights for guiding rational vaccine design. Our experiments comparing dermal DNA vaccination with H56 or H56_E constructs and subcutaneous vaccination with BCG or BCG *::H56* demonstrated that the two vaccines elicited distinct immune responses, due to vaccine differences. BCG shares numerous mycobacterial antigens with *Mtb*, including Ag85B (but not ESAT6 or Rv2660c) and thus contains multiple vaccine antigens, while the DNA tattoo immunization elicits specific responses only against H56. Mice vaccinated with BCG or BCG *::H56* accordingly had relatively high levels of *Mycobacterium*-specific antibodies, while mice administered cDNA *i.d.* (particularly the unmodified H56 sequence) developed mainly Ag85B specific antibody responses. All vaccines containing H56 (either BCG *::H56* or the H56 and H56_E cDNA) elicited H56-specific $CD4^+$ and $CD8^+$ T cells, but $CD8^+$ responses against H56 were most pronounced in mice vaccinated with DNA intradermally. Ultimately, mice vaccinated with BCG *s.c.*, and particularly BCG *::H56,* tended to be more protected against *Mtb* challenge

than mice that received H56 cDNA *i.d.* in a homologous regimen, suggesting that broader anti-mycobacterial responses were more protective than a strong specific responses to H56. The observed improved immune protection in BCG-vaccinated mice may be due to the persistence and dissemination of live BCG within the host, compared to the short-lived availability of the DNA vaccines. Previously we found that BCG disseminates to the lungs after *s.c.* vaccination, where it persists for about 45 days [14]. Dermal tattoo vaccination with BCG showed a trend towards lower efficacy than subcutaneous vaccination, potentially because the BCG are killed during the tattoo procedure.

Following testing of the single vaccine candidates, we tested heterologous and homologous prime-boost combinations. Priming with H56_E or H56 cDNA *i.d.* followed by a *s.c.* boost with BCG *::H56* appeared to boost the expansion of $CD4^+$ T_{EM} cells, H56-specific $CD4^+$ T cells secreting IFNγ, IL17, IL2 and TNFα, and to lead to the most consistently high Ag85B specific antibody responses. This regimen also induced H56-specific $CD8^+$ T cells, targeting the majority of epitopes studied. Homologous H56_E cDNA prime-boost *i.d.* induced the most vigorous H56-specific $CD8^+$ T cell responses, but these mice showed the highest bacterial burdens after *Mtb* challenge, indicating that this response was not protective.

Interestingly, homologous H56_E prime-boosted mice hardly produced any *Mtb*- and Ag85B-specific IgG, with only a few mice producing Ag85B-specific IgG2c. Mice receiving BCG *::H56* at the boost (either homologous prime or heterologous prime) produced higher levels of Ag85B specific antibodies than mice receiving H56_E cDNA *i.d.* at the boost in a heterologous regimen. *Mycobacterium* specific antibodies in these groups must therefore be induced by BCG. It can be speculated that alterations to the H56_E sequence may have led to a change in B cell Ag85B epitopes or skewing of immune responses away from Ag85B antibody-producing conditions, since also in the single dose vaccination experiments, H56 cDNA led to higher antibody production than H56_E cDNA. Remarkably, H56 or H56_E cDNA *i.d.* primed BCG *::H56 s.c.* boosted mice produced anti-Ag85B specific IgG1 and IgG2c whereas BCG *::H56* vaccinated mice did not produce much Ag85B-specific antibodies in single vaccine dose experiments. Since antibodies produced following single vaccination were measured only at early time points, it is possible that antibodies against BCG *::H56* –derived Ag85B are generated later after vaccination, due to the persistence of BCG.

Understanding the underlying mechanisms leading to immune protection against *Mtb* will assist in the rational design of efficacious vaccines. In our model,

protection appeared to be associated with increased $CD4^+T_{EM}$ and *Mycobacterium*-specific antibody levels, although mice vaccinated by intradermal BCG tattoo showed increased levels of antibodies without increased protection, indicating that the higher antibody titers in other protected groups may not correlate with protection. It is possible that in our study $CD4^+T_{EM}$ play a dominating role due to the relatively short time course of our vaccination regime, and that $CD4^+T_{CM}$, by virtue of their capacity to generate new $CD4^+T_{EM}$, are important in the long term. Recently it was reported that boosting of a BCG primed immune response with the subunit Apa, a cell-surface adhesion factor which is a secreted glycoprotein of all members of the *Mtb*-complex [40-42], was more successful if the booster was given once the primary response was contracted, rather than at the peak of the BCG-induced response [39]. Therefore, it is possible that the H56_E cDNA *i.d.* boosters may boost the immune response more effectively if administered in the memory phase. Although H56 or H56_E cDNA did not induce protective responses when given as a single vaccine, implying that it does not induce optimal responses required for immunity against tuberculosis in mice, it did appear to lead to stronger immune responses when given as a *i.d.* prime in combination with *s.c.* BCG or BCG *::H56* boost.

In summary, we have tested intradermal DNA tattoo vaccination using H56 and H56_E constructs in combination with subcutaneous injection of BCG or BCG *::H56*. Our data suggests that broader specificity of T cell responses is more effective in controlling TB infection compared to highly specific responses targeted to a specific antigen. In addition, the sequence of different immunizations determines the magnitude of induced responses and should be carefully considered when designing vaccine regimens.

Acknowledgments

Support was by European Union's Seventh Framework Programme [FP7/2007-2013] - Grant No. 280873 ADITEC to A.S. and S.K., Boehringer Ingelheim fonds travelgrant and EFIS travel grant to A.P. We thank Dr. Donatella Negri for providing the 15-mers of H56.

Abbreviations

TB Tuberculosis
Mtb Mycobacterium tuberculosis
BCG *Mycobacterium bovis* bacillus Calmette-Guérin
i.d. intradermal
s.c. subcutaneous

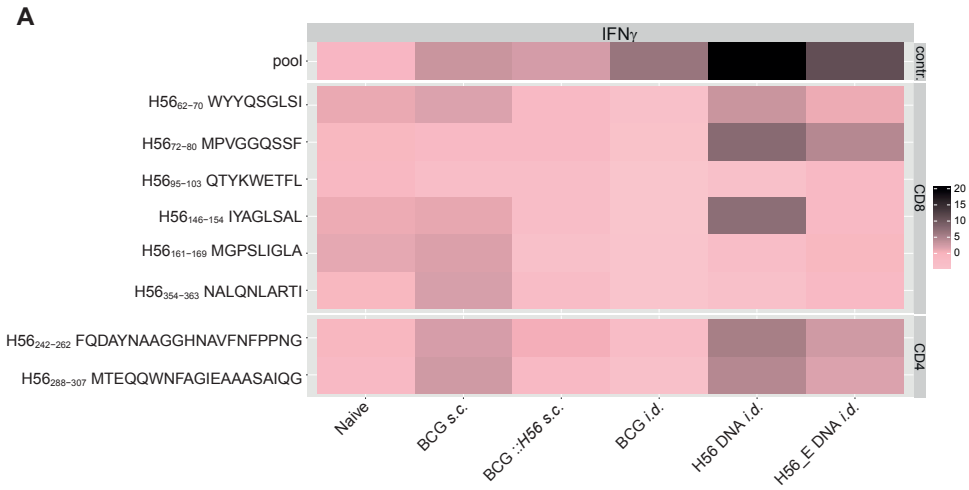

Supplementary Figure 1. Heat map of H56-specific IFNγ producing cells in lymph nodes after different vaccination methods. The heat map represents mean number of IFNγ- producing cells per million lymph node cells after peptide stimulation, normalized to medium incubated cells. IFNγ ELISpots were performed at day 21 post vaccination on lymph node cells re-stimulated with peptides. The peptide pools consisted of eighty-five 15-mer peptides spanning the entire sequence of H56. $CD4^+$ T cell epitopes included H56$_{242-262}$ (Ag85B derived) and H56$_{288-307}$ (ESAT6 derived). The $CD8^+$ T cell epitopes included H56$_{354-363}$ (ESAT6 derived) and five epitopes of Ag85B. The results show pooled data from two independent experiments (n=10 in total).

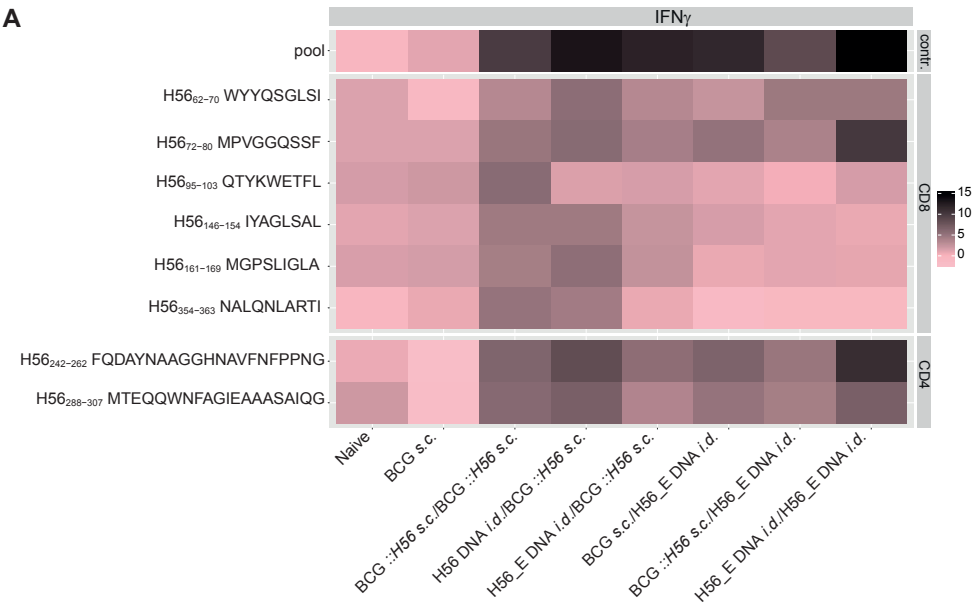

Supplementary figure 2. Heat map of H56-specific IFNγ producing cells in lymph nodes after different prime-boost vaccination methods. The heat map represents mean number of IFNγ- producing cells per million lymph node cells after peptide stimulation, normalized to medium incubated cells. IFNγ ELISpots were performed two weeks after the booster vaccination on lymph node cells re-stimulated with peptides. The peptide pools consisted of eighty-five 15-mer peptides spanning the entire sequence of H56. $CD4^+$ T cell epitopes included $H56_{242-262}$ (Ag85B derived) and $H56_{288-307}$ (ESAT-6 derived). The $CD8^+$ T cell epitopes included $H56_{354-363}$ (ESAT-6 derived) and five epitopes of Ag85B. The results show pooled data from two independent experiments (n=10 in total).

5

References

1. WHO. Global tuberculosisreport 2015. WHO Press,Geneva, Switzerland. (2015).
2. Kaufmann, S. H. Fact and fiction in tuberculosis vaccine research: 10 years later. *The Lancet Infectious Diseases* **11**, 633-640 (2011).
3. Calmette, A. Sur la vaccination préventive des enfants nouveau-néscontre la tuberculose par le BCG. **Ann Inst Pasteur**, 41:201–232 (1927).
4. Aaby, P., Kollmann, T. R. & Benn, C. S. Nonspecific effects of neonatal and infant vaccination: Public-health, immunological and conceptual challenges. *Nat. Immunol.* **15**, 895-899 (2014).
5. Andersen, P. & Doherty, T. M. The success and failure of BCG - Implications for a novel tuberculosis vaccine. *Nat. Rev. Microbiol.* **3**, 656-662 (2005).
6. Bertholet, S. *et al*. A defined tuberculosis vaccine candidate boosts BCG and protects against multidrug-resistant mycobacterium tuberculosis. *Sci. Transl. Med.* **2** (2010).
7. Skeiky, Y. A. W. *et al*. Differential immune responses and protective efficacy induced by components of a tuberculosis polyprotein vaccine, Mtb72F, delivered as naked DNA or recombinant protein. *J. Immunol.* **172**, 7618-7628 (2004).
8. Dietrich, J., Billeskov, R., Doherty, T. M. & Andersen, P. Synergistic effect of bacillus calmette guerin and a tuberculosis subunit vaccine in cationic liposomes: Increased immunogenicity and protection. *J. Immunol.* **178**, 3721-3730 (2007).
9. Nandakumar, S. *et al*. Boosting BCG-primed responses with a subunit Apa vaccine during the waning phase improves immunity and imparts protection against Mycobacterium tuberculosis. *Sci. Rep.* **6** (2016).
10. Orr, M. T. *et al*. Immune subdominant antigens as vaccine candidates against Mycobacterium tuberculosis. *J. Immunol.* **193**, 2911-2918 (2014).
11. Agger, E. M. Novel adjuvant formulations for delivery of anti-tuberculosis vaccine candidates. *Adv. Drug Deliv. Rev.* **102**, 73-82 (2016).

12. Grode, L. *et al*. Increased vaccine efficacy against tuberculosis of recombinant Mycobacterium bovis bacille Calmette-Guérin mutants that secrete listeriolysin. *J. Clin. Invest.* **115,** 2472-2479 (2005).
13. Vogelzang, A. *et al*. Central memory $CD4^+$ T cells are responsible for the recombinant Bacillus Calmette-Guérin ΔureC::hly vaccine's superior protection against tuberculosis. *J. Infect. Dis.* **210,** 1928-1937 (2014).
14. Gengenbacher, M. *et al*. Deletion of nuoG from the Vaccine Candidate Mycobacterium bovis BCG DeltaureC::hly Improves Protection against Tuberculosis. *MBio* **7,** 10.1128/mBio.00679-16 (2016).
15. Bold, T. D., Banaei, N., Wolf, A. J. & Ernst, J. D. Suboptimal activation of antigen-specific cD4+ effector cells enables persistence of M. tuberculosis in vivo. *PLoS Pathog.* **7** (2011).
16. Kupz, A. *et al*. ESAT-6-dependent cytosolic pattern recognition drives noncognate tuberculosis control in vivo. *J. Clin. Invest.* **126,** 2109-2122 (2016).
17. Flynn, J. L., Goldstein, M. M., Triebold, K. J., Koller, B. & Bloom, B. R. Major histocompatibility complex class I-restricted T cells are required for resistance to Mycobacterium tuberculosis infection. *Proc. Natl. Acad. Sci. U. S. A.* **89,** 12013-12017 (1992).
18. Wang, J. *et al*. Single mucosal, but not parenteral, immunization with recombinant adenoviral-based vaccine provides potent protection from pulmonary tuberculosis. *J. Immunol.* **173,** 6357-6365 (2004).
19. Foreman, T. W. *et al*. CD4+ T-cell-independent mechanisms suppress reactivation of latent tuberculosis in a macaque model of HIV coinfection. *Proc. Natl. Acad. Sci. U. S. A.* **113,** E5636-E5644 (2016).
20. Achkar, J. M. & Casadevall, A. Antibody-mediated immunity against tuberculosis: Implications for vaccine development. *Cell Host and Microbe* **13,** 250-262 (2013).
21. Abebe, F. & Bjune, G. The protective role of antibody responses during Mycobacterium tuberculosis infection. *Clin. Exp. Immunol.* **157,** 235-243 (2009).
22. Aagaard, C. *et al*. A multistage tuberculosis vaccine that confers efficient protection before and after exposure. *Nat. Med.* **17,** 189-195 (2011).
23. Olsen, A. W., Van Pinxteren, L. A. H., Okkels, L. M., Rasmussen, P. B. & Andersen, P. Protection of mice with a tuberculosis subunit vaccine based on a fusion protein of antigen 85B and ESAT-6. *Infect. Immun.* **69,** 2773-2778 (2001).
24. Betts, J. C., Lukey, P. T., Robb, L. C., McAdam, R. A. & Duncan, K. Evaluation of a nutrient starvation model of Mycobacterium tuberculosis persistence by gene and protein expression profiling. *Mol. Microbiol.* **43,** 717-731 (2002).
25. Rappuoli, R. & Medaglini, D. ADITEC: Joining forces for next-generation vaccines. *Sci. Transl. Med.* **4** (2012).
26. Woodworth, J.S., Cohen, S.B., Moguche, A.O., Plumlee, C.R., Agger, E.M., Urdahl, K.B., & Andersen,P. Subunit vaccine H56/CAF01 induces a population of circulating CD4 T cells that traffic into the *Mycobacterium tuberculosis*-infected lung.*Mucosal Immunol*. **4,**1933-0219 (2016)
27. Lindenstrøm, T., Knudsen, N. P. H., Agger, E. M. & Andersen, P. Control of chronic Mycobacterium tuberculosis infection by CD4 KLRG1 - IL-2-secreting central memory cells. *J. Immunol.* **190,** 6311-6319 (2013).
28. Knudsen, N. P. H. *et al*. Different human vaccine adjuvants promote distinct antigen-independent immunological signatures tailored to different pathogens. *Sci. Rep.* **6** (2016).
29. Lin, P. L. *et al*. The multistage vaccine H56 boosts the effects of BCG to protect cynomolgus macaques against active tuberculosis and reactivation of latent Mycobacterium tuberculosis infection. *J. Clin. Invest.* **122,** 303-314 (2012).

30. Platteel, A. C. M. *et al*. Strategies to enhance immunogenicity of cDNA vaccine encoded antigens by modulation of antigen processing. *Vaccine* **34,** 5132-40 (2016).
31. Bins, A. D. *et al*. A rapid and potent DNA vaccination strategy defined by in vivo monitoring of antigen expression. *Nat. Med.* **11,** 899-904 (2005).
32. Nieuwenhuizen, N. Manuscript in preparation. (2016).
33. Oosterhuis, K. *et al*. Preclinical development of highly effective and safe DNA vaccines directed against HPV 16 E6 and E7. *International Journal of Cancer* **129,** 397-406 (2011).
34. Oosterhuis, K., Van Den Berg, J. H., Schumacher, T. N. & Haanen, J. B. A. G. DNA vaccines and intradermal vaccination by DNA tattooing. *Curr. Top. Microbiol. Immunol.* **351,** 221-250 (2012).
35. Snelgrove, R. J. *et al*. OX40 ligand fusion protein delivered simultaneously with the BCG vaccine provides superior protection against murine Mycobacterium tuberculosis infection. *J. Infect. Dis.* **205,** 975-983 (2012).
36. Bo, Y. J. *et al*. Mycobacterium bovis BCG immunization induces protective immunity against nine different Mycobacterium tuberculosis strains in mice. *Infect. Immun.* **76,** 5173-5180 (2008).
37. Huygen, K. *et al*. Mapping of TH1 helper T-cell epitopes on major secreted mycobacterial antigen 85A in mice infected with live Mycobacterium bovis BCG. *Infect. Immun.* **62,** 363-370 (1994).
38. Brandt, L., Oettinger, T., Holm, A., Andersen, Å B. & Andersen, P. Key Epitopes on the ESAT-6 Antigen Recognized in Mice during the Recall of Protective Immunity to Mycobacterium tuberculosis. *J. Immunol.* **157,** 3527-3533 (1996).
39. Nandakumar, S. *et al*. Boosting BCG-primed responses with a subunit Apa vaccine during the waning phase improves immunity and imparts protection against Mycobacterium tuberculosis. *Sci. Rep.* **6,** 25837 (2016).
40. Ragas, A., Roussel, L., Puzo, G. & Riviere, M. The Mycobacterium tuberculosis cell-surface glycoprotein apa as a potential adhesin to colonize target cells via the innate immune system pulmonary C-type lectin surfactant protein A. *J. Biol. Chem.* **282,** 5133-5142 (2007).
41. Horn, C. *et al*. Decreased capacity of recombinant 45/47-kDa molecules (Apa) of Mycobacterium tuberculosis to stimulate T lymphocyte responses related to changes in their mannosylation pattern. *J. Biol. Chem.* **274,** 32023-32030 (1999).
42. Dobos, K. M., Khoo, K. -., Swiderek, K. M., Brennan, P. J. & Belisle, J. T. Definition of the full extent of glycosylation of the 45-kilodalton glycoprotein of Mycobacterium tuberculosis. *J. Bacteriol.* **178,** 2498-2506 (1996).

5

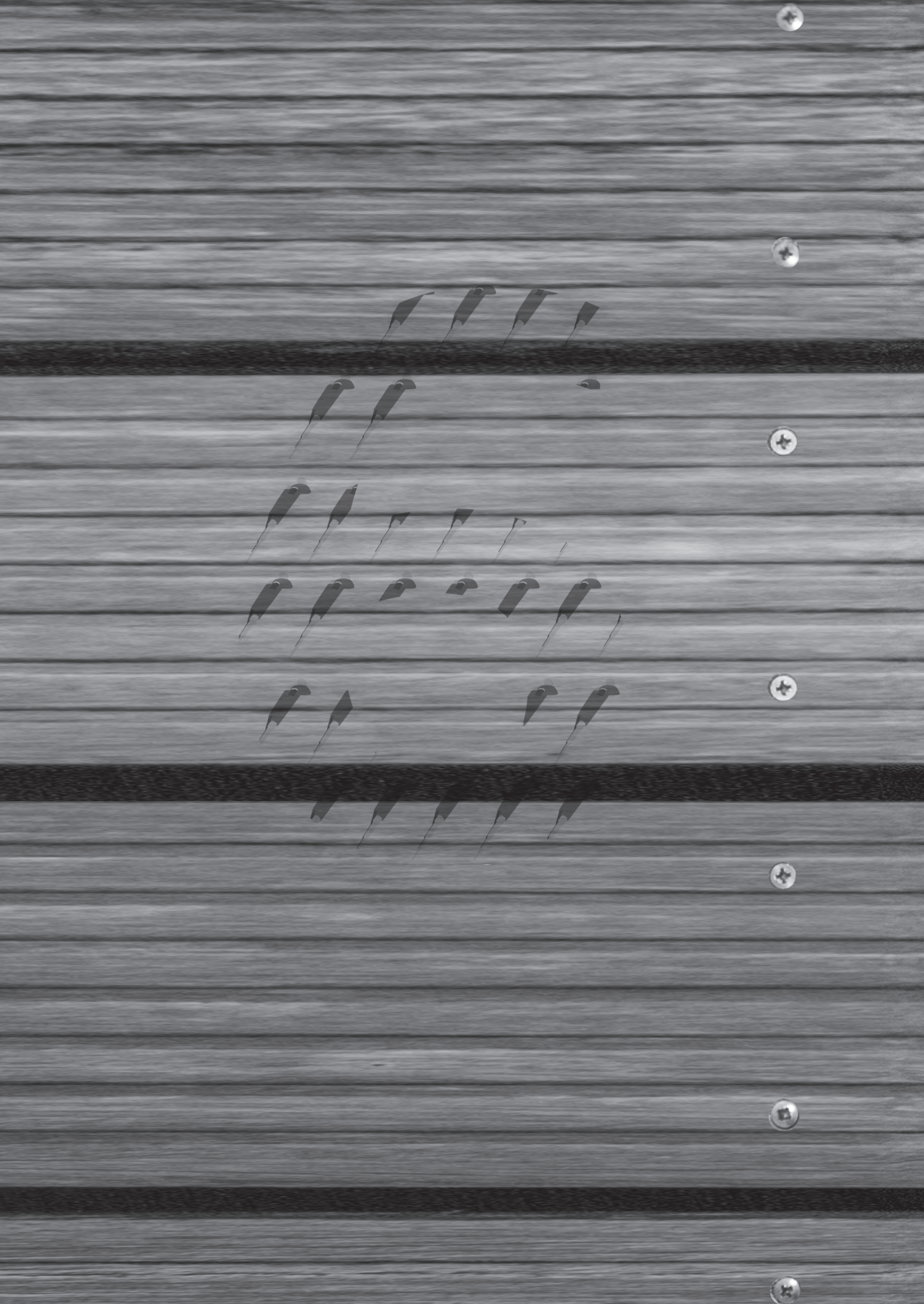

Summarizing discussion

6

Together with the discovery of antibiotics and improved hygiene practices, the introduction of vaccines has had major impact on human longevity and health and is therefore considered as the most significant and cost-effective health achievement of the 20th century [1]. In the present century however, it has become clear that vaccines against causative agents of global pandemics such as HIV, malaria and tuberculosis require a more in depth understanding of the interaction between the pathogens and the host immune system. Extended knowledge and clearer definitions are needed of ways to modulate immune responses in order to accomplish protective immunity. The work described in this thesis can contribute to this knowledge because we studied new ways of MHC class I antigen processing as well as strategies to modulate this process, and consequences for the $CD8^+$ T cell response.

Opportunitites for the modulation of antigen processing

Vaccine design against intracellular pathogens often focuses on activation of the cellular arm of the immune system, in particular the $CD8^+$ T cell response. The proteasome plays a key role in generating the epitopes that are targeted by these $CD8^+$ T cells. Modulation of the proteasome results in an altered peptide pool and this can lead to altered $CD8^+$ T cell responses.

The efficiency of antigen processing *i.e.* how fast epitopes are generated and how many antigen is needed for that, has major consequences for the $CD8^+$ T cell response. It is known that these efficiencies can vary extensively [2, 3]. Differences in efficiency of antigen processing can be caused by immunosubunit incorporation, as shown in **Chapter 3**, in which we identified $CD8^+$ T cells that can be cross-reactive to $LLO_{294/297-304}$, that shares sequence similarity with $LLO_{296-304}$. We showed that all potential spliced epitopes from LLO were generated by immunoproteasomes. We compared these digests with digests of proteasomes from spleens of $LMP7^{-/-}$ $MECL1^{-/-}$ mice and found that the generation efficiency, measured as pmol peptide *per* nmol of substrate consumed over time, of $LLO_{291-298/300-304}$ and $LLO_{291-300/302-304}$ (N-terminally extended precursors of $LLO_{295-298/300-304}$, $LLO_{296-298/300-304}$ and $LLO_{296-300/302-304}$) was decreased in the proteasomes from $LMP7^{-/-}MECL1^{-/-}$ mice. This decreased efficiency can be one of the underlying mechanisms for the fact that we did not detect a specific $CD8^+$ T cell response targeted to these epitopes because low efficiency can result in low abundance or delayed presentation of epitopes on the cell surface. The correlation between delayed presentation and the failure to induce a $CD8^+$ T cell response was already reported [4]. These authors used infection with a recombinant *Listeria monocytogenes* strain expressing an earlier identified Adeno virus- derived fusion antigen, which encompasses the

immunoproteasome-dependent $E1B_{192-200}$ and immunoproteasome-independent $E1A_{234-243}$ epitope. It was shown that antigen presenting cells of $LMP7^{-/-}MECL1^{-/-}$ mice processed and presented the immunoproteasome dependent $E1B_{192-200}$, but they did so with delayed kinetics [5]. These delayed kinetics were responsible for the failure of the mice to respond in infection with rLM-E1 to the immunoproteasome dependent $E1B_{192-200,}$ while they mounted normal responses to $E1A_{234-243}$. Using splenocytes from the infected $LMP7^{-/-}$ $MECL1^{-/-}$ mice, taken at later time points in infection and transferred into naïve $LMP7^{-/-}$ $MECL1^{-/-}$ mice, it was shown that the recipient mice responded normally to $E1B_{192-200}$. This illustrates that there were sufficient quantities of the epitope on the cell surface and there is no gap in the T cell repertoire. The delayed presentation kinetics were responsible for the failure of the infected $LMP7^{-/-}$ $MECL1^{-/-}$ mice to respond to the immunoproteasome dependent epitope [4]. Besides the presentation kinetics, the epitope abundance at the cell surface is also directly correlated with the magnitude of the $CD8^+$ T cell responses, as illustrated in viral models [6, 7]. In the study of La Gruta et al., the influenza-derived epitopes $NP_{366-374}$ and $PA_{224-233}$ were shifted within the same viral context, which equalized the epitope abundance on the cell surface, and hence altered the $CD8^+$ T cell response specific for these epitopes [7]. These data illustrate the influence of generation efficiency on the $CD8^+$ T cell response via the presentation kinetics or abundance of epitopes on the cell surface.

Flanking residue modulation, in which amino acids adjacent to the epitope are changed, is a way to modulate efficiency of antigen processing and has been shown to have major consequences for the immune responses [8-13]. Characteristics of amino acids close to the cleavage site have been studied [14], although the studied dataset does not allow for generalizations. The authors found that immuno- and constitutive proteasomes favor cleaving between hydrophobic large residues and polar large/small residues. Several of the six H56-derived epitopes we used in **Chapter 4** to illustrate a complete strategy to enhance immunogenicity, displayed hydrophobic residues at both P1 and P1′. In order to liberate them from the H56 protein context, the proteasome has to cleave between these two hydrophobic residues. We hypothesized that proteasome-mediated liberation might be increased if the residue at P1′ was substituted for a polar glutamic acid. For $H56_{72-80}$ MPVGGQSSF, we proved that the efficiency was indeed enhanced. Unfortunately, this effect was not seen for all epitopes, potentially due to substitution-dependent alterations of the substrate transport or regulation of non-catalytic modifier sites [15]. These authors showed that substrate transport and regulation sites greatly influence hydrolysis by the proteasome. If the substitutions alter the transport through the cavity of the proteasome which

results in decreased hydrolysis, the amount of epitope produced is less, which might cause a decrease in the magnitude of the specific $CD8^+$ T cell response. These studies show that modulation of antigen processing can be very adequately done by C-terminal flanking residue modulation of epitopes but that more research is needed to unravel all underlying mechanisms.

More indirect ways of antigen processing modulation are also known, *e.g.* those affecting the stability of the antigen [16] or providing $CD4^+$ T cell help by linking the antigen of interest to an antigen that has a strong $CD4^+$ T cell epitope, which is of uttermost importance in DNA tattoo immunization [17-19]. In our studies described in **Chapter 4**, we adapted the latter strategy and linked the cDNA encoding antigen H56 to the cDNA of proteins with immunogenicity enhancing properties. We found an enhancement of H56-targeted $CD4^+$ and $CD8^+$ T cell response when this antigen was linked to tetanus toxin fragment C (TTFC) or ubiquitin (UB). The immunogenicity enhancing effect of TTFC is probably due to the presence of a strong $CD4^+$ T cell epitope [18], but this cannot be the case for UB, since this is a self-derived protein. It has, however, already been reported before to enhance immunogenicity [20]. These observations are in contrast with an earlier study by Wolkers et al., who concluded that successful vaccination is significantly hampered if the cDNA of the antigen is linked to cDNA of a self-derived protein [19]. Wolkers et al., used vaccination with GFP containing constructs in GFP-transgenic mice that express GFP in all nucleated cells, or vaccination with Dby in male mice in which Dby is located on the Y chromosome. The reason that these authors did not find an immunogenicity enhancing effect with these self-derived antigens, while we did find a positive effect using UB, potentially lies in different function of UB under steady state conditions. Additionally, unlike Wolkers et al., who used truncated versions of influenza- or papilloma virus antigens [19], in our studies H56 cDNA was used which encodes for 3 full length proteins in which known $CD4^+$ T cell epitopes are present [21, 22]. These $CD4^+$ T cell epitopes could have been of beneficial influence in our experimental setup. This work shows that providing $CD4^+$ T cell help is an effective way to modulate the responses elicited by the antigens but that differences in the study set-up and choice of vaccine-antigens is of great influence and should be studied more.

By mathematical modelling of proteasome behavior, consequences of attempts to modulate antigen processing can be studied more effectively. This modelling is based on detailed *in vitro* kinetics of epitope generation. The more such knowledge is gathered, the more the prediction of how the epitopes are generated becomes accurate. By modelling proteasome behavior, novel epitopes

can also be predicted, as already widely used for linear epitopes [23]. In **Chapter 2** we developed a multi-level strategy, based on an *in silico* based prediction algorithm, to identify epitopes generated by proteasome-catalyzed peptide splicing (PCPS) within antigens. Additionally, we successfully tested this in a murine *L. monocytogenes* infection model. Two Listeria PlcB-derived spliced epitopes, composed of sequences that in their linear context are not recognized by $CD8^+$ T cells, were identified. As described in the supplementary figures, the prediction algorithm was further specified for HLA haplotypes and would make it possible to synthesize HLA specific - *i.e.* personalized - vaccines. For example, minigene constructs that encode a series of epitopes [24], or a cocktail of DNA constructs, each containing individual epitopes [25], could be used.

Currently, our understanding of antigen processing and how to modulate it is growing. However, by further developing new tools such as *in silico* prediction algorithms this can be further enhanced, which contributes to rational vaccine design.

Possibilties for the navigation of $CD8^+$ T cells towards a desired response

In order to navigate the $CD8^+$ T cells towards a response which is protective in a vaccine setting, modulation of antigen processing can be performed, but the responding $CD8^+$ T cells to an antigen display kinetics that also impose possibilities for further steering. In vaccine design, usually the aim is to elicit a broad response in which both vaccine-derived immunodominant, but also subdominant epitopes are targeted. In this way the chances of immune evasion are smaller and massive IFNγ production, which results in side effects such as tissue damage, are also decreased. Additionally, vigorous responses specific for an immunodominant epitope are not necessarily protective, and can even be associated with increased fitness of the pathogen [26-28] or with higher viral load [29], whereas responses specific for subdominant epitopes have been associated with lower viral- or bacterial loads [30, 31]. If more knowledge becomes available on how activation kinetics of $CD8^+$ T cells and the subsequent immunodominance hierarchy can be modulated, the desired, broad response is easier accomplished.

The activation kinetics of $CD8^+$ T cells responding to natural infection are complex phenomena of which not all influencing factors have been identified. The complexity in the activation kinetics of a total $CD8^+$ T cell response is mainly due the fact that the contribution to responses in primary- and recall infection of one T cell family, *i.e.* one naive T cell and its progeny, differs from

the function of another T cell family [32-34]. These differences arise from the fact that on an individual cell level, proliferation and differentiation of $CD8^+$ T cells occurs heterogeneously. After a primary infection, the immunological memory is maintained in $CD8^+$ T_{CM}, $CD8^+$ T_{EM} and $CD8^+$ T_{RM} populations that develop from $CD8^+$ T_{EFF} cells, while in recall expansion, the individual $CD8^+$ T cells follow the $CD8^+$ T_{CM} population →$CD8^+$ T_{EM} population→$CD8^+$ T_{EFF} population model [35, 36]. The differentiation-variability of an individual $CD8^+$ T cell in this population model has been shown to be tremendous [37] and it is tempting to speculate how the different families of $CD8^+$ T cells are channeled to proliferate and differentiate in specific phases of infection. This is probably influenced by intrinsic variation as well as variation in extrinsic signals, such as the specific environment. Asymmetric division is also believed to contribute to assigning different functions to different families [38], but more research is needed to study the contribution of these underlying mechanisms. Knowledge on how to channel the responses can be used for vaccine design against *e.g.* pathogens, for which the characteristics of the memory populations that confer protection at certain specific sites are known. In the murine *Mycobacterium tuberculosis* model, especially the $CD4^+$ T_{CM} cells, which secrete IFNγ and TNFα, have been shown to be protective in the lungs [39]. The different vaccination strategies used in **Chapter 5**, in which we studied homologous and heterologous prime-boost regimens with dermal DNA tattoo and subcutaneous injection with BCG, were shown to elicit different $CD8^+$ and $CD4^+$ T cell responses. BCG vaccination results in a broad immunological effect compared to the narrow and specific response which is elicited by the H56 cDNA tattoo immunization. By combining the two we found that especially a prime with dermal H56 or H56_E cDNA tattoo immunization, followed by a boost with BCG *::H56* given subcutaneously, resulted in immune responses that are associated with protection. We found enhanced H56 specific secretion of IFNγ, IL17, IL2 and TNFα by $CD4^+$ T cells and increased $CD4^+$ T_{EM} populations compared to the other vaccination regimes. Additionally, H56-specific antibodies in these mice were found to be higher in comparison to mice of other groups that were vaccinated with homologous regimens. The heterologous regimens were effective in decreasing bacterial burdens however, the absolute necessity of at least one subcutaneous injection of BCG is shown, by the fact that a homologous regimen using H56 cDNA tattoo immunization did not result in any protective effect. These examples illustrate that by varying immunization regimes, a desired response can be successfully and safely channeled.

Timing of immunization in a vaccine setting can also greatly influence $CD8^+$ and $CD4^+$ T cell responses. As illustrated in an earlier prime-boost study by

Nandakumar et al., BCG drives persistent immune-activation and this should be taken into account in vaccine strategies [40]. The authors studied T cell responses specific for the cell-surface adhesion factor Apa, which is a secreted glycoprotein of all members of the *Mtb*-complex [41-43], in BCG- or Apa subunit-primed mice. In the study by Nandakumar et al., the animals were boosted during the peak- or contraction phase of this response in a homologous- or heterologous regimen with BCG or Apa-subunit vaccine, and the protective capacity was measured. The authors concluded that boosting with a heterologous vaccine may be ideal once the specific persisting effector responses have contracted, but in this model this was achieved after only 78 weeks [40]. This result might explain the fact that in **Chapter 5** we detected more specific $CD4^+$ and $CD8^+$ T cells in the DNA primed and BCG boosted animals compared to the BCG primed and DNA boosted animals. Probably, in the BCG primed-DNA boosted animals, the immune response elicited by the prime was not contracted enough to have a significant effect of the boost, since the boost took place six weeks after the prime. In the human population there can be years between various vaccinations, which is not easily mimicked in a mouse model, however, such studies should be considered with respect to timing or sequence of the different immunizations.

Activation kinetics of $CD8^+$ T cells responding to pathogen-derived antigens in infection are complex phenomena. It is important to study these kinetics in order to acquire knowledge as a basis for rational vaccine design.

Future perspectives of navigating immune responses for improvement of vaccine design

Modulation of antigen processing and the navigation of $CD8^+$ T cell responses is aimed to result in improved vaccine design. The immune system is then successfully steered towards a desired and broad response with subsequent memory that is protective upon infection with the real pathogen. Cross-reactive $CD8^+$ T cells, that are specific for one pathogen-derived epitope but can also be activated by a different pathogen-derived epitope that shares sequence similarity with the initial epitope, can enhance vaccine efficacy in this setting. However, these cross-reactive $CD8^+$ T cells can also impose risks such as induction of auto-immunity.

Positive effects of $CD8^+$ T cell cross-reactivity have been described with cross-reactive $CD8^+$ T cells that recognize epitopes derived from the same pathogen. In our study described in **Chapter 3** we detected spliced epitope $LLO_{294/297-304}$-specific $CD8^+$ T cells *ex vivo.* This spliced epitope shares sequence similarity with

the linear epitope $LLO_{296-304}$ [44]. We stained splenocytes from infected mice *ex vivo* with MHC class I multimers folded with the two epitopes and found a double positive population and some cells still recognizing $LLO_{296-304}$ while all $LLO_{294/297-304}$ had shifted into the double positive population. From this we inferred that most likely a portion of $CD8^+$ T cells primed by $LLO_{296-304}$ can also recognize $LLO_{294/297-304}$ but it is unclear whether $LLO_{294/297-304}$ is presented and participates in $CD8^+$ T cell priming during infection as well. However, these cross-reactive $CD8^+$ T cells may decrease the immune evasion by the pathogens.

Several studies have also reported positive effects of $CD8^+$ T cells activated in one infection to be protective in another infection, as shown for cross-reactive $CD8^+$ T cells specific for lymphocytic choriomeningitis virus which were functionally activated during acute infection with vaccinia virus [45] or pichinde virus [46]. In **Chapter 2** we used Listeria-derived PlcB as a model antigen to prove that our *in silico* prediction method worked and successfully predicted and identified spliced epitopes that are important immunological targets in infection while their N- and C-terminal parts were not immunogenic in the context of their natural flanking sequences. No linear peptides with full sequence similarity were found with identified spliced epitopes $PlcB_{189-191/163-167}$ or $PlcB_{189-192/164-167}$ in any proteome of prokaryotes or eukaryotes, but the amino acid sequence from which the epitopes are generated by PCPS shares similarity with a sequence found in other bacteria. This domain conveys a zinc dependent phospholipase C activity and is found in a monomeric phospholipase C of *Bacillus cereus* (62% similarity with binding motive for $H\text{-}2K^b$ XXXXF/MZZL [47] present as well as 3 out of 4 amino acids of C-terminal part):

L.monocytogenes $PlcB_{162-196}$ AFYKLGLAIHYYTDISQPMHANNFTAISYPPGYH

Sequence of *B. cereus* AFFYLGLSLHYLGDVNQPMHAANFTNLSYPQGFH

The binding motive for $H\text{-}2K^b$ as well as 3 out of 4 amino acids of the C-terminal part are also found in the Phospholipase C precursor of *Streptococcus pneumoniae* which displays 61% similarity with the PlcB sequence of *Listeria monocytogenes*. In all these pathogenic bacteria the function of the proteins is associated with haemolysis and cell rupture. Sequence similarity of 50% is found in the alpha toxin of *Clostridium perfringens* and *Clostridium bifermentans* but then the binding motive for $H\text{-}2K^b$ is not maintained. In a study in which variants of $NP_{418-426}$ were studied in a human population [48], the authors found *in vivo* existence of $CD8^+$ T cells cross-reactive with homo- or heterosubtypic variants of the epitope in other

influenza viruses. They showed that certain positions in these epitopes were the crucial determinants of T cell specificity, which resulted in sequence similarity of approximately 50%. Whether the PlcB-derived epitopes in our study, which share the same degrees of similarity with phospholipase C of other bacteria, are immunogenic in infection with those bacteria as well, remains to be determined but it might indicate an additional immunological relevance of PCPS.

Cross-reactive T cells have also been described in infection as the cause of disease, which is a great risk when modulating antigen processing of vaccine-derived antigens. Influenza specific $CD8^+$ T cells have been shown to also recognize an epitope from Epstein Barr virus (EBV) despite only 33% sequence similarity. This results in massive proliferation and subsequently the overzealous $CD8^+$ T cell responses as seen in EBV-associated infectious mononucleosis [49]. Influenza specific $CD8^+$ T cells were also shown to cross-recognize a peptide derived from hepatitis C virus by which they contribute to immune mediated liver pathology [50, 51]. Next to immune mediated pathology, the risk often associated with cross-reactivity is auto immune disease. In many auto-immune diseases in which $CD8^+$ T cells play a role, epitope specificity and the underlying processes leading to the initial activation of auto-reactive $CD8^+$ T cells, are unclear.

The fact that few studies are describing cross-reactive $CD8^+$ T cells that are cross-reactive to self-antigens and thereby induce auto-immunity, should not lead to neglecting the potential dangers. However, the opportunities should also be explored, especially by identifying responses that can be protective in infections with other pathogens.

Conclusion

Knowledge of new ways of antigen processing as well as strategies to modulate it, forms the basis for successful and rational vaccine design. Vaccine efficacy can be greatly enhanced if the immune system is neatly navigated towards development of the desired response. However, negative consequences with respect to cross-reactivity should not be neglected.

References

1. Berkley, S. Improving access to vaccines through tiered pricing. *Lancet* **383**, 2265-2267 (2014).
2. Villanueva, M. S., Sijts, A. J. A. M. & Pamer, E. G. Listeriolysin is processed efficiently into an MHC class I-associated epitope in Listeria monocytogenes-infected cells. *Journal of Immunology* **155**, 5227-5233 (1995).
3. Villanueva, M. S., Fischer, P., Feen, K. & Pamer, E. G. Efficiency of MHC class I antigen processing: A quantitative analysis. *Immunity* **1**, 479-489 (1994).
4. Deol, P., Zaiss, D. M. W., Monaco, J. J. & Sijts, A. J. A. M. Rates of processing determine the immunogenicity of immunoproteasome-generated epitopes. *Journal of Immunology* **178**, 7557-7562 (2007).
5. Sijts, A. J. A. M. *et al*. MHC class I antigen processing of an adenovirus CTL epitope is linked to the levels of immunoproteasomes in infected cells. *Journal of Immunology* **164**, 4500-4506 (2000).
6. Tenzer, S. *et al*. Antigen processing influences HIV-specific cytotoxic T lymphocyte immunodominance. *Nat. Immunol.* **10**, 636-646 (2009).
7. La Gruta, N. L. *et al*. A virus-specific CD8+ T cell immunodominance hierarchy determined by antigen dose and precursor frequencies. *Proc. Natl. Acad. Sci. U. S. A.* **103**, 994-999 (2006).
8. Le Gall, S., Stamegna, P. & Walker, B. D. Portable flanking sequences modulate CTL epitope processing. *J. Clin. Invest.* **117**, 3563-3575 (2007).
9. Mo, A. X. Y., Van Lelyveld, S. F. L., Craiu, A. & Rock, K. L. Sequences that flank subdominant and cryptic epitopes influence the proteolytic generation of MHC class I-presented peptides. *J. Immunol.* **164**, 4003-4010 (2000).
10. Beekman, N. J. *et al*. Abrogation of CTL epitope processing by single amino acid substitution flanking the C-terminal proteasome cleavage site. *Journal of Immunology* **164**, 1898-1905 (2000).

11. Ossendorp, F. *et al*. A single residue exchange within a viral CTL epitope alters proteasome-mediated degradation resulting in lack of antigen presentation. *Immunity* **5,** 115-124 (1996).
12. Del Val, M., Schlicht, H. -., Ruppert, T., Reddehase, M. J. & Koszinowski, U. H. Efficient processing of an antigenic sequence for presentation by MHC class I molecules depends on its neighboring residues in the protein. *Cell* **66,** 1145-1153 (1991).
13. Seifert, U. *et al*. Hepatitis C virus mutation affects proteasomal epitope processing. *J. Clin. Invest.* **114,** 250-259 (2004).
14. Mishto, M. *et al*. Proteasome isoforms exhibit only quantitative differences in cleavage and epitope generation. *Eur. J. Immunol.* **44,** 3508-3521 (2014).
15. Liepe, J. *et al*. Quantitative time-resolved analysis reveals intricate, differential regulation of standard- and immuno-proteasomes. *eLife 2015;4:e07545* (2015).
16. Bins, A. D., Wolkers, M. C., Van Den Boom, M. D., Haanen, J. B. A. G. & Schumacher, T. N. M. In vivo antigen stability affects DNA vaccine immunogenicity. *J. Immunol.* **179,** 2126-2133 (2007).
17. Oosterhuis, K. *et al*. Preclinical development of highly effective and safe DNA vaccines directed against HPV 16 E6 and E7. *International Journal of Cancer* **129,** 397-406 (2011).
18. Oosterhuis, K., Aleyd, E., Vrijland, K., Schumacher, T. N. & Haanen, J. B. Rational design of DNA vaccines for the induction of human papillomavirus type 16 E6- and E7-specific cytotoxic T-cell responses. *Hum. Gene Ther.* **23,** 1301-1312 (2012).
19. Wolkers, M. C., Toebes, M., Okabe, M., Haanen, J. B. A. G. & Schumacher, T. N. M. Optimizing the efficacy of epitope-directed DNA vaccination. *J. Immunol.* **168,** 4998-5004 (2002).
20. Rodriguez, F., Zhang, J. & Whitton, J. L. DNA immunization: Ubiquitination of a viral protein enhances cytotoxic T-lymphocyte induction and antiviral protection but abrogates antibody induction. *J. Virol.* **71,** 8497-8503 (1997).
21. Huygen, K. *et al*. Mapping of TH1 helper T-cell epitopes on major secreted mycobacterial antigen 85A in mice infected with live Mycobacterium bovis BCG. *Infect. Immun.* **62,** 363-370 (1994).
22. Brandt, L., Oettinger, T., Holm, A., Andersen, Å B. & Andersen, P. Key Epitopes on the ESAT-6 Antigen Recognized in Mice during the Recall of Protective Immunity to Mycobacterium tuberculosis. *J. Immunol.* **157,** 3527-3533 (1996).
23. Lundegaard, C., Lund, O. & Nielsen, M. Accurate approximation method for prediction of class I MHC affinities for peptides of length 8, 10 and 11 using prediction tools trained on 9mers. *Bioinformatics* **24,** 1397-1398 (2008).
24. Livingston, B. D. *et al*. Optimization of epitope processing enhances immunogenicity of multiepitope DNA vaccines. *Vaccine* **19,** 4652-4660 (2001).
25. Rodriguez, F., Harkins, S., Slifka, M. K. & Whitton, J. L. Immunodominance in virus-induced CD8+ T-cell responses is dramatically modified by DNA immunization and is regulated by gamma interferon. *J. Virol.* **76,** 4251-4259 (2002).
26. Coscolla, M. *et al*. M. tuberculosis T cell epitope analysis reveals paucity of antigenic variation and identifies rare variable TB antigens. *Cell Host and Microbe* **18,** 538-548 (2015).
27. Dorhoi, A. & Kaufmann, S. H. E. Pathology and immune reactivity: understanding multidimensionality in pulmonary tuberculosis. *Semin. Immunopathol.* **38**(2):153-66 (2015).
28. Woodworth, J. S. & Andersen, P. Reprogramming the T Cell Response to Tuberculosis. *Trends Immunol.* **37** 81-83 (2016).
29. Kiepiela, P. *et al*. CD8+ T-cell responses to different HIV proteins have discordant associations with viral load. *Nat. Med.* **13,** 46-53 (2007).

30. Orr, M. T. *et al*. Immune subdominant antigens as vaccine candidates against Mycobacterium tuberculosis. *J. Immunol.* **193,** 2911-2918 (2014).
31. Frahm, N. *et al*. Control of human immunodeficiency virus replication by cytotoxic T lymphocytes targeting subdominant epitopes. *Nat. Immunol.* **7,** 173-178 (2006).
32. Busch, D. H., Pilip, I. M., Vijh, S. & Pamer, E. G. Coordinate regulation of complex T cell populations responding to bacterial infection. *Immunity* **8,** 353-362 (1998).
33. Gilchuk, P. *et al*. Discovering naturally processed antigenic determinants that confer protective T cell immunity. *J. Clin. Invest.* **123,** 1976-1987 (2013).
34. Choi, E. Y. *et al*. Immunodominance of H60 is caused by an abnormally high precursor T cell pool directed against its unique minor histocompatibility antigen peptide. *Immunity* **17,** 593-603 (2002).
35. Buchholz, V. R. *et al*. Disparate individual fates compose robust CD8+ T cell immunity. *Science* **340,** 630-635 (2013).
36. Gerlach, C. *et al*. Heterogeneous differentiation patterns of individual CD8+ T cells. *Science* **340,** 635-639 (2013).
37. Stemberger, C. *et al*. A Single Naive CD8+ T Cell Precursor Can Develop into Diverse Effector and Memory Subsets. *Immunity* **27,** 985-997 (2007).
38. Chang, J. T. *et al*. Asymmetric T lymphocyte division in the initiation of adaptive immune responses. *Science* **315,** 1687-1691 (2007).
39. Vogelzang, A. *et al*. Central memory $CD4^+$ T cells are responsible for the recombinant Bacillus Calmette-Guérin ΔureC::hly vaccine's superior protection against tuberculosis. *J. Infect. Dis.* **210,** 1928-1937 (2014).
40. Nandakumar, S. *et al*. Boosting BCG-primed responses with a subunit Apa vaccine during the waning phase improves immunity and imparts protection against Mycobacterium tuberculosis. *Sci. Rep.* **6,** 25837 (2016).
41. Ragas, A., Roussel, L., Puzo, G. & Riviere, M. The Mycobacterium tuberculosis cell-surface glycoprotein apa as a potential adhesin to colonize target cells via the innate immune system pulmonary C-type lectin surfactant protein A. *J. Biol. Chem.* **282,** 5133-5142 (2007).
42. Horn, C. *et al*. Decreased capacity of recombinant 45/47-kDa molecules (Apa) of Mycobacterium tuberculosis to stimulate T lymphocyte responses related to changes in their mannosylation pattern. *J. Biol. Chem.* **274,** 32023-32030 (1999).
43. Dobos, K. M., Khoo, K. -., Swiderek, K. M., Brennan, P. J. & Belisle, J. T. Definition of the full extent of glycosylation of the 45-kilodalton glycoprotein of Mycobacterium tuberculosis. *J. Bacteriol.* **178,** 2498-2506 (1996).
44. Geginat, G., Schenk, S., Skoberne, M., Goebel, W. & Hof, H. A novel approach of direct ex vivo epitope mapping identifies dominant and subdominant CD_4 and CD8 T cell epitopes from Listeria monocytogenes. *Journal of Immunology* **166,** 1877-1884 (2001).
45. Chen, H. D. *et al*. Memory CD8+ T cells in heterologous antiviral immunity and immunopathology in the lung. *Nat. Immunol.* **2,** 1067-1076 (2001).
46. Selin, L. K., Nahill, S. R. & Welsh, R. M. Cross-reactivities in memory cytotoxic T lymphocyte recognition of heterologous viruses. *J. Exp. Med.* **179,** 1933-1943 (1994).
47. Falk, K., Rötzschke, O., Stevanovic, S., Jung, G. & Rammensee, H. -. Allele-specific motifs revealed by sequencing of self-peptides eluted from MHC molecules. *Nature* **351,** 290-296 (1991).
48. Boon, A. C. M. *et al*. Recognition of Homo- and Heterosubtypic Variants of Influenza A Viruses by Human CD8+ T Lymphocytes. *J. Immunol.* **172,** 2453-2460 (2004).
49. Clute, S. C. *et al*. Cross-reactive influenza virus-specific CD8+ T cells contribute to lymphoproliferation in Epstein-Barr virus-associated infectious mononucleosis. *J. Clin. Invest.* **115,** 3602-3612 (2005).

50. Wedemeyer, H., Mizukoshi, E., Davis, A. R., Bennink, J. R. & Rehermann, B. Cross-reactivity between hepatitis C virus and influenza a virus determinant-specific cytotoxic T cells. *J. Virol.* **75,** 11392-11400 (2001).
51. Urbani, S. *et al*. Heterologous T cell immunity in severe hepatitis C virus infection. *J. Exp. Med.* **201,** 675-680 (2005).

Summary

Cover

The sailboat on the cover embodies the immune system. Using results presented in this thesis about new ways of antigen processing and strategies to modulate it, the immune system, mainly $CD8^+$ T cells, can be navigated or steered towards a specific response. In this way the harbor is safely reached. The harbor of Den Helder symbolizes this desired place as the situation in which the appropriate immune response is accomplished. The gained knowledge can therefore be used in vaccine design.

In this thesis

This thesis can roughly be divided into two parts. In the first part we study a new mechanism of antigen processing and its immunological consequences. In a series of two chapters we discuss our research on proteasome-catalyzed peptide splicing (PCPS) and its immunological relevance in *Listeria monocytogenes* infection. In the last two chapters we focus on modulation of antigen processing in order to enhance $CD8^+$ T cell responses for vaccine design. We first present a complete strategy to increase immunogenicity of a *Mycobacterium tuberculosis* cDNA encoded antigen and subsequently test this in a heterologous prime-boost vaccination regimen. The latter was performed at the Max Planck Institute of Infection Biology in Berlin. These results will be briefly summarized per chapter and are followed by the main conclusions.

In **Chapter 2** we show how we developed a novel approach to identify spliced epitopes in a bacterial infection. More and more evidence of spliced epitopes is available but due to insufficient tools to predict them, their identification remains challenging. We developed a reverse immunology-based multi-level approach to identify spliced epitopes that are targeted by $CD8^+$ T cells in *Listeria monocytogenes* infection. Our data show that we can predict such epitopes with high accuracy, and also demonstrate the immunological relevance of PCPS in infection. The spliced epitope-specific $CD8^+$ T cells detected in our studies recognized only the spliced epitopes, not the peptides in their natural flanking residues. This opens a whole range of opportunities for immunotherapies or vaccine design.

We continue with PCPS in studies described in **Chapter 3**. Here, by digestion of substrates with purified 20S proteasomes, we show that PCPS indeed increases the variety of peptides that is produced. Both immuno- and constitutive proteasomes were found to produce spliced peptides next to linear peptides.

Furthermore, we show that $CD8^+$ T cells that are activated by a linear epitope derived from a *Listeria monocytogenes* antigen, can be cross reactive to spliced epitopes that share sequence similarity with the linear epitope and are derived from the same antigen. Such a mechanism may reduce the chances of immune evasion because infected cells can present multiple versions of one epitope that can be recognized by the same $CD8^+$ T cells.

T cell priming by vaccines is often not optimal. We therefore aimed to increase vaccine-specific T cell responses in the studies reported in **Chapter 4**. In this chapter we show a complete strategy to enhance vaccine' immunogenicity. The multistage cDNA vaccine H56, encoding three secreted *Mycobacterium tuberculosis* (*Mtb*) antigens, was used as a model vaccine and delivered using dermal DNA tattoo immunization. We started by predicting H56 epitopes. Their antigen processing was optimized using flanking residue modulation and immunogenicity was increased by linkage of the cDNA of the antigen to cDNA of proteins with immunogenicity enhancing properties. This complete strategy can be used for vaccine design.

The H56 cDNA was also used in studies described in **Chapter 5**, in which we studied the effectiveness of a heterologous prime-boost strategy using dermal H56 DNA tattoo immunization in combination with BCG *::H56* subcutaneous injection. BCG is the only licenced vaccine against *Mtb* but it lacks efficacy in certain situations. We therefore tested whether we can successfully boost the effect of BCG by incorporating it in a heterologous prime boost regimen. We first measured the immunization strategies separately and scored cellular and humoral responses as well as efficacy. We continued by testing different combinations of the immunization strategies and scored the same immunological parameters. We conclude that broad immune responses are necessary to fight *Mtb*. Heterologous prime-boost using a combination of a dermal H56 cDNA prime and a subcutaneously given BCG *::H56* boost resulted in immune responses associated with protection. We show that responses differ depending on the sequence and type of the immunizations that are given, and that this has consequences for the disease burden.

In conclusion

In this thesis, antigen processing and $CD8^+$ T cell activation was studied. In the first chapters we proved the immunological relevance of PCPS in bacterial infection and in the last chapters we showed a complete vaccination strategy that will contribute to effectively fight *Mycobacterium tuberculosis*. We can conclude that these results give more insight in how modulation of antigen processing influences immune responses, mainly $CD8^+$ T cells. This knowledge will contribute to improved vaccine design.

Samenvatting

Op de voorkant

De zeilboot op de voorkant symboliseert het immuunsysteem. Met behulp van kennis over nieuwe mechanismen of strategieën die beschreven zijn in dit proefschrift, kan je het immuunsysteem beïnvloeden, voor o.a. vaccinatie doeleinden. Het immuunsysteem wordt op deze manier in de goede richting gestuurd ofwel genavigeerd. De boot komt dan op de gewenste plek, de haven, aan. De haven van Den Helder symboliseert deze gewenste situatie waarin het immuunsysteem verkeert nadat het succesvol beïnvloed is. Hierin is de sturing van het immuunsysteem door bijvoorbeeld een vaccinatie succesvol geweest en kan het lichaam toekomstige ziekteverwekkers zonder veel schade uitschakelen.

$CD8^+$ T cellen

Het immuunsysteem is een complex systeem met allerlei cellen die samenwerken en met elkaar communiceren. Sommige cellen zijn deel van de aangeboren afweer. Deze cellen zijn de eersten die maatregelen nemen als er een ziekteverwekker, bijvoorbeeld een bacterie of virus, binnen komt, maar ze zijn niet specifiek voor die ziekteverwekker. Deze cellen kunnen de groei van de ziekteverwekker beperken maar voor echte opruiming is vaak de hulp nodig van cellen die horen bij de aangeleerde afweer, die wel specifiek zijn voor de ziekteverwekker. Het duurt echter even voordat deze cellen gemobiliseerd zijn. Cellen van de aangeboren afweer nemen stukjes van de ziekteverwekker mee en presenteren die op major histocompatibility complex (MHC) moleculen, een soort dienblaadjes, aan cellen van de aangeleerde afweer. Een klein deel van deze cellen kan het stukje herkennen en gaat delen. Door deze vermenigvuldiging ontstaat een relatief groot percentage specifieke cellen voor deze ziekteverwekker. Het duurt echter ongeveer een week voordat dit hele proces voltooid is en daarom is het effect van de aangeleerde afweer pas later merkbaar. Dit effect kan echter wel heel lang voortbestaan omdat de aangeleerde afweer immunologisch geheugen aanlegt. Hierdoor word je de volgende keer dat de ziekteverwekker je lichaam binnen komt niet meer ziek, we zeggen dan dat je 'immuun' bent voor die specifieke ziekteverwekker. Tegen verschillende soorten ziekteverwekkers heb je verschillende soorten cellen nodig van de aangeleerde afweer. Er zijn daarom verschillende cellen in deze populatie, bijvoorbeeld B cellen of T cellen. Binnen deze populatie cellen van de aangeleerde afweer bestaan er verschillende soorten T cellen, de $CD8^+$ T cellen zijn de cellen waar dit proefschrift over gaat. Deze cellen zijn in staat

cellen te herkennen die geïnfecteerd zijn met bijvoorbeeld virussen. Virussen zijn ziekteverwekkers die ín de cellen zitten en zijn daardoor voor andere cellen niet te zien aan de buitenkant.

Vaccinaties

Vaccinatie, of wel inenting, tegen virussen of andere ziekteverwekkers die in de cellen van het lichaam zitten in plaats van vrij rondzwemmen tussen de cellen, is vaak gericht op het activeren van T cellen, onder andere de $CD8^+$ T cellen. Vaccinatie berust op het feit dat je het lichaam al in contact brengt met een stukje van de ziekteverwekker. Het eerder beschreven proces van presentatie aan T cellen vindt dan al plaats wat betekent dat er al immunologisch geheugen wordt aangelegd. Als de werkelijke ziekteverwekker dan het lichaam binnen komt, kunnen de specifieke T cellen meteen in actie komen en is er wel sprake van infectie, maar zijn de ziekteverschijnselen veel minder erg.

In dit proefschrift

In het onderzoek beschreven in dit proefschrift hebben we onderzocht hoe $CD8^+$ T cellen geactiveerd raken en hoe ze kunnen worden beïnvloed en gestuurd. In de eerste twee hoofdstukken bestuderen we een nieuw mechanisme waarop de stukjes ziekteverwekker door het lichaam worden samengesteld om vervolgens aan het immuunsysteem te worden gepresenteerd. We laten zien dat dit mechanisme immunologisch relevant is omdat we $CD8^+$ T cellen aangetoond hebben die de stukjes die op deze nieuwe manier gemaakt worden, ook echt kunnen herkennen. In het tweede deel van het proefschrift wordt beschreven hoe het immuunsysteem beïnvloed kan worden voor vaccinatie doeleinden. We laten een strategie zien hoe de stukjes ziekteverwekker kunnen worden veranderd ter verbetering van de $CD8^+$ T cel respons. Tenslotte tonen we aan dat ook de manier waarop het vaccin, wat bestaat uit deze gemodificeerde stukjes van de ziekteverwekker, wordt gegeven van belang is voor het opwekken van de gewenste immuun respons. Hier volgt een samenvatting van wat er is onderzocht in de verschillende hoofdstukken en wat de belangrijkste conclusies waren.

In het onderzoek beschreven in **Hoofdstuk 2** hebben we een nieuwe manier bestudeerd hoe stukjes ziekteverwekker aan het immuunsysteem worden gepresenteerd. We hebben ontdekt dat dit niet alleen gebeurt met een schaar die de ziekteverwekker opdeelt in stukjes, zoals tot nu toe bekend, maar dat er ook een soort plakstift is die kleine stukjes ziekteverwekker samen kan plakken zodat ze groot genoeg zijn om aan het immuunsysteem te laten zien. Dit fenomeen van knippen en plakken kan worden voorspeld met wiskundige modellen. We

hebben laten zien dat het model wat wij hebben ontwikkeld werkt, en dat het kan voorspellen welke stukken worden gepresenteerd. Vervolgens hebben we aangetoond dat deze stukken van belang zijn bij immuun responsen tegen een ziekteverwekker. Het feit dat het immuunsysteem dit kan, betekent dat er tegen veel meer stukjes immuun responsen kunnen worden opgebouwd dan wat we tot nu toe dachten, en dit kan van groot belang worden in vaccinatie strategieën. We gaan verder met het principe van knippen en plakken in het onderzoek beschreven in **Hoofdstuk 3** waarin we hebben laten zien dat $CD8^+$ T cellen die 'ouderwets' geknipte stukjes ziekteverwekker herkennen, ook stukjes kunnen herkennen die hierop lijken maar gemaakt zijn door knippen én plakken. Dit herkennen van meerdere stukjes door één $CD8^+$ T cel noemen we kruis reactiviteit. Het belang van het knip-en-plak mechanisme wordt hierdoor groter. De reden hiervoor is dat als $CD8^+$ T cellen meerdere stukjes kunnen herkennen die op elkaar lijken, het minder gevaarlijk is als de ziekteverwekker een deel van zijn stukjes verandert. Sommige ziekteverwekkers veranderen, ook wel muteren genoemd, heel vaak en snel waardoor het immuunsysteem altijd achter de feiten aan loopt en de infectie niet goed kan worden gestopt. Aangezien $CD8^+$ T cellen stukjes kunnen herkennen die op elkaar lijken maar via verschillende mechanismen worden gemaakt, kan het immuunsysteem je beter beschermen tegen deze snel veranderende ziekteverwekkers.

In de studies beschreven in **Hoofdstuk 4** hebben we gewerkt aan een streng genetische informatie, DNA, wat codeert voor stukjes van de ziekteverwekker die tuberculose veroorzaakt. Dit stuk DNA kan worden gebruikt als model-vaccin. We hebben een strategie laten zien hoe dit stuk DNA kan worden verbeterd, waardoor er meer $CD8^+$ T cellen geactiveerd worden. Door het ontwikkelen van dit soort strategieën kunnen bestaande vaccins verbeterd worden, opdat ze meer $CD8^+$ T cellen activeren.

Dit verbeterde model-vaccin hebben we ook gebruikt voor het project beschreven in **Hoofdstuk 5**. Deze studies zijn gedaan aan het Max Planck Instituut voor Infectie Biologie in Berlijn. We hebben getest of het model-vaccin een goede combinatie kan zijn met het huidige vaccin voor tuberculose. De achterliggende gedachte is dat wanneer je niet één, maar twee keer vaccineert, en op verschillende plaatsen in het lichaam, er een betere activatie is van het immuunsysteem. We hebben geconcludeerd dat dit inderdaad het geval is maar ook dat het uitmaakt in welke volgorde je de vaccins geeft. Deze kennis kan goed toegepast worden op het huidige vaccinatie regime tegen tuberculose.

Conclusies

In dit proefschrift stonden de $CD8^+$ T cellen centraal. We kunnen concluderen dat de beschreven resultaten meer inzicht geven in hoe ze functioneren en beïnvloed kunnen worden. Ten eerste omdat we de immunologische relevantie aan hebben getoond van een nieuw mechanisme hoe de ziekteverwekkers worden verwerkt en gepresenteerd aan het immuunsysteem. Ten tweede omdat we een direct toepasbare strategie hebben laten zien die werkt tegen tuberculose. Deze kennis zal bijdragen aan het verbeteren van vaccins.

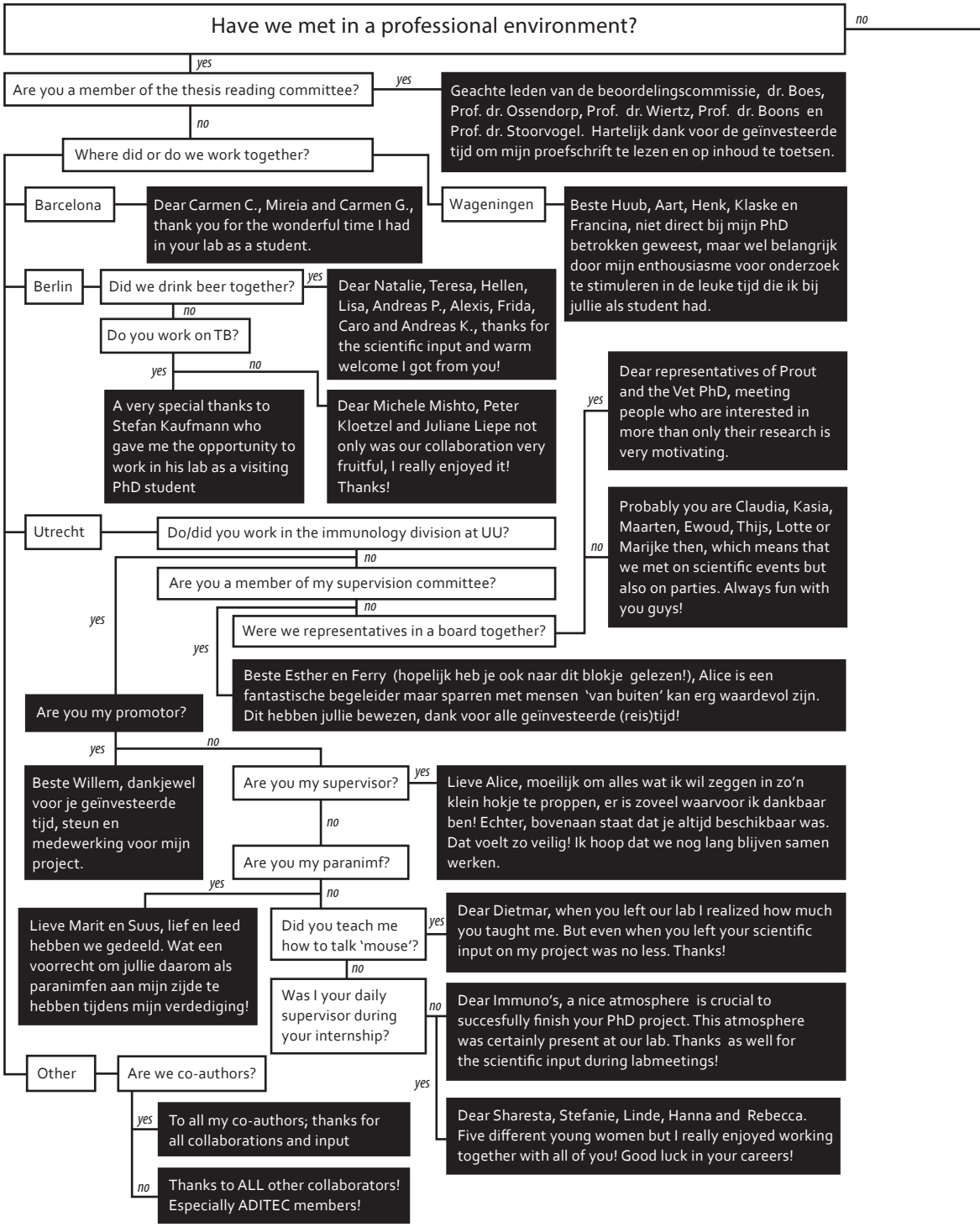
Have we met in a professional environment?
no
yes
Are you a member of the thesis reading committee?
yes
Geachte leden van de beoordelingscommissie, dr. Boes, Prof. dr. Ossendorp, Prof. dr. Wiertz, Prof. dr. Boons en Prof. dr. Stoorvogel. Hartelijk dank voor de geïnvesteerde tijd om mijn proefschrift te lezen en op inhoud te toetsen.
no
Where did or do we work together?
Barcelona
Dear Carmen C., Mireia and Carmen G., thank you for the wonderful time I had in your lab as a student.
Wageningen
Beste Huub, Aart, Henk, Klaske en Francina, niet direct bij mijn PhD betrokken geweest, maar wel belangrijk door mijn enthousiasme voor onderzoek te stimuleren in de leuke tijd die ik bij jullie als student had.
Berlin
Did we drink beer together?
yes
Dear Natalie, Teresa, Hellen, Lisa, Andreas P., Alexis, Frida, Caro and Andreas K., thanks for the scientific input and warm welcome I got from you!
no
Do you work on TB?
yes
A very special thanks to Stefan Kaufmann who gave me the opportunity to work in his lab as a visiting PhD student
no
Dear Michele Mishto, Peter Kloetzel and Juliane Liepe not only was our collaboration very fruitful, I really enjoyed it! Thanks!
Utrecht
Do/did you work in the immunology division at UU?
yes
Are you my promotor?
no
Are you a member of my supervision committee?
yes
Were we representatives in a board together?
yes
Dear representatives of Prout and the Vet PhD, meeting people who are interested in more than only their research is very motivating.
no
Probably you are Claudia, Kasia, Maarten, Ewoud, Thijs, Lotte or Marijke then, which means that we met on scientific events but also on parties. Always fun with you guys!
Beste Esther en Ferry (hopelijk heb je ook naar dit blokje gelezen!), Alice is een fantastische begeleider maar sparren met mensen 'van buiten' kan erg waardevol zijn. Dit hebben jullie bewezen, dank voor alle geïnvesteerde (reis)tijd!
yes
Beste Willem, dankjewel voor je geïnvesteerde tijd, steun en medewerking voor mijn project.
no
Are you my supervisor?
yes
Lieve Alice, moeilijk om alles wat ik wil zeggen in zo'n klein hokje te proppen, er is zoveel waarvoor ik dankbaar ben! Echter, bovenaan staat dat je altijd beschikbaar was. Dat voelt zo veilig! Ik hoop dat we nog lang blijven samen werken.
no
Are you my paranimf?
yes
Lieve Marit en Suus, lief en leed hebben we gedeeld. Wat een voorrecht om jullie daarom als paranimfen aan mijn zijde te hebben tijdens mijn verdediging!
no
Did you teach me how to talk 'mouse'?
yes
Dear Dietmar, when you left our lab I realized how much you taught me. But even when you left your scientific input on my project was no less. Thanks!
no
Was I your daily supervisor during your internship?
no
Dear Immuno's, a nice atmosphere is crucial to succesfully finish your PhD project. This atmosphere was certainly present at our lab. Thanks as well for the scientific input during labmeetings!
yes
Dear Sharesta, Stefanie, Linde, Hanna and Rebecca. Five different young women but I really enjoyed working together with all of you! Good luck in your careers!
Other
Are we co-authors?
yes
To all my co-authors; thanks for all collaborations and input
no
Thanks to ALL other collaborators! Especially ADITEC members!

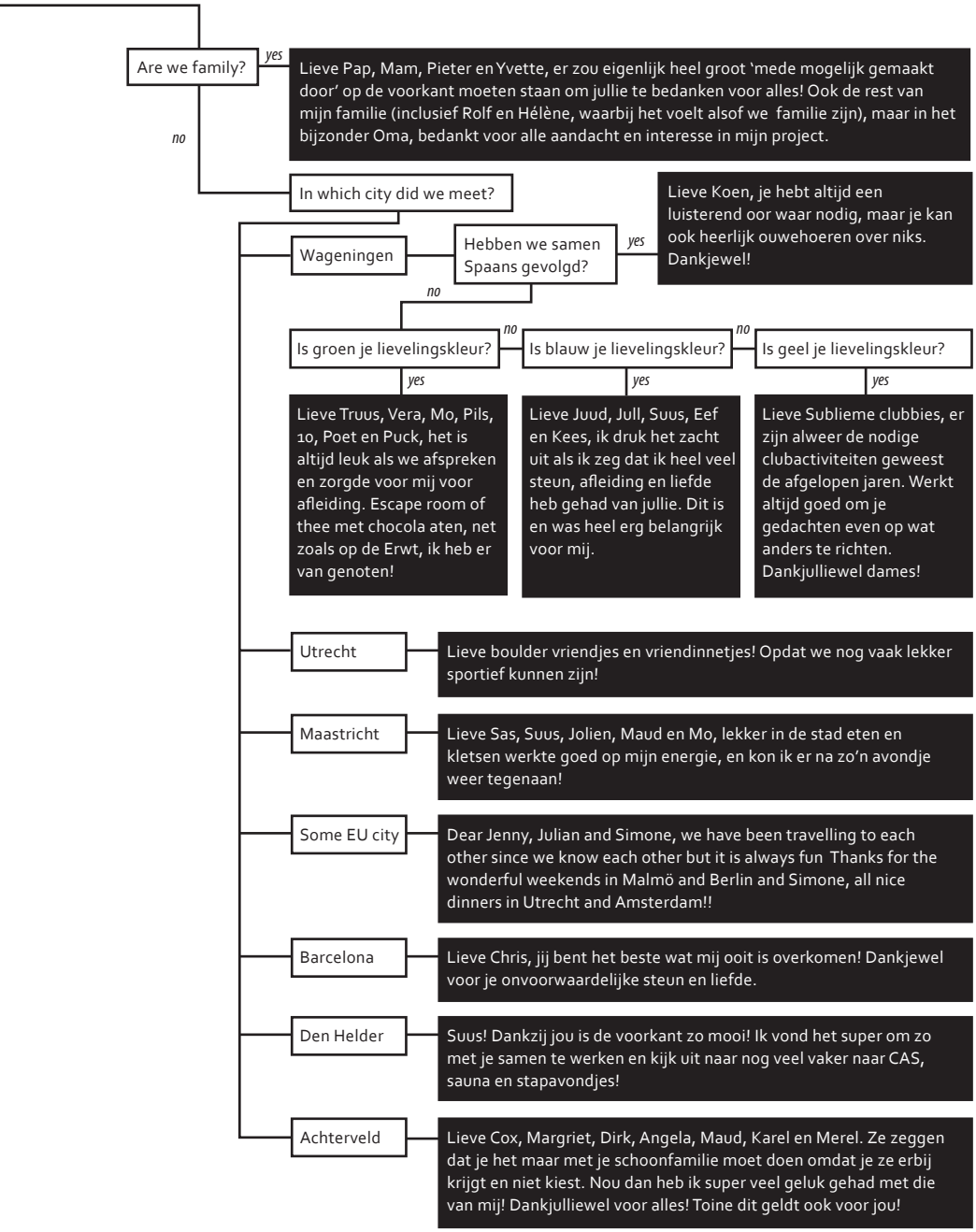
Are we family?
yes
Lieve Pap, Mam, Pieter en Yvette, er zou eigenlijk heel groot 'mede mogelijk gemaakt door' op de voorkant moeten staan om jullie te bedanken voor alles! Ook de rest van mijn familie (inclusief Rolf en Hélène, waarbij het voelt alsof we familie zijn), maar in het bijzonder Oma, bedankt voor alle aandacht en interesse in mijn project.
no
In which city did we meet?
Wageningen
Hebben we samen Spaans gevolgd?
yes
Lieve Koen, je hebt altijd een luisterend oor waar nodig, maar je kan ook heerlijk ouwehoeren over niks. Dankjewel!
no
Is groen je lievelingskleur?
no
Is blauw je lievelingskleur?
no
Is geel je lievelingskleur?
yes
Lieve Truus, Vera, Mo, Pils, 10, Poet en Puck, het is altijd leuk als we afspreken en zorgde voor mij voor afleiding. Escape room of thee met chocola aten, net zoals op de Erwt, ik heb er van genoten!
yes
Lieve Juud, Jull, Suus, Eef en Kees, ik druk het zacht uit als ik zeg dat ik heel veel steun, afleiding en liefde heb gehad van jullie. Dit is en was heel erg belangrijk voor mij.
yes
Lieve Sublieme clubbies, er zijn alweer de nodige clubactiviteiten geweest de afgelopen jaren. Werkt altijd goed om je gedachten even op wat anders te richten. Dankjulliewel dames!
Utrecht
Lieve boulder vriendjes en vriendinnetjes! Opdat we nog vaak lekker sportief kunnen zijn!
Maastricht
Lieve Sas, Suus, Jolien, Maud en Mo, lekker in de stad eten en kletsen werkte goed op mijn energie, en kon ik er na zo'n avondje weer tegenaan!
Some EU city
Dear Jenny, Julian and Simone, we have been travelling to each other since we know each other but it is always fun Thanks for the wonderful weekends in Malmö and Berlin and Simone, all nice dinners in Utrecht and Amsterdam!!
Barcelona
Lieve Chris, jij bent het beste wat mij ooit is overkomen! Dankjewel voor je onvoorwaardelijke steun en liefde.
Den Helder
Suus! Dankzij jou is de voorkant zo mooi! Ik vond het super om zo met je samen te werken en kijk uit naar nog veel vaker naar CAS, sauna en stapavondjes!
Achterveld
Lieve Cox, Margriet, Dirk, Angela, Maud, Karel en Merel. Ze zeggen dat je het maar met je schoonfamilie moet doen omdat je ze erbij krijgt en niet kiest. Nou dan heb ik super veel geluk gehad met die van mij! Dankjulliewel voor alles! Toine dit geldt ook voor jou!

CV

Anouk Cecile Maria Platteel was born on February 6, 1987 in Den Helder, the Netherlands. In September 2005 she started her studies in Animal Sciences at Wageningen University, Wageningen. She wrote her bachelor thesis under supervision of Prof. dr. ir. H.F.J. Savelkoul and obtained her degree in 2008. During her master Anouk was active as a member of the Student Council and student representative in the board of the Education Institute of Wageningen University and European Students' Union. She was admitted to the Research Master track of Animal Sciences in which Anouk fulfilled her first internship at the Adaptation Physiology department of Wageningen University under supervision of dr. A. Lammers. She worked on the immunomodulatory influence of lectins in the diet of young laying hens. Anouk went to Barcelona, Spain to IDIBELL (Bellvitge Biomedical Research Institute) for her second internship, which she did under supervision of dr. C. Cabellos. She studied the activities of combination treatment with daptomycin and fosfomycin against methicillin resistant *Staphylococcus aureus* in rats. Her supervisor in the Netherlands for this internship was dr. H.K. Parmentier. For her third internship, Anouk worked on the effect of systemic inflammation on muscle of elderly at Nutricia Research, now based in Utrecht, the Netherlands, under supervision of dr. K. van Norren and Ing. F. Dijk. Prof. dr. ir. H.F.J. Savelkoul was her supervisor from Wageningen University. In June 2012 Anouk graduated in both specializations Animal Health and Applied Zoology.

Anouk started her PhD training in September 2012 at the "Infection & Immunity Center Utrecht" in Utrecht, the Netherlands and performed her research in the lab of dr. E.J.A.M. Sijts at the department of Infectious Diseases and Immunology, Division of Immunology of Utrecht University. She studied new ways of antigen processing as well as strategies to modulate it, in order to elicit robust and broad $CD8^+$ T cell responses for vaccine design. Part of these studies were conducted in the lab of Prof. dr. S.H.E. Kaufmann at the Max Planck Institute of Infection Biology in Berlin, Germany. For these studies Anouk received short stay fellowships grants from Boehringer Ingelheim Fonds and the European Federation of Immunological Societies (EFIS). The results obtained during this PhD project are presented in this thesis. Also during her PhD project, Anouk was active in education policy. She was a member of the Infection & Immunity educational board, Prout (Promovendi Overleg Utrecht) and Veterinary PhD council, aiming at contributing to the education of Life Science master students and PhD candidates of Utrecht University.

Currently Anouk is working at the department of Infectious Diseases and Immunology, Division of Immunology of Utrecht University.

List of publications

VIVAS, M., FORCE, E., GARRIGOS, C., TUBAU, F., **PLATTEEL, A.C.M**, ARIZA, J. and CABELLOS, C., 2014. Experimental study of the efficacy of daptomycin for the treatment of cephalosporin-resistant pneumococcal meningitis. *The Journal of antimicrobial chemotherapy,* June;69(11):, pp. 3020-3026.

PLATTEEL, A.C.M., MISHTO, M., TEXTORIS-TAUBE, K., KELLER, C., LIEPE, J., BUSCH, D.H., KLOETZEL, P.M., SIJTS, E.J.A.M. 2016. $CD8^+$ T cells of *Listeria monocytogenes*-infected mice recognize both linear and spliced proteasome products. *European Journal of Immunology,* May;46(5):1109-18.

PLATTEEL, A.C.M., DE GROOT, A.M., KELLER, C., ANDERSEN, P., OVAA, H., KLOETZEL, P.M., MISHTO, M., AND SIJTS, E.J.A.M. 2016. Strategies to enhance immunogenicity of cDNA vaccine encoded antigens by modulation of antigen processing. *Vaccine,* Sep;34(42):5132-40.

PLATTEEL, A.C.M., LIEPE, J., TEXTORIS-TAUBE, K., SCHALKWIJK, H.H., KLOETZEL, P.M., MISHTO, M., SIJTS, E.J.A.M. 2016. Multi-level strategy identifies proteasome-generated spliced epitopes targeted by $CD8^+$ T cells in *Listeria monocytogenes* infection*. In review.*

PLATTEEL, A.C.M., NIEUWENHUIZEN, N., DOMASZEWSKA, T., VOGELZANG, A., SCHEURER, S,. ZEDLER, U., WEINER, J., GENGENBACHER, M., SIJTS, E.J.A.M., KAUFMANN, S.H.E. 2016. Efficacy of heterologous prime-boost vaccination using dermal H56 cDNA tattoo and subcutaneous injection of BCG *::H56* against *Mycobacterium tuberculosis. Submitted.*

PLATTEEL, A.C.M., ZAISS, D.M., HENRI, S., SIJTS, E.J.A.M. 2016. Correlating antigen processing and presentation in skin vaccination strategies. *Submitted.*